SUPERPARAMAGNETIC RESONANCE STUDIES
ON
MAGNETIC NANOPARTICLES

by

Hüseyin KAVAS

July   2006

SUPERPARAMAGNETIC RESONANCE STUDIES
ON
MAGNETIC NANOPARTICLES

by

Hüseyin KAVAS

A thesis submitted to

the Graduate Institute of Sciences and Engineering

of

Fatih University

in partial fulfillment of the requirements for the degree of

Master of Science

in

Physcis

July 2006
Istanbul, Turkey

APPROVAL PAGE

I certify that this thesis satisfies all the requirements as a thesis for the degree of Master of Science.

Prof. Dr. Mustafa KUMRU
Head of Department

This is to certify that I have read this thesis and that in my opinion it is fully adequate, in scope and quality, as a thesis for the degree of Master of Science.

Assist. Prof. Dr. Yüksel KÖSEOĞLU
Supervisor

Examining Committee Members

Prof. Dr. Mustafa KUMRU   …………………………………………..

Assist. Prof. Dr. Yüksel KÖSEOĞLU   …………………………………………..

Assist. Prof. Dr. Abdülhadi BAYKAL   …………………………………………..

It is approved that this thesis has been written in compliance with the formatting rules laid down by the Graduate Institute of Sciences and Engineering.

Asst. Prof. Dr. Nurullah ARSLAN

Director

July 2006

**SUPERPARAMAGNETIC RESONANCE STUDIES
ON
MAGNETIC NANOPARTICLES**

Hüseyin KAVAS

M. S. Thesis - Physics
July 2006

Supervisor: Assist. Prof. Dr. Yüksel KÖSEOĞLU

ABSTRACT

Magnetic nanoparticles have attracted great interest due to their mesoscopic properties and their potential for applications. The widely used and the well known magnetic nanoparticle is the magnetite (Fe_3O_4). In this study, the theory of the Superparamagnetic Resonance (SPR) and its application on superparamagnetic Fe_3O_4 nanoparticles in a size range of 1.1-11 nm were studied. The size and surface effects on temperature and frequency dependent magnetic properties of these particles were investigated. We used a theoretical formalism based on a distribution of diameters or volumes of the nanoparticles following lognormal proposed by Berger et al. The nanoparticles are considered as single magnetic domains with random orientations of magnetic moments and thermal fluctuations of anisotropic axes. The individual line shape function is derived from the damped precession equation of Landau-Lifshitz. Magnetic properties of the samples were strongly temperature and size dependent. When the

temperature is decreased, while the SPR line width is increasing the resonance field is decreasing. This means the anisotropy field is increasing by decreasing the temperature. At high T's, the SPR line shape is governed by the core anisotropy and the thermal fluctuations. On decreasing T, as the shell spins increase their magnetic susceptibility, they produce an effective field on the core, leading to a decrease of B_r from its high T value. As the shell spins begin to order, the effective anisotropy increases following its surface value more closely. So, the results can be interpreted by a simple model, in which each single-domain nanoparticle is considered as a core-shell system, with uniaxial anisotropy on the core and surface anisotropy on the shell. Also a linear microwave frequency dependence was observed. Furthermore, the blocking temperature of the particles is also increasing by the particle size.

MANYETİK NANO PARÇAÇIKLARDA
SÜPERPARAMANYETİK REZONANS ÇALIŞMALARI

Hüseyin KAVAS

Yüksek Lisans Tezi - Fizik
Temmuz 2006

Tez Yöneticisi: Yrd.Doç. Dr. Yüksel KÖSEOĞLU

ÖZ

Manyetik nano parçacıklar, uygulama alanlarının genişliği ve mesoskopik özelliklerinden dolayı çok yaygın olarak çalışılmaktadır. En yaygın kullanılan ve en iyi bilinen magnetic nano parçacıklardan birisi mıknatıs (Fe_3O_4). Bu çalışmada, Süperparamanyetik Rezonans (SPR) teorisi ve 1.1-11 nm arasında büyüklüklere sahip süperparamanyetik Fe_3O_4 numunelerindeki uygulaması incelenmiştir. Sıcaklığa ve frekansa bağlı manyetik özellikleri olan bu nano parçacıklarda büyüklük ve yüzey etkileri araştırılmıştır. Kullanılan teorik yaklaşım Berger ve çalışma arkadaşlarına ait parçacık çaplarının veya hacimlerinin lognormal dağılımına dayanmaktadır. Rastgele yönelmiş manyetik momentler ve anisotropi ekseninin ısısal dalgalanmalarıdan dolayı bu nanoparçacıkların tek alanlı (single domain) oldukları kabul edilmiştir. Tek çizgi fonsiyonu Landau-Lifshitz'in sönümlü presesyon denkleminden elde edilmiştir. Numunelerin manyetik özelliklerinin büyüklüklerine ve sıcaklığa şiddetli bağımlı olduğu gözlenmiştir. Sıcaklık düşerken SPR çizgi genişliği artarken rezonans alanı azalmıştır. Bunun anlamı düşen sıcaklıkla anisotropy alanının artmasıdır. Yüksek sıcaklıklarda SPR çizgi şekli çekirdek anisotrpisi ve ısısal dalgalanmalardan etkilenmiştir. Azalan sıcaklıkla birlikte

kabuk spinleri numunelerin manyetik alınganlığını artıracakları için bunlar çekirdek üzerinde etkin bir manyetik alan oluştururlar ve buda rezonans alanının B_r yüksek sıcaklardaki değerinden daha küçük değerlere sahip olmasına sebep olur. Kabuk spinleri düzenli hale geldikçe etkin anisotropi artar ve yüzey alanının sahip olduğu değere yaklaşır. Dolayısıyla bu sonuçları basit bir model ile açıklayabiliriz. Bu modele göre her bir tek alanlı nano parçacıklar, çekirdek-kabuk yapılı sistemler olarak düşünülebilir. İlave olarak lineer mikrodalga frekans bağlılığı ve blok sıcaklığının parçacık büyüklüğü ile arttığı gözlenmiştir.

Anahtar Kelimeler: SPR, süperparamanyetizma, spinel yapılar, nanoparçacıklar, Fe_3O_4.

ACKNOWLEDGEMENT

TABLE OF CONTENTS

LIST OF FIGURES

LIST OF TABLES

LIST OF SYMBOLS AND ABBREVIATIONS

SYMBOL/ABBREVIATION

SPR	:	Superparmagetic Resonance
ESR	:	Electron Spin Resonance
EPR	:	Electron Paramagnetic Resonance
FMR	:	Ferromagnetic Resonance
NMR	:	Nuclear Magnetic Resonance
DPPH	:	Difenilpicrilhidracil, Antioxidant Free Radical
p	:	Pole strengths
m	:	Magnetic moment or magnetic dipole moment of bar magnet
$\vec{\tau}_{max}$	:	Maximum torque
T	:	Period
e	:	Charge of electron
γ	:	Gyromagnetic ratio constant
μ	:	The electronic or atomic moment
m$_{av}$	:	Average magnetic moment
μ_B	:	Bohr Magneton
μ_r	:	Relative magnetic Permeability
μo	:	Magnetic Permeability of free space
μ_s	:	Spin Magnetic Moment
A	:	Area
L	:	Angular Momentum Vector
S	:	Spin Vector
J	:	Total Angular Momentum Vector ($\mathbf{J} = \mathbf{L} + \mathbf{S}$)
M	:	Magnetization vector
M$_s$	:	Saturation Magnetization

B	:	Total Magnetic Field
$\mathbf{B}_0$	:	Applied (external) Field
H_d	:	Demagnetizing filed
N_d	:	Demagnetizing factor
χ	:	Magnetic Susceptibility
χ'	:	Real part of the susceptibility
χ''	:	Imaginary part of the Susceptibility
T_c	:	Curie Temperature (Critical temperature)
T_N	:	Neél Temperature
D_{SP}	:	Superparamagnetic size
D_S	:	Single domain particle size
K	:	Anisotropy constant
f_o	:	Attempt frequency
T_B	:	Blocking temperature
η	:	Dynamic viscosity
H_K	:	Internal magnetic field due to anisotropy
F	:	Helmholtz free energy
G	:	Gibbs free energy
G_L	:	Landau free energy
H_1	:	Hamiltonian of first particle
V_{12}	:	Coulomb repulsion between the two electrons
$\psi_1(\vec{r}_1)$	:	Eigenfunctions of first particles hamiltonian H_1
$\psi_{spatial}$	:	Spatial wave functions of electrons
φ_{spin}	:	Spin wave functions of electrons
J_{12}	:	Exchange Coulomb energy constant
E_{exc}	:	The exchange energy
E_{ani}	:	The magnetocrystalline anisotropy energy
E_{ms}	:	The magnetostatic energy

E_{ext}	:	The Zeeman energy in an external field
C	:	Curie constant
k	:	Boltzman Constant
J	:	Exchange Constant
h	:	Planck's constant
$\hbar$	:	Constant ($\hbar = $ h $/2\pi$)
F	:	Force
G	:	Magnetic Field Unit, Gauss
T	:	Magnetic Field Unit, Tesla
kN	:	Pressure Unit, Kilo-Newton
g	:	Lande Splitting factor
H	:	Effective Magnetic Field
dP/dH	:	First Derivative of Absorption Peak
L(x)	:	Langevin Function
Mr	:	Remenance
Hc	:	Coercivity
E_{exc}	:	Heisenberg Exchange Energy
m_s	:	Electron Spin Moment Quantum Number
w	:	Angular Frequency
ν	:	Larmour Precession Frequency
T_1	:	Spin-Lattice Relaxation Time
T_2	:	Spin-Spin Relaxation Time
fcc	:	Face Centered Cubic
Hr	:	Resonance Field
ΔH	:	Line Width
a.u.	:	Arbitrary Unit

CHAPTER 1

INTRODUCTION

Magnetism is a subject, which has been studied for nearly three thousands years. The navigational magnetic compass was the first technological product resulting from this study. The first known magnetic material is magnetite (Fe_3O_4). Although its history is not certainly known, its power to attract iron was known to have been before Christ. The name of magnet came from Magnesia, a district of Turkey and the Greeks coined it by referring to this district. William Gilbert made the first effective scientific study of magnetism in 1600 [1]. People did not know that an electric current produces a magnetic field until it was discovered by H. C. Oersted in 1820 and the discovery of electromagnet followed five years later. With further contributions by Faraday, Maxwell, Hertz and many others, the new science of electromagnetism developed.

During the 1930's researches on 'soft ferrites' continued, primarily in Japan and Netherlands. However, it was not until 1945 that J. L. Snoek of the Phillips Research Laboratories in Netherlands succeeded in producing a 'soft ferrite' for commercial applications. The term ''ferrite'' is derived from the Latin word ''ferrum'', meaning iron. Ferrites are homogeneous ceramic materials composed of various oxides containing iron oxide as their main constituent.

Magnetic nanoparticles have attracted great interest due to their mesoscopic properties and their potential for applications. There are a lot of studies on magnetic properties of many kinds of nanoparticles. They have a wide field of applications, such as; recording tapes, permanent magnets, hard disc recording media, flexible recording media, read-write heads, active components of ferrofluids, color imaging, magnetic refregration, detoxification of biological fluids, magnetically controlled transport of anti-cancer drugs, magnetic resonance imaging (MRI) contrast enhancement and magnetic cell separation, etc [2-11].

In this study, size and surface effects on temperature and frequency dependent magnetic properties of superparamagnetic Fe_3O_4 nanoparticles in a size range of 1.1-11 nm are investigated by Superparamagnetic Resonance (SPR) technique.

In this study, the theory of magnetism will be explained firstly and basically in the first chapter. Then the nanoparticles' magnetism is going to be studied with details. The following chapter contains synthesis and characterization of samples and the SPR measurements. After experimental part, the way of the theoretical analysis of experimental results will be given. In Chapter 6, experimental and theoretical fit results explained in the name of results and discussions. Finally we have conclusions in our study.

CHAPTER 2

THEORY OF MAGNETISM

2.1 MAGNETIC POLES

The law of interaction between magnetic poles was discovered independently by Michell in 1750, and by Coulomb in 1785. They found the following empirical equation that the force between two magnetic poles is proportional to the product of their pole strengths, p, and inversely proportional to the square of the distance between them:

$$\vec{F} = \frac{p_1 p_2}{r^2} \qquad \text{(cgs).} \qquad (2.1)$$

This is analogous to Coulomb's law for electric charges; with one important difference that single magnetic pole (magnetic monopole) does not exist. Above equation can be written in SI units as follows:

$$\overline{F} = \frac{1}{4\pi\mu_0} \frac{p_1 p_2}{r^2} \qquad \text{(SI)} \qquad (2.2)$$

where μ_0 is called the permeability of free space, and has the value $4\pi \times 10^{-7}$ Wb/Am (weber/ampere meter). To understand what causes the force, we can think of the first pole generating a magnetic field, H, which in turn exerts a force on the second pole. So

$$\vec{F} = \left(\frac{p_1}{r^2}\right) p_2 = \vec{H} p_2 \qquad \text{(cgs)} \qquad (2.3)$$

giving, by definition,

$$\vec{H} = \frac{p}{r^2} \quad \text{(cgs)} \qquad \text{and} \qquad \vec{H} = \frac{p}{4\pi\mu_0 r^2} \quad \text{(SI)} \qquad (2.4)$$
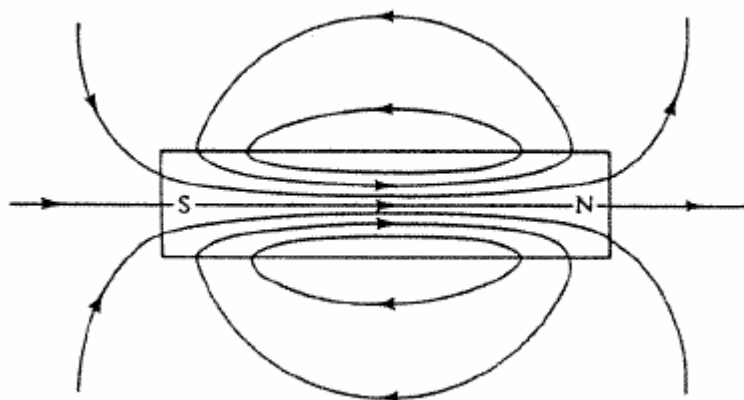
Figure 2.1 Magnetic field lines in a bar magnet [12].

So, a field of strength is one, which exerts a force of one dyne on a unit pole. By convention, the North Pole is the *source* of magnetic field, and the South Pole is the *sink,* it can be seen in Fig. 2.1. The units of magnetic field strength are oersteds (Oe) in cgs units and ampere/meter (A/m) in SI units; 1 Oe = $(1000/4\pi)$ A/m. The symbol H denotes the magnetic field strength and is called simply magnetic field.

2.2 MAGNETIC FLUX

The conveying of field of magnetic pole to a distant place by something called as a *magnetic flux,* ϕ. Rigorously the flux is defined the surface integral of the normal component of the magnetic field. This means that the amount of flux passing through unit area perpendicular to the field is equal to the field strength. So the field strength is equal to amount of flux per unit area,

$$\phi = HA \quad \text{(cgs)} \qquad \text{and} \qquad \phi = \mu_0 HA \quad \text{(SI)} \qquad (2.5)$$

and units of it are oersted.cm^2 (maxwell) in cgs units and weber in SI units. Magnetic flux is important because a changing flux generates an electric current in any circuit, which it intersects. In fact we define the 'electromotive force', ε, equal to the rate of change of the flux linked with the circuit:

$$\varepsilon = -\frac{d\phi}{dt}.$$ (2.6)

The above equation is known as Faraday's law of electromagnetic induction. The minus sign in Eqn 2.6 shows that the current sets up a magnetic field that acts in the opposite direction to the magnetic flux (This is known as Lenz's law).

2.3 MAGNETIC MOMENT

Next we need to introduce the concept of magnetic moment, which is moment of dipole of couple exerted on either a bar magnet or a current loop when it is in an external field. Again we can define the magnetic moment either in terms of poles, or in terms of currents.
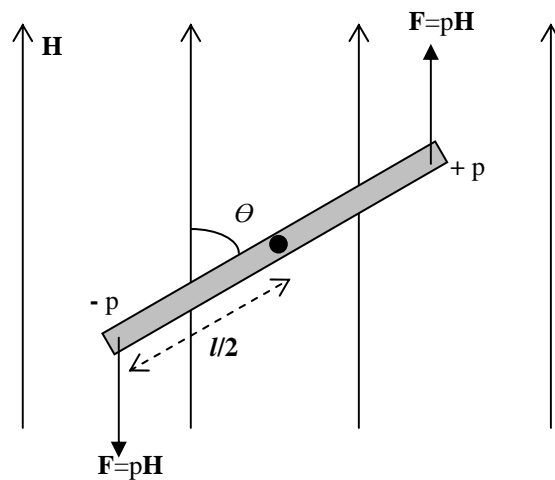
Figure 2.2 Bar magnet in a uniform field [1].

Imagine a bar magnet is at an angle Θ to a magnetic field, **H**, as shown in Fig 2.2. The force on each pole is $\boldsymbol{F} = p\boldsymbol{H}$. So, the moment acting on the magnet, which is just the force times the perpendicular distance from the center of mass, is

$$pH\sin\theta\frac{l}{2} + pH\sin\theta\frac{l}{2} = plH\sin\theta$$ (2.7)

When H = 1 Oe and $\theta = 90°$, the moment is given by

$$\vec{m} = pl \qquad . \qquad\qquad\qquad (2.8)$$

where **m** is the *magnetic moment* of the magnet.

Alternatively, if we want to explain the magnetic moment in terms of currents then we can look at the current loop in a uniform magnetic field like in the following Fig. 2.3. A rectangular loop carrying a current I is placed in a medium with a uniform magnetic induction or magnetic flux density which is denoted by a symbol of B. Both magnetic field strength H and magnetic induction B are called simply magnetic field and the difference between them will be explained below (Fig. 2.3 (a)). No magnetic force acts on sides 1 and 3 because those wires are parallel to the field.

(a)

(b)
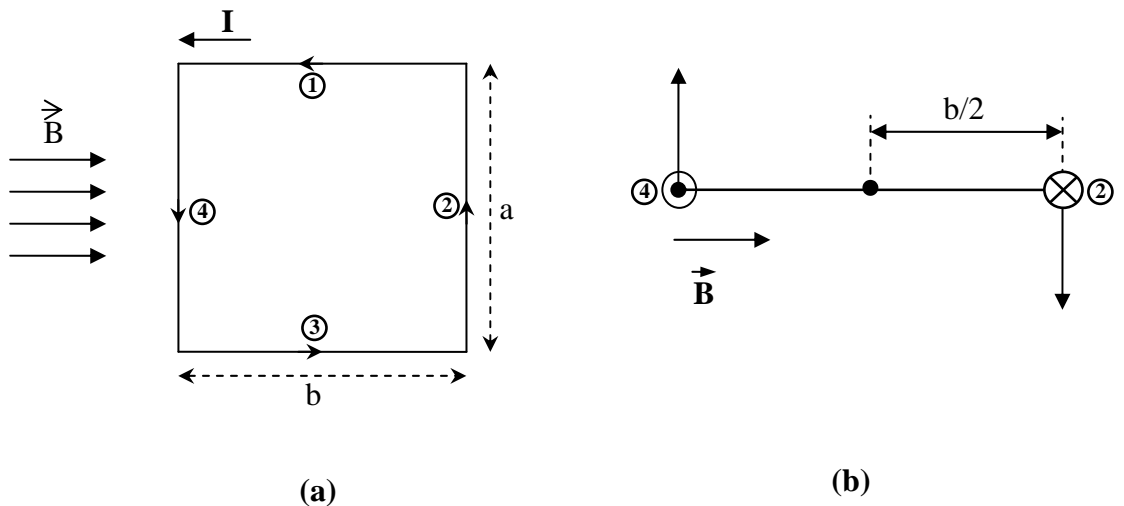
Figure 2.3 (a) Overhead view of rectangular current loop in a uniform magnetic field, which is parallel to sides 1 and 3 and perpendicular to sides 2 and 4, **(b)** edge view of loop [13].

However, magnetic forces do act on sides 2 and 4 because these sides are oriented perpendicular to the field. The magnitude of forces is from a well-known equation of magnetic force acting on a current carrying conductor, as follows

$$F_2 = F_4 = IaB . \qquad\qquad\qquad (2.9)$$

Note that the two forces point in opposite directions but are not directed along the same line of action as in the Fig. 2.3. (b). If the loop is pivoted so that it can rotate about point O, these two forces produce a torque about O that rotates the loop in the clock-wise direction. The magnitude of this Torque $\vec{\tau}_{max}$ is

$$\tau_{max} = F_2 \frac{b}{2} + F_4 \frac{b}{2} = (IaB)\frac{b}{2} + (IaB)\frac{b}{2} = IabB, \tag{2.10}$$

where moment arm about O is b/2 for each force. Because the area enclosed by the loop is A= a .b, then we can express the maximum torque as

$$\vec{\tau}_{max} = IAB. \tag{2.11}$$

Remember that this maximum resultant torque is valid only when the magnetic field is parallel to the plane of the loop. Now let us suppose that the magnetic field makes an angle $\theta < 90^o$ with a line perpendicular to the plane of the loop as shown in Fig. 2.4. Note that the moment arm of F_1 about the point O is equal to $(a/2)\sin\theta$ as the moment arm F_3. Because $F_1 = F_3 = IbB$, the net torque about O has the magnitude

$$\vec{\tau}_{max} = F_1 \frac{a}{2} Sin\theta + F_3 \frac{a}{2}\sin\theta = IbB\left(\frac{a}{2}Sin\theta\right) + IbB\left(\frac{a}{2}Sin\theta\right) = IabBSin\theta$$

$$\vec{\tau}_{max} = IABSin\theta \tag{2.12}$$

where $A = ab$ is the area of a rectangular loop.

A convenient expression for the torque exerted on a loop placed in a uniform magnetic field B is

$$\vec{\tau}_{max} = I\vec{A} \times \vec{B} \tag{2.13}$$
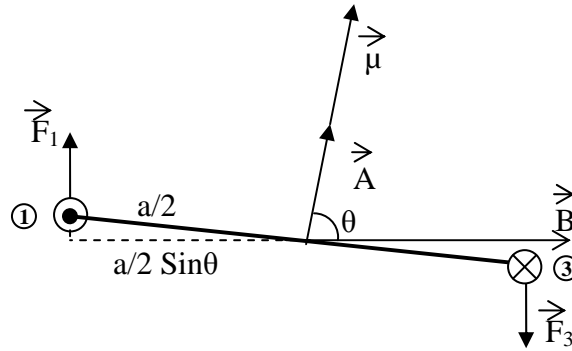
Figure 2.4 Edge view of the loop sighting downsides [13].

where **A**, the vector shown in Fig. 2.4, is perpendicular to the plane of the loop has a magnitude equal to the area of the loop. The direction of **A** is determined by using right hand rule. The product I**A** is defined to be the magnetic dipole moment **m,** (often simply called "magnetic moment") of the loop [13]:

$$\vec{m} = I\vec{A} \tag{2.14}$$

The SI unit of the magnetic dipole moment is ampere-meter^2 (A.m^2). By using the Eqn. 2.13 and 2.14, we can express the torque in terms of magnetic moment as follows:

$$\vec{\tau} = \vec{m} \times \vec{B}. \tag{2.15}$$

In this sense it will be better to examine the potential energy of dipole moment in a uniform magnetic field. Returning to Fig. 2.2, the energy of magnetic dipole is defined to be zero when the dipole is perpendicular to magnetic field. So the work done (in ergs) in turning through an angle $d\theta$ against the field is

$$dE = 2(pH \sin\theta)\frac{l}{2}d\theta = mH \sin\theta d\theta \tag{2.16}$$

and the energy of dipole at an angle θ to a magnetic field is

$$E = \int_{\pi/2}^{\theta} mH \sin\theta d\theta = -mH \cos\theta = -\vec{m}\cdot\vec{H} \tag{2.17}$$

This energy expression is in cgs units and it can be expressed in SI units as

$$E = -\mu_0\vec{m}\cdot\vec{H} \ , \tag{2.18}$$

where μ_0 is the permeability of free space.

2.4 MAGNETIC MOMENT OF ELECTRONS

There are two kinds of electron motion, orbital and spin, and each has magnetic moment associated with it.

The orbital motion of an electron around the nucleus constitutes a tiny current loop (because it is a moving charge), and the magnetic moment of electron is associated with this orbital motion. Consider an electron moving in a constant speed V in a circular orbit of radius r about the nucleus as shown Fig. 2.5. Because the electron travels the distance of $2\pi r$ (the circumstance of circle) in a period T, it's orbital speed is $v = 2\pi r/T$. The current I associated with this orbiting electron is its charge e divided by T. using T=$2\pi r/v$, we have

$$I = \frac{e}{T} = \frac{ev}{2\pi r} \tag{2.19}$$

The magnetic moment associated with this current loop is equal to current times area of the loop from Eq. 2.14, where $A = \pi r^2$ is the area enclosed by the orbit. Therefore we can write

$$\mu = IA = \left(\frac{ev}{2\pi r}\right)\pi r^2 = \frac{1}{2}evr \ . \tag{2.20}$$
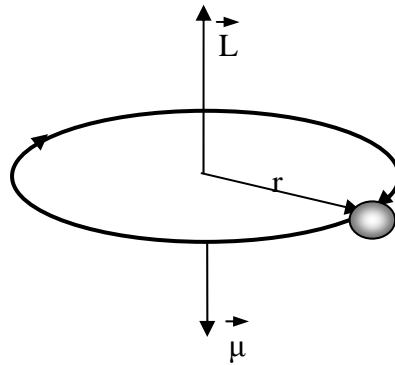
Figure 2.5 An electron moving in a circular orbit of radius r has angular momentum L in one direction and a magnetic moment μ in the opposite direction [12].

(here μ is the electronic or atomic magnetic moment). Because the magnitude of angular momentum of electron is $L = m_e vr$ the magnetic moment can be expressed as

$$\mu = \gamma L \tag{2.21}$$

where γ is the proportionality constant and called as gyromagnetic ratio$\left(\gamma = \dfrac{e}{2m_e}\right)$ [1].

An additional assumption of Bohr theory was angular momentum of the electron must be integral multiple of $\hbar$ (which is equal to $\dfrac{h}{2\pi}$) where h is Planck's constant. Therefore,

$$m_e vr = n\hbar \ . \tag{2.22}$$

Combining Eqs. 2.20 and 2.22, we have

$$\mu(orbit) = \frac{e\hbar}{2m_e} \qquad (2.23)$$

for the magnetic moment of electron in the first ($n = 1$) Bohr orbit.

The electron behaves as if it were spinning about its own axis, as well as moving in an orbit about the nucleus, associated with the spin are definite amounts of magnetic moment and angular momentum. It is found experimentally and theoretically that the magnetic moment due to electron's spin is equal to

$$\mu(spin) = \frac{e\hbar}{2m_e} = 0.927 \times 10^{-20} \, erg \, / \, Oe. \qquad (2.24)$$

Thus the magnetic moment due to spin and that due to motion in the first Bohr orbit are exactly equal. Because it is such a fundamental quantity, this amount of magnetic moment is given a special symbol μ_B and a special name, the *Bohr Magneton* [12]. Thus,

$$\mu_B = 0.927 \times 10^{-20} \, erg \, / \, Oe. \qquad (2.25)$$

2.5 MAGNETIZATION AND FIELD

The quantity of the magnetic moment per unit volume describes the extent to which the magnets are magnetized. It is called the *intensity of magnetization*, or simply the *magnetization* as follows,

$$\vec{M} = \frac{\vec{\mu}}{v}, \qquad (2.26)$$

where v is the volume.

In free space (vacuum) there is no magnetization. The magnetic field can be described by the vector fields **B** and **H** which are linearly related by

$$\vec{B} = \mu_0 \vec{H} \tag{2.27}$$

The magnetic fields **B** has unit of Tesla (T). In a magnetic solid the relation between **B** and **H** is more complicated and the two vector fields may be very different in magnitude and direction. The general relationship is

$$\vec{B} = \mu_0 (\vec{H} + \vec{M}) \tag{2.28}$$

In the special case that the magnetization **M** is linearly related to the magnetic field **H**, and we write

$$\vec{M} = \chi \vec{H} \tag{2.29}$$

where χ is dimensionless quantity called the magnetic susceptibility and we can rewrite the Eq. 2.28 as follows

$$\vec{B} = \mu_0 (1 + \chi) \vec{H} = \mu_0 \mu_r \vec{H} \tag{2.30}$$

where $\mu_r = 1 + \chi$ is the relative permeability of the material. We can now characterize the magnetic behavior of various kinds of substances by their corresponding values of χ and μ_r (The classification will be studied later with more detail):

1. Empty space: $\chi = 0$, since there is no matter to magnetize, and $\mu_r = 1$

2. Diamagnetic. χ is small and negative, and μ_r slightly less than 1

3. Paramagnetic and antiferromagnetic: χ is small and positive, and μ_r slightly greater than 1

4. Ferromagnetic and ferrimagnetic: χ and μ_r are large and positive [1].

2.6 THE HYSTERESIS LOOP AND MAGNETIC PROPERTIES

A great deal of information can be learned about the magnetic properties of a material by studying its hysteresis loop. A hysteresis loop shows the relationship between the induced magnetic flux density **B** and the magnetic field strength **H** (magnetizing force field). It is often referred to as the B-H loop. An example for the hysteresis loop is shown below.

The loop is generated by measuring the magnetic flux **B** of a ferromagnetic material while the magnetizing force **H** is changed. A ferromagnetic material that has never been previously magnetized or has been thoroughly demagnetized will follow the dashed line as **H** is increased. As the line demonstrates, the greater the amount of current applied **(H+)**, the stronger the magnetic field in the component **(B+)**. At point "a" almost all of the magnetic domains are aligned and an additional increase in the magnetizing force will produce very little increase in magnetic flux. The material has reached the point of magnetic saturation. When **H** is reduced back down to zero, the curve will move from point "a" to point "b." At this point, it can be seen that some magnetic flux remains in the material even though the magnetizing force is zero. This is referred to as the point of retentivity on the graph and indicates the remanence or level of residual magnetism in the material. (Some of the magnetic domains remain aligned but some have lost their alignment.)
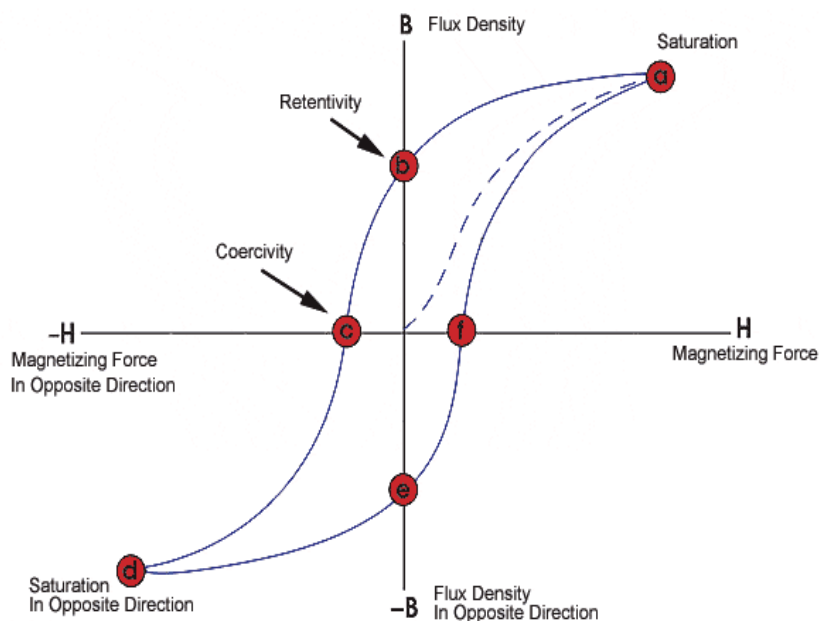
Figure 2.6 Sample hysteresis loop for a ferromagnet [1].

As the magnetizing force is reversed, the curve moves to point "c", where the flux has been reduced to zero. This is called the point of coercivity on the curve. (The reversed magnetizing force has flipped enough of the domains so that the net flux within the material is zero.) The force required to remove the residual magnetism from the material, is called the coercive force or coercivity of the material.

As the magnetizing force is increased in the negative direction, the material will again become magnetically saturated but in the opposite direction (point "d"). Reducing **H** to zero brings the curve to point "e". It will have a level of residual magnetism equal to that achieved in the other direction. Increasing **H** back in the positive direction will return **B** to zero. Notice that the curve did not return to the origin of the graph because some force is required to remove the residual magnetism. The curve will take a different path from point "f" back the saturation point where it with complete loop.

From the hysteresis loop, a number of primary magnetic properties of a material can be determined.

1. *Retentivity* - A measure of the residual flux density corresponding to the saturation induction of a magnetic material. In other words, it is a material's ability to retain a certain amount of residual magnetic field when the magnetizing force is removed after achieving saturation. (The value of **B** at point B on the hysteresis curve.)

2. *Residual Magnetism* or *Residual Flux* - the magnetic flux density that remains in a material when the magnetizing force is zero. Note that residual magnetism and retentivity are the same when the material has been magnetized to the saturation point. However, the level of residual magnetism may be lower than the retentivity value when the magnetizing force did not reach the saturation level.

3. *Coercive Force* - The amount of reverse magnetic field which must be applied to a magnetic material to make the magnetic flux return to zero. (The value of **H** at point "c" on the hysteresis curve.)
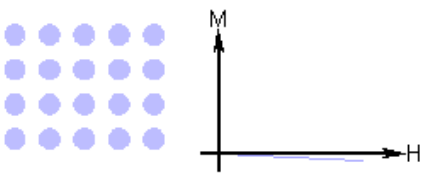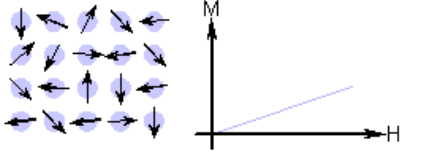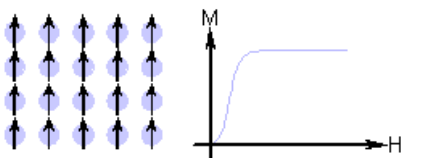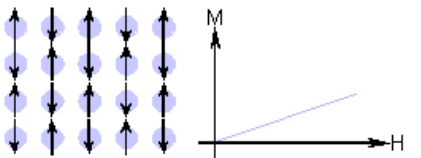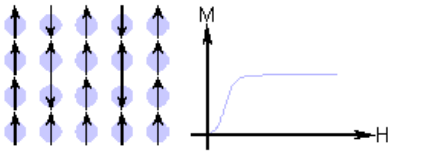
2.7 CLASIFICATION OF MAGNETIC MATERIALS

Materials are classified by their response to an externally applied magnetic field. Descriptions of orientations of the magnetic moments in a material help to identify different forms of magnetism observed in nature (Table 2.1). Five basic types of magnetism can be described: diamagnetism, paramagnetism, ferromagnetism, antiferromagnetism and ferrimagnetism.

In the presence of an externally applied magnetic field the atomic current loops created by the orbital motion of electrons respond to oppose the applied field. All materials display this type of weak repulsion to a magnetic field known as ***diamagnetism***. However, diamagnetism is very weak and therefore any other form of magnetic behavior that a material may possess usually over-powers the effects of the current loops. In terms of electronic configurations of materials, diamagnetism is observed in materials with filled electronic sub-shells where the magnetic moments are paired and overall cancel each other. Diamagnetic materials have a negative susceptibility ($\chi < 0$) and weakly repel an applied magnetic field. The effect of these atomic current loops overcomes if the material displays a net magnetic moment or has long-range ordering of magnetic moments [14].

All of the other types of magnetic behaviors observed in materials are at least partially attributed to unpaired electrons in atomic shells, often in the 3d or 4f shells of each atom. Materials whose atomic magnetic moments are uncoupled display ***paramagnetism***. Therefore, paramagnetic materials` moments have no long-range order. A generalized description of paramagnetism is enhancement of the magnetic flux density as a result of each atom carries a magnetic moment, which partially aligns in an applied magnetic field. The field acts independently on each atomic dipole. Hence, there is no long-range order and there is a small positive magnetic susceptibility ($\chi < 0$)[15]. Materials that possess **f*erromagnetism*** have aligned atomic magnetic moments of equal magnitude and their crystalline structure allows for direct coupling interactions between the moments, which may strongly enhance the flux density. Furthermore, the aligned moments in ferromagnetic materials can confer a spontaneous magnetization in the absence of an applied magnetic field.

Table 2.1: Summary of different types of magnetic behavior [16].

Type of Magnetism	Susceptibility	Atomic Behavior	Magnetic Behavior
Diamagnetism	Small & Negative Au...... -2.74×10^{-6} Cu.......-0.77×10^{-6}	Atoms have no magnetic moment	
Paramagnetism	Small & Positive β-Sn.... 0.19×10^{-6} Pt........21.04×10^{-6} Mn.....66.10×10^{-6}	Atoms have randomly oriented magnetic moments	
Ferromagnetism	Large & positive, function of applied field, microstructure dependent Fe....... ~100,000	Atoms have parallel aligned magnetic moments	
Antiferromagnetism	Small & positive Cr.........3.6×10^{-6}	Atoms have mixed parallel and anti-parallel aligned magnetic moments	
Ferrimagnetism	Large & positive, function of applied field, microstructure dependent Ba ferrite.......~3	Atoms have anti-parallel aligned magnetic moments	

Materials that retain permanent magnetization in the absence of an applied field are known as hard magnets. Materials having atomic magnetic moments of equal magnitude are arranged in an antiparallel fashion display ***antiferromagnetism***. The exchange interaction couples the moments such that they are antiparallel hence leaving

a zero net magnetization [17]. Above the Néel temperature (T_N), thermal energy is sufficient to cause the equal and oppositely aligned atomic moments to randomly fluctuate leading to a disappearance of their long-range order. In this state the material exhibits paramagnetic behavior. ***Ferrimagnetism*** is similar to antiferromagnetism in that two different sub-lattices exist and antiferromagnetic exchange interactions occur. However, the magnitudes of the two different types of moments, arranged antiparallel, are not equal in magnitude and hence a net magnetization is produced.

2.8 THEORY OF FERROMAGNETISM AND FERRIMAGNETISM

Weiss first developed the molecular theory of ferromagnetism in the early 1900s, which sufficed as a semi-quantitative description. The theory is based on the assumption that each atomic dipole is subject to a local field that is proportional to the magnetization summed over all the other dipoles in the material [14, 17, 18,19].

Later, the development of quantum mechanics led to the concept of exchange interactions between two atoms and spin-dependent Coulombic interactions. The spin exchange interaction is derived from the Pauli exclusion principles, where antiparallel spin arrangements in an atomic shell are forbidden [20]. The exchange interaction is essentially the difference in Coulombic energies for different spin configurations in a sample [19]. Above a certain temperature, known as the Curie temperature (T_C), the alignment of the moments in ferromagnetic and ferrimagnetic materials is lost due to thermal energy and the material displays paramagnetic behavior.

Ferrimagnetism is similar to antiferromagnetism since the spin arrangements are antiparallel; however the sub-lattice magnetic moments are of unequal magnitude and therefore produce a net magnetization in an applied field. The net magnetization observed in ferrimagnetic materials is typically lower than that of ferromagnetic materials primarily because of the antiparallel spin arrangement in the former. Despite the differences in moment alignments, the theories that describe ferromagnetism can be applied to ferrimagnetism with modifications to account for the existence of the sub-lattice interactions and antiparallel orientations of spins.

The ferrimagnetic crystalline structure is comprised of two different magnetic ions occupying two kinds of lattice sites, tetrahedral (A) and octahedral (B) [18, 19, 21]. For spinel crystalline structures, such as magnetite, surprisingly all of the exchange interactions (AA, AB and BB) favor antiparallel alignment. The ferrimagnetic behavior is due to the strong AB interaction. The favorable A antiparallel B interaction induces all of the A spins to parallel arrangements and all of the B spins parallel with each other [18]. Some ferromagnetic and ferrimagnetic materials possess spontaneous magnetization and are referred to as permanent magnets. However, most ferromagnetic and ferrimagnetic materials are unmagnetized until an external magnetic field is applied. In the early 1900s, Weiss developed the theory of magnetic domains to explain the lack of large demagnetization forces, which result if the entire ferromagnetic material is uniformly magnetized throughout [22].

CHAPTER 3

MAGNETISM OF NANOPARTICLES

The aligned spin arrangements in ferromagnetic, antiferromagnetic and ferrimagnetic materials are subdivided into regions (domains) throughout the bulk material. The boundary between two neighboring domains is a domain wall, which consists of a rotation of the direction of the magnetic moment between discrete domains (Figure 3.1) [18]. The formation of domains is a process driven by the balance between the magnetostatic energy and the domain wall energy. The magnetostatic energy increases proportionally to the volume of the material, while the domain wall energy increases proportionally to the surface area. If the sample size is reduced, these points intuitively to the existence of a critical volume below which the reduction of the magnetostatic energy becomes less than the minimum energy required to form a domain wall. Consequently, below this size a ferromagnetic material exists as a *single-domain* particle. This means that the particle is in a state of *uniform magnetization*.
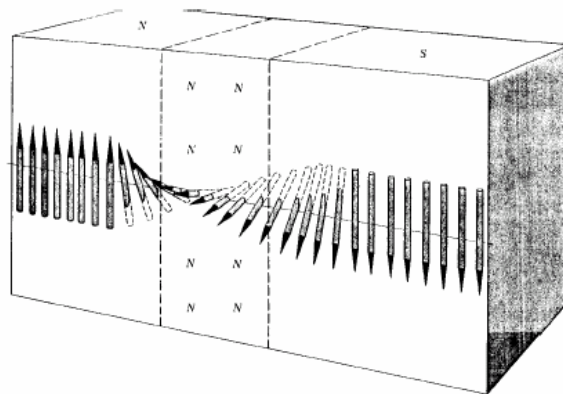
Figure 3.1 Domain wall [18].

The constituent spins, at temperatures well below the Curie temperature, rotate in unison. The exchange energy is strong enough to hold all spins tightly parallel to each

other and determines the value of the particle magnetic moment, while its direction is determined by the total anisotropy energy. The typical size of a single-domain particle is in the order of a few tens of nanometers depending on the material and contributions from various anisotropy energy terms. Therefore, it can be concluded that single domain particles are in general not isotropic, but they will have anisotropic contributions to their total energy associated with their external shape, the magnetocrystalline structure itself and the imposed stress.

In principle, single-domain particles must reverse their magnetization by coherent spin rotation. This is a comparatively difficult process, if the particle has a significant magnetic anisotropy. Consequently, single-domain particles are expected have a high coercivity, which is the basis of most of their applications. This (non thermal) magnetization reversal mechanism was first studied by Stoner and Wohlfarth in 1948 [23]. Neel predicted that at nonzero temperature the magnetization can overcome the energy barrier as a result of thermal agitation [24]. Later, Brown derived the Fokker-Planck equation for the probability distribution of spin orientations, starting from the stochastic Landau-Lifshitz equation, and calculated approximate expression for the relaxation time of particles with uniaxial anisotropy [25]. Theoretically most well studied systems are noninteracting classical spins (representing the magnetization of the nanoparticles) with axially symmetric magnetic anisotropy.
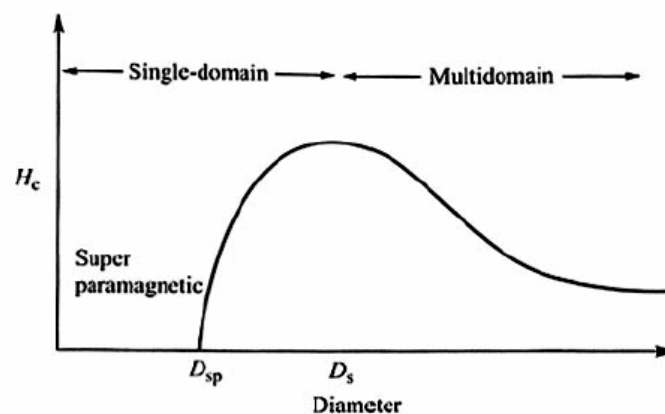
Figure 3.2 Coercivity as a function of particle size, where D_{SP} is the superparamagnetic size and D_S is the single domain particle size [17].

Frenkel and Dorfman first formulated theorizes regarding the single domain nature of particles below a critical diameter in 1930 [26]. In this critical size range the

nanoparticles are single domain materials (Figure 3.2). In the presence of an applied magnetic field, the spin's orientation and subsequent magnetic saturation is achieved with lower field strengths than with the analogous bulk materials. The magnetic moment of each particle is ~105 times larger than for transition metal ions and saturation magnetization is reached at applied magnetic fields as low as 1 kOe [27]. When the field is decreased, demagnetization is dependent on coherent rotation of the spins, which results in large coercive forces [28]. The large coercive force in single domain particles is due to magnetocrystalline and shape anisotropies for nonspherical particles. As the single domain particles' size decrease, the coercive force decrease (Figure 3.2).

Moreover, the shape anisotropy increases as the aspect ratio of a particle increases. Therefore, elongated single-domain particles can display large coercive forces [29, 30].

3.1 SUPERPARAMAGNETISM

The magnetic anisotropy, which keeps a particle magnetized in specific direction, is generally proportional to the volume of a particle [31]. As the size of the particle decreases, the energy associated with the uniaxial anisotropy (K) decreases until thermal energy is sufficient to overcome any preferential orientation of the moment in the particle.

a   b   c
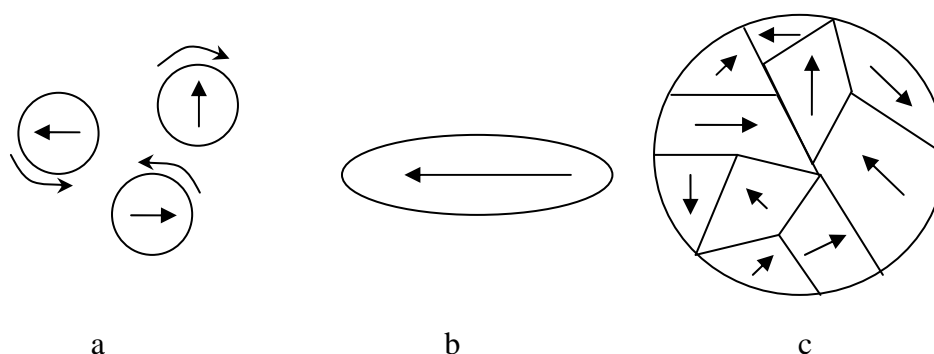
Figure 3.3 Domain structures observed in magnetic particles: a) superparamagnetic; b) single domain particle; c) multi-domain particle [29].

A single domain particle that reaches magnetization equilibrium at experimental temperatures in short times relative to the measurement time is commonly referred to as *superparamagnetic*. (Figure 3.3 a) [29]. The uniformly magnetized single domain structure and the multi domain particle can be seen in Figure 3.3 b and c.

3.2 MAGNETIC RELAXATION IN SUPERPARAMAGNETIC PARTICLES

When placed in an external magnetic field the magnetic moments of these particles align in the direction of the field via moment and particle rotation. When the field is removed the frequency of thermally activated reversals is given by

$$f = f_o e^{-\frac{E}{kT}} \tag{3.1}$$

where f_o is the "attempt frequency" which is approximately 10^9 s^{-1}. Conceptually, the frequency is the rate at which the particles approach thermal equilibrium [32]. For relaxation times of ~100 seconds the critical energy barrier is

$$\Delta E_{crit} = \ln(tf_o)kT = 25kT \tag{3.2}$$

for thermal equilibrations. The condition for superparamagnetism is observed when a particle with uniaxial anisotropy displays zero coercive force as mathematically defined by

$$KV = 25kT \tag{3.3}$$

where K is the effective magnetic anisotropy energy constant (a function of the magnetocrystalline, shape and surface anisotropies), V is the volume of the particle and kT is the thermal energy [17, 32]. Particles with relaxation times greater than 100 seconds or with diameters larger than the critical values (Figure 3.2) are called blocked [17, 18, 33]. The **blocking temperature** (T$_B$) of a material is given by

$$T_B = \frac{KV}{25k} . \tag{3.4}$$

Below T_B the anisotropy of the particle blocks the free movement of the moment [17]. Above the T_B the moment is free to align in an applied magnetic field and appears superparamagnetic.

In an applied field at temperature T, assuming the particles' moments have achieved some level of thermal equilibrium, there will be a Boltzmann distribution of moments aligned in the direction of the applied field. This relation is essentially the case prescribed for classical paramagnetism, where the degree of orientation is given by the Langevin function

$$m_{av} = m(\coth \alpha - \frac{1}{\alpha}) \qquad \text{where} \qquad \alpha = \frac{mH}{kT} \qquad (3.5)$$

where m_{av} is the average magnetic moment, k is Boltzmann's constant and T is the absolute temperature [29]. The fundamental difference is that the moment is a single atom in the paramagnetic case, whereas the moment is considered as a single domain particle, which contains more than 105 atoms coupled ferro- or ferrimagnetically in the superparamagnetic case [34]. The term superparamagnetism originates from this relation. The magnetization of an individual superparamagnetic particle is given by $M = nm_{av}$, where n is the number of particles per volume.

The defining factor between single domain and superparamagnetic particles is essentially the relaxation time relative to the experimental time. The superparamagnetic nature of the nanoparticles is derived from the randomization of aligned spins governed by Brownian motion and Néel rotation when the gradient field is removed. Brownian motion and Néel rotation are magnetic relaxation mechanisms due to particle and spin rotation, respectively. Brownian relaxation is achieved via bulk rotational diffusion of the particles in a fluid. The relaxation time for Brownian motion is given by

$$\tau_B = \frac{3V'\eta}{kT} \qquad (3.6)$$

where V' is the hydrodynamic volume of the particle, η is the dynamic viscosity, k is Boltzmann.s constant and T is the absolute temperature. Néel relaxation (Eq. 3.7) is attributed to the rotation of the magnetization vector or moment in the particle with a relaxation time given by

$$\tau_N = \tau_O \exp\left(\frac{\Delta E}{kT}\right) \qquad \text{where} \qquad \Delta E = KV(1 - h^2) \qquad (3.7)$$

τ_O is typically estimated to be 10^{-9} s, ΔE is the energy barrier assuming uniaxial on interacting particles, h = H/H_K is the reduced magnetic field and H_K is the internal magnetic field due to anisotropy [33]. Experimental conditions for superparamagnetism are

1) relaxation times faster than the measurement times (commonly ~100 s),
2) the magnetization curve does not display hysteresis.

3.3 HAMILTONIAN OF FERROMAGNETIC SYSTEM

The Hamiltonian of a single isolated nanoparticle consists of the Zeeman energy (which is the interaction energy between the magnetic moment and an external field) and the magnetic anisotropy (which creates preferential directions of the magnetic moment orientation). In the system, the nanoparticles are supposed to be well separated by a nonmagnetic medium (i.e., a ferrofluid in which the particle are coated with a surfactant and particle dispersed in a diamagnetic medium). The only relevant interparticle interaction mechanism is therefore the dipole-dipole interaction. By using the thermodynamic relations, magnetic field H, magnetic moment μ, temperature T and Helmholtz free energy F dependent Gibbs free energy G(H,T) is introduced to characterize the states of magnetic system. The energy of intermediate states can be characterized by Landau free energy G_L with below equation:

$$G_L(\vec{\mu}; \vec{H}, T) = F - \mu_O \vec{\mu} \cdot \vec{H} . \qquad (3.8)$$

The G_L means that the spin relaxation time over which individual elementary volumes reach thermal equilibrium with respect to the given local value of the magnetization that is shorter than the time over which the system as a whole approaches equilibrium through time changes of magnetization.

For ferromagnetic systems there are four important contributions to the Landau free energy of a ferromagnetic body: the exchange energy, the magnetocrystalline anisotropy energy, the magnetostatic energy and the Zeeman energy in an external field [35]. Another contribution, magnetoelastic energy, which arises from magnetostriction, is omitted for two reasons. When a ferromagnet is magnetized it shrinks (or expands) in the direction of the magnetization. As a result, the volume and the saturation magnetization changes are defined as the magnetic moment in saturation per unit volume. However, in micromagnetics it is a basic assumption, that the saturation magnetization remains constant. Secondly, a large part of the internal magnetostriction in a ferromagnetic crystal can be expressed in the same mathematical form as magnetocrystalline anisotropy. If the anisotropy constants are taken from experiment as in our case, the effect of magnetostriction is already included, and therefore we do not have to consider it in an additional energy term.

3.3.1 The exchange interaction energy

Electrons in neighboring orbitals in certain crystals move according to each other's spin states. In order to avoid sharing the same orbital with the same spin (hence having the same quantum numbers - not allowed from Pauli's exclusion principle), electronic spins in such crystals act in a coordinated fashion. They will be either aligned parallel or antiparallel according to the details of the interaction. To understand the origin of the exchange interaction, consider the Hamiltonian for a 2-electron system

$$H = \frac{p_1^2}{2m} + \frac{p_2^2}{2m} - \left(\frac{Ze^2}{r_1}\right) - \left(\frac{Ze^2}{r_2}\right) + \left(\frac{e^2}{|\vec{r}_1 - \vec{r}_2|}\right) = H_1 + H_2 + V_{12} \qquad (3.9)$$

where p_1 and p_2 are momentums of first and the second electron, Z atomic number, e elementary charge, r_1 and r_2 are position vectors of first and the second electron, and here

$$H_1 = \frac{p_1^2}{2m} - \left(\frac{Ze^2}{r_1} \right) \qquad \text{and} \qquad H_2 = \frac{p_1^2}{2m} - \left(\frac{Ze^2}{r_2} \right) \qquad (3.10\text{-}11)$$

$$V_{12} = \frac{e^2}{\left| \vec{r}_1 - \vec{r}_2 \right|} \, . \qquad (3.12)$$

The one-electron Hamiltonians H_1 and H_2 can be solved directly, on the other hand, the interaction term V_{12} expresses the Coulomb repulsion between the two electrons and cannot be simply written in terms of the one-electron wavefunctions which diagonalize H_1 and H_2. The Coulomb energy would be found approximately by perturbation theory using for our unperturbed states the eigenfunctions of H_1 and H_2 which are written as $\psi_1(\vec{r}_1)$ and $\psi_2(\vec{r}_2)$. We thus write the so-called Coulomb energy

$$E_{12} = \int \psi_1^*(\vec{r}_1) \psi_2^*(\vec{r}_2) \left(\frac{e^2}{\left| \vec{r}_1 - \vec{r}_2 \right|} \right) \psi_1(\vec{r}_1) \psi_2(\vec{r}_2) d^3 r_1 d^3 r_2 \qquad (3.13)$$

Table 3.1 Allowed combinations of the exchange symmetries

of the spatial and spin wave functions of electrons.

$\psi_{spatial}$	φ_{spin}
symmetric	anti-symmetric (S = 0)
anti-symmetric	symmetric (S = 1)

This Coulomb energy term is for 2-electron system which are identical and indistinguishable. We are also required to satisfy the Pauli Exclusion Principle which states that the 2-electron wave function must be totally antisymmetric under the interchange of the 2 electrons as in Table 3.1 (this is equivalent to saying that we cannot put two electrons in exactly the same state). In writing the wave function for an electronic system, we normally write the total wave function as a product of a spatial wave function with a spin function. In this situation, we have two options in making an antisymmetric state:

Table 3.2 Spin and spatial wave functions for a two-electron atom where the (1) and (2) refer to r_1 and r_2 for electrons 1 and 2 and the subscript on ψ refers to the quantum numbers labeling the one-electron eigen-states of the unperturbed Hamiltonians H_1 and H_2.

$S = S_1 + S_2$	Ms	φ_{spin}	$\psi_{spatial}$
0	0	$\frac{1}{\sqrt{2}}[\alpha(1)\beta(2) - \beta(1)\alpha(2)]$	$\frac{1}{\sqrt{2}}[\psi_1(1)\psi_2(2) + \psi_1(2)\psi_2(1)]$
1	1	$\alpha(1)\alpha(2)$	$\frac{1}{\sqrt{2}}[\psi_1(1)\psi_2(2) - \psi_1(2)\psi_2(1)]$
	0	$\frac{1}{\sqrt{2}}[\alpha(1)\beta(2) + \beta(1)\alpha(2)]$	
	-1	$\beta(1)\beta(2)$	

The above Coulomb energy term can be found by computing the expectation value of the Coulomb repulsion Hamiltonian:

$$E_{12} = \int\int \psi_{spatial}^* \frac{e^2}{|\vec{r}_1 - \vec{r}_2|} \psi_{spatial} d^3r_1 d^3r_2 \qquad (3.14)$$

The spin wave functions do not appear here because the Hamiltonian does not affect the spin directly, and so the spin wave functions just integrate out to unity.
By inserting spatial from Table 3.2, we find:

$$E_{12} = \frac{1}{2}\int\int [\psi_1^*(1)\psi_2^*(2) \pm \psi_1^*(2)\psi_2^*(1)]V_{12}[\psi_1(1)\psi_2(2) \pm \psi_1(2)\psi_2(1)]d^3r_1 d^3r_2$$

$$(3.15)$$

where the + sign applies for singlet states and the - sign for triplets. This breaks into four terms:

$$E_{12} = \frac{1}{2}\int\int \psi_1^*(1)\psi_2^*(2)\left(\frac{e^2}{|\vec{r}_1 - \vec{r}_2|}\right)\psi_1(1)\psi_2(2)d^3$$

$$+\frac{1}{2}\int\int\psi_1^*(2)\psi_2^*(1)\left(\frac{e^2}{|\vec{r}_1-\vec{r}_2|}\right)\psi_1(2)\psi_2(1)d^3r_1d^3r_2$$

$$\pm\frac{1}{2}\int\int\psi_1^*(1)\psi_2^*(2)\left(\frac{e^2}{|\vec{r}_1-\vec{r}_2|}\right)\psi_1(2)\psi_2(1)d^3r_1d^3r_2 \tag{3.16}$$

$$\pm\frac{1}{2}\int\int\psi_1^*(2)\psi_2^*(1)\left(\frac{e^2}{|\vec{r}_1-\vec{r}_2|}\right)\psi_1(1)\psi_2(2)d^3r_1d^3r_2$$

The first two terms are identical, as are the third and fourth. We therefore obtain:

$$E_{12}=C_{12}\pm J_{12} \tag{3.17}$$

where the + sign is for singlets and the - sign is for triplets. C_{12} is the direct Coulomb energy given by:

$$C_{12}=\int\psi_1^*(1)\psi_2^*(2)\left[\frac{e^2}{\vec{r}_1-\vec{r}_2}\right]\psi_1(1)\psi_2(2)d^3r_1d^3r_2 \tag{3.18}$$

and J_{12} is the exchange Coulomb energy given by

$$J_{12}=\int\psi_1^*(1)\psi_2^*(2)\left[\frac{e^2}{\vec{r}_1-\vec{r}_2}\right]\psi_1(2)\psi_2(1)d^3r_1d^3r_2 \tag{3.19}$$

and $J_{12}=J_{21}$. If $J_{12}>0$, the triplet state (with a symmetric spin function and an antisymmetric spatial function) lies lower. Here the spins are lined up and S = 1. For the singlet state we have S = 0. We then can write:

$$\vec{S}=\vec{S}_1+\vec{S}_2 \tag{3.20}$$

so that

$$S^2=\left(\vec{S}_1+\vec{S}_2\right)\cdot\left(\vec{S}_1+\vec{S}_2\right)=S_1^2+S_2^2+2S_1\cdot S_2 \tag{3.21}$$

Consider the eigenvalues of 2-electron system ($s_1 = s_2 = 1/2$), for Eq. 3.21.

$$2S_1 \cdot S_2 = s(s+1) - s_1(s_1+1) - s_2(s_2+1) = s(s+1) - \frac{3}{4} - \frac{3}{4} \qquad (3.22)$$

For the triplet state ($s = 1$), Eq. 3.22 yields

$$2S_1 \cdot S_2 = 2 - (3/4) - (3/4) = (1/2) \qquad (3.23)$$

and for the singlet ($s = 0$), Eq. 3.22 yields

$$2S_1 \cdot S_2 = 0 - (3/4) - (3/4) = (-3/2). \qquad (3.24)$$

Therefore we can write

$$\left(\frac{1}{2}\right) + 2S_1 \cdot S_2 = 1 \qquad (3.25)$$

for the spin symmetric (triplet) state, and

$$\left(\frac{1}{2}\right) + 2S_1 \cdot S_2 = -1 \qquad (3.26)$$

for the spin antisymmetric (singlet) state, which allows us to write the expectation value for the Coulomb potential V_{12} in a spin dependent form as

$$\Delta E_{12} = C_{12} \pm J_{12} = C_{12} - (1/2)J_{12} - 2S_1 \cdot S_2 J_{12} \qquad (3.27)$$

The term $-2S_1 \cdot S_2 J_{12}$ is called the Heisenberg Hamiltonian. This exchange energy's hamiltonian generally written in the form of

$$H_{exch} = -\sum_{i,j=1}^{N} J_{ij} \vec{S}_i \cdot \vec{S}_j \tag{3.28}$$

where J_{ij} is the exchange integral [36]. If replace the spin operators by classical vectors and rewrite the dot product, above equation change to

$$E_{exch} = -JS^2 \sum_{i,j|i\neq j} \cos\phi_{ij} \tag{3.29}$$

where ϕ_{ij} is the angle between spin vectors. For small angles the cosine can be developed by Taylor series expansion. By removing the constant term and after some basic calculations, it can written in final form

$$E_{exch} = JS^2 \sum_{NN} \phi_{ij}^2 \tag{3.30}$$

If angle interpreted by $\vec{m} = \vec{M}/M_S$ and the position vectors for small angles and finally change the summation to integral over ferromagnetic body

$$E_{exch} = \int_V A\left[(\nabla m_x)^2 + (\nabla m_y)^2 + (\nabla m_z)^2\right] d^3r , \tag{3.31}$$

where A is the exchange constant [37].

3.3.2 Magnetocrystalline (crystal) anisotropy energy

The most common type of anisotropy is the magnetocrystalline anisotropy, which is caused by the spin-orbit interaction of the electrons. The electron orbits are linked to the crystallographic structure, and by their interaction with the spins they make the latter prefer to align along well-defined crystallographic axes. Therefore, there are directions in space, in which a magnetic material is easier to magnetize than in others. In other words, the energy of moments aligned along different directions in magnetite and they are in directions that have the highest energy (ie.. [001, 010, 100]

are hard directions, Fig. 3.4. The lowest energy is along the body diagonal ([111] is easy direction). This crystal axis dependent energy is called as the magnetocrystalline anisotropy energy, E_a. The Russian physicist Akulov showed in 1929 that E_a can be expressed in terms of a series expansion of direction cosines of M_S relative to the crystal axes. In a cubic crystal M_S make an angles with the crystallographic axes [100, 010, 001] and let α_1, α_2 and α_3 be the cosines of these angles [1]. Then

$$E_a = K_1(\alpha_1^2\alpha_2^2 + \alpha_2^2\alpha_3^2 + \alpha_3^2\alpha_1^2) + K_2(\alpha_1^2\alpha_2^2\alpha_3^2) + ... \qquad (3.32)$$

where K_1 and K_2 are empirically determined magnetocrystalline anisotropy constants and in above equation angle independent constants are ignored. The magnetocrystalline energy is usually small compared to the exchange energy. But the direction of the magnetization is determined only by the anisotropy, because the exchange interaction just tries to align the magnetic moments parallel, no matter in which direction.
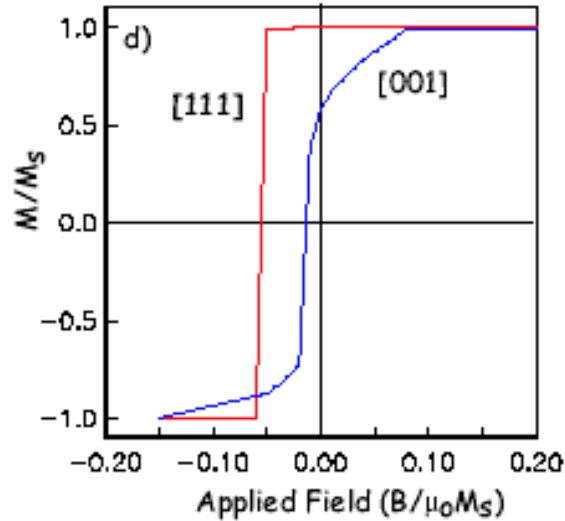
Figure 3.4 Numerical simulation of the magnetization of a cube of magnetite as the applied field is brought down from saturation to zero [38]

In hexagonal crystals the anisotropy energy is a function of only one parameter, that is the angle between the magnetization and the c-axis. Experiments show, that it is symmetric with respect to the base plane, and so odd powers of $\cos\theta$ can be omitted in

a power series expansion for the anisotropy energy density E_{ani}. The first two angle dependent terms are thus

$$E_{ani} = -K_1 \cos^2 \theta + K_2 \cos^4 \theta = -K_1 m_z^2 + K_2 m_z^4 \qquad (3.33)$$

where z is parallel to the c-axis. It is known from experiment, that terms of higher order, and in most cases even K_2 are negligible. If $K_1 > 0$, then the c-axis is an easy axis, which means it is a direction of minimal energy. For K1 < 0 it is a hard axis with an easy plane perpendicular to it [37].

3.3.3 Magnetostatic (shape anisotropy) energy

The origin of domains still cannot be explained by the two energy terms above. Another contribution comes from the magnetostatic self-energy, which originates from the classical interactions between magnetic dipoles. These dipoles constitute a field inside the specimen and when the external filed is applied to it, this internal field tends to demagnetize. The demagnetizing filed H_d of a body is proportional to the magnetization which creates it,

$$H_d = N_d M \qquad (3.34)$$

where N_d is the demagnetizing factor and depends mainly on the shape of the body , and can be calculated exactly only for ellipsoid. For a arbitrary shaped ferromagnet the magnetic fields **H** and **B** are separated two components:

$$H = H_{ext} + H_d \qquad (3.35)$$

$$B = B_{ext} + B_d \qquad (3.36)$$

where external filed is $H_{ext} = B_{ext} / \mu_O$ and demagnetizing field is H_d and B_d is written as a sum of flux density due to the magnetizing field $\mu_O H_d$ and $\mu_O M$ inside the material, $B_d = \mu_O (H_d + M)$. The demagnetizing filed is arises from the dipoles as mentioned above which are produced on the surface of the magnetic body wherever

$\nabla \cdot M \neq 0$. Since $\nabla \times H_d = 0$ and demagnetizing field can be written in terms of gradient of scalar function the below requirement is obtained [39].

$$\int_V B_d H_d d^3 r = 0.$$

(3.37)

If the external field is not present, then the energy E of the demagnetizing field is simply the integral over the energy density $\frac{1}{2}\mu_o H_d^2$. This can be converted to integral inside the volume V of the body, so that the energy can be expressed as

$$E_{ms} = \frac{\mu_o}{2}\int_V H_d^2 d^3 r = -\frac{1}{2}\int_V (B_d - \mu_o M) \cdot H_d d^3 r = -\frac{\mu_o}{2}\int_V M \cdot H_d d^3 r$$

$$E_{ms} = -\frac{\mu_o}{2}\int_V M \cdot H_d d^3 r$$

(3.38)

where outside the body magnetization is equal to zero.

3.3.4 Zeeman energy

If there is an external field, then the energy of the specimen may be written as the difference between the energy density in the total field and in the external field. Using the boundary of $\frac{1}{2}\mu_o H^2$ and the energy density in the external field $\frac{1}{2}\mu_o H_{ext}^2$. This removes the infinite energy contribution from a uniform external field and integrated over all space. Thus, the energy can be written as

$$E_{ext} = \frac{\mu_o}{2}\int_V (H^2 - H_{ext}^2) d^3 r$$

(3.39)

Using the fact that $\nabla \times H_{ext} = 0$, we have

$$\int\limits_V H_{ext} B_d d^3 r = 0 \tag{3.40}$$

Hence, by also using the fallowing equations:

$$H^2 = H_{ext}^2 + 2H_d \cdot H_{ext} + H_d^2 \tag{3.41}$$

$$H_d \cdot H_{ext} = H_{ext} \cdot \left(\frac{B_d}{\mu_O} - M \right) \tag{3.42}$$

from the $H_d \cdot H_{ext}$ the energy of a magnetic body in the external field is obtained as:

$$E_{ext} = -\mu_o \int\limits_V M \cdot H_{ext} d^3 r \tag{3.43}$$

All these abovementioned energy term can be added due to the Maxwell's equations' linearity.

3.4 ENERGY MINIMIZATION

The Landau free energy G_L is can be written the summation of exchange energy, the magnetocrystalline anisotropy energy, the magnetostatic energy and the Zeeman energy in an external field as:

$$G_L = E_{exc} + E_{ani} + E_{ms} + E_{ext} \tag{3.44}$$

$$= \int\limits_V \left\{ A[(\nabla m_x)^2 + (\nabla m_y)^2 + (\nabla m_z)^2] - K_1 m_z^2 + K_2 m_z^4 - \frac{\mu_o}{2} M \cdot H_d - \mu_o M \cdot H_{ext} \right\} d^3 r$$

From this equation Landau free energy can be calculated, if the magnetization of the specimen is known. Brown [40] proposed a variational method to minimize the Landau free energy which is required for determination of magnetization distribution in specimen. He considered a small variation of the direction of the magnetization vector, rather a small variation of the magnetization distribution function by arbitrary functions. At an energy minimum the coefficients of the linear term for any choice of the variation should vanish. Proper application of this variational principle [36] finally leads to

Brown's equations. They have to be solved together with Maxwell's equations for the magnetostatic field and the proper boundary conditions. And it is necessary to check, if the solution is a minimum or a maximum, for which the variation vanishes, too. Static energy minimization using the finite element method is very efficient in calculating equilibrium magnetization distributions and nucleation fields of poly-crystalline permanent magnets [37]. The solutions of Brown's equation will be examined in the next section.

3.5 PHONOMENOLOGICAL EQUATIONS FOR RELAXATION PROCESS

The solution of Brown's equations gives the magnetization distribution in equilibrium [41]. However the important thing is dynamic properties and time evolution of the magnetization. Magnetic moment of circulating electron with charge e, velocity ϑ has a magnetic moment $m = IA$ in Eq.2.14 can written as $|m| = \dfrac{e\vartheta r}{2}$ where r is radius of circular path, A is area of that closed path and t is period of it motion. When we write magnetic moment in terms of resultant angular momentum

$$|\mu| = \frac{e|J|}{2m} \qquad \text{or} \qquad (3.45)$$

$$|\mu| = \gamma |J| \qquad (3.46)$$

Total magnetic moment M is sum of the magnetic moment of electrons

$$M = \sum \mu \qquad (3.47)$$

Then, the rate of change of resultant magnetic moment can be written as

$$\frac{dM}{dt} = \gamma \frac{dJ}{dt} \ . \qquad (3.48)$$

By using the moment equations, one can derive that the time derivative of total angular momentum is equal to torque

$$\frac{d\vec{J}}{dt} = \frac{d(\vec{r} \times m\vec{v})}{dt} = \vec{r} \times m\frac{d(\vec{v})}{dt} = \vec{r} \times m\vec{a} = \vec{r} \times \vec{F} = \vec{\tau} \tag{3.49}$$

and so

$$\tau = \frac{dJ}{dt} = \frac{1}{\gamma}\frac{dM}{dt} \tag{3.50}$$

Here torque on a finite current loop in magnetic field can be taken as

$$\tau = M \times B_{eff} , \tag{3.51}$$

as a result, if one neglects the damping [41], the motion of the magnetization vector M is described by the magnetic torque equation

$$\frac{1}{\gamma}\frac{dM}{dt} = M \times B_{eff} \qquad \text{or} \qquad M' = \gamma(M \times B_{eff}) \tag{3.52}$$

Magnetization in static field ($\vec{B} = B_z\hat{k}$) since $B_z = B$.

$$M \times B_{eff} = \begin{vmatrix} \hat{i} & \hat{j} & \hat{k} \\ M_x & M_y & M_z \\ 0 & 0 & B \end{vmatrix} = M_y B\hat{i} - M_x B\hat{j} \tag{3.53}$$

$$\frac{dM_x}{dt} = \gamma B M_y \tag{3.54}$$

$$\frac{dM_y}{dt} = -\gamma B M_x \tag{3.55}$$

$$\frac{dM_z}{dt} = 0 \tag{3.56}$$

Consider relaxation effect, if system subjected sudden change in the magnitude and direction of $\vec{B}$, then M_x, M_y and M_z in general relaxation to their new equilibrium values of different rates [42]. So there must be correction terms in the relaxation equations. Assume M_x and M_y relax with the same rate of $\frac{1}{T_2}$ and M_z with $\frac{1}{T_1}$.

$$\frac{dM_x}{dt} = \gamma B M_y - \frac{M_x}{T_2} \tag{3.57}$$

$$\frac{dM_y}{dt} = -\gamma B M_x - \frac{M_y}{T_2} \tag{3.58}$$

$$\frac{dM_z}{dt} = \frac{M_z^o - M_z}{T_1} \tag{3.59}$$

The oscillating field with only oscillate in the x direction and so $B_y = 0$ and $B_z \neq 0$

First equation is reorganized with relaxation terms and called **Bloch equation** [43]:

$$\vec{M}' = \gamma \vec{M} \times \vec{B}_{eff} - \frac{\vec{M} - \delta_{iz} M_o}{\vec{T}} \qquad \begin{cases} \delta_{iz} = 1 & \text{if} \quad i = z \\ \delta_{iz} = 0 & \text{if} \quad i \neq z \end{cases} \tag{3.60}$$

where $\vec{M} = (M_x \quad M_y \quad M_z)$, $\vec{T} = (T_2 \quad T_2 \quad T_1)$ and $\vec{\delta}_{iz} = (0 \quad 0 \quad 1)$. The Eq. 3.60 can be rewritten as

$$\frac{1}{\gamma}\vec{M}' = \vec{M} \times \vec{B}_{eff} - \frac{\vec{M} - \delta_{iz} M_o}{\gamma \vec{T}} \tag{3.61}$$

Here

$$\vec{M}' = \frac{dM_x}{dt}\hat{i} + \frac{dM_y}{dt}\hat{j} + \frac{dM_z}{dt}\hat{k} \tag{3.62}$$

$$M \times B_{eff} = \begin{vmatrix} \hat{i} & \hat{j} & \hat{k} \\ M_x & M_y & M_z \\ B_x & B_y & B_z \end{vmatrix} = (M_y B_z - M_z B_y)\hat{i} - (M_x B_z - M_z B_x)\hat{j} + (M_x B_y - M_y B_x)\hat{k}$$

$$\tag{3.63}$$

$$\frac{\vec{M} - \delta_{iz}M_o}{\gamma \vec{T}} = \frac{M_x}{\gamma T_2}\hat{i} + \frac{M_y}{\gamma T_2}\hat{j} + \frac{M_z - M_o}{\gamma T_1}\hat{k} \tag{3.64}$$

So

$$\frac{1}{\gamma}\frac{dM_x}{dt} = (M_y B_z - M_z B_y) - \frac{M_x}{\gamma T_2} \tag{3.65}$$

$$\frac{1}{\gamma}\frac{dM_y}{dt} = (M_z B_x - M_x B_z) - \frac{M_y}{\gamma T_2} \tag{3.66}$$

$$\frac{1}{\gamma}\frac{dM_z}{dt} = (M_x B_y - M_y B_x) - \frac{M_z - M_o}{\gamma T_1} \tag{3.67}$$

Here $\quad \vec{M} = \begin{vmatrix} \chi & -i\kappa \\ i\kappa & \chi \end{vmatrix}\vec{B} \quad$ and $\quad \vec{B} = B_o e^{\mp iwt}$, so that

$$M_x = (\chi - i\kappa)B_o e^{+iwt}$$

$$\tag{3.68}$$

$$M_y = (\chi + i\kappa)B_o e^{+iwt} \tag{3.69}$$

The first derivative of M_x and M_y with respect to t is

$$M_x^{'} = i\omega M_x \qquad \text{and} \qquad M_y^{'} = i\omega M_y \qquad \text{(3.70-3.71)}$$

The volume susceptibility's imaginary part is proportional with the absorption spectra (dynamic) in FMR. So it is related with magnetization in y direction.

$$\frac{dP}{dB} \alpha \frac{d\chi''}{dB}$$

(3.72)

Absoption power and imaginary part of susceptibility are proportional to each other

$$\chi'' = \frac{M_y^{''}}{B_{\perp}}$$

(3.73)

3.5.1 Bloch-Bloembergen Equation

Bloembergen adapted Bloch's Equation to FMR, as follows:

$$\vec{M}' = \gamma \vec{M} \times \vec{B}_{eff} - \frac{\vec{M} - \delta_{iz} M_o}{\vec{T}}$$

(3.74)

with $\vec{M} = (M_x \quad M_y \quad M_z)$, $\vec{T} = (T_2 \quad T_2 \quad T_1)$ and $\vec{\delta}_{iz} = (0 \quad 0 \quad 1)$ and T_1 and T_2 are referrred to spin-lattice (in $\hat{z}$ direction) and spin-spin (in $\hat{x}$ and $\hat{y}$ direction) relaxation time respectively [44].

$$\vec{M}' = \frac{dM_x}{dt}\hat{i} + \frac{dM_y}{dt}\hat{j} + \frac{dM_z}{dt}\hat{k}$$

(3.75)

$$M \times B_{eff} = \begin{vmatrix} \hat{i} & \hat{j} & \hat{k} \\ M_x & M_y & M_z \\ B_x & B_y & B_z \end{vmatrix} = (M_y B_z - M_z B_y)\hat{i} - (M_x B_z - M_z B_x)\hat{j} + (M_x B_y - M_y B_x)\hat{k}$$

(3.76)

$$\frac{\vec{M} - \delta_{iz}M_o}{\gamma \vec{T}} = \frac{M_x}{\gamma T_2}\hat{i} + \frac{M_y}{\gamma T_2}\hat{j} + \frac{M_z - M_o}{\gamma T_1}\hat{k} \qquad (3.77)$$

Use the Eqs. 3.75-3.77 in the Eq. 3.74, then

$$\frac{1}{\gamma}\frac{dM_x}{dt} = (M_y B_z - M_z B_y) - \frac{M_x}{\gamma T_2} \qquad (3.78)$$

$$\frac{1}{\gamma}\frac{dM_y}{dt} = (M_z B_x - M_x B_z) - \frac{M_y}{\gamma T_2} \qquad (3.79)$$

$$\frac{1}{\gamma}\frac{dM_z}{dt} = (M_x B_y - M_y B_x) - \frac{M_z - M_o}{\gamma T_1} \qquad (3.80)$$

Substitude Eqs. 3.70 and 3.71 in Eqs. 3.78 and 3.79 then

$$i\frac{\omega}{\gamma}M_x = (M_y B_z - M_z B_y) - \frac{M_x}{\gamma T_2} \qquad (3.81)$$

$$i\frac{\omega}{\gamma}M_y = (M_z B_x - M_x B_z) - \frac{M_y}{\gamma T_2} \qquad (3.82)$$

Use the relations $\Delta_B = \frac{1}{\gamma T_2}$, $B_o = -\frac{\omega}{\gamma}$, $M_z = M$ and; the magnetic field traveling along

z-axis $B_z = B$ and in y-direction $B_y = B_\perp$ so $B_x = 0$,

$$(-iB_o + \Delta_B)M_x - BM_y = -MB_\perp \qquad (3.83)$$

$$BM_x + (-iB_o + \Delta_B)M_y = 0 \qquad (3.84)$$

here take $a = -iB_o + \Delta_B$, $b = B$ and $c = -MB_\perp$ then Eqs. 3.83. and 3.84 take the forms

of

$$aM_x - bM_y = c \tag{3.85}$$

$$bM_x + aM_y = 0 \tag{3.86}$$

From the above relation $M_x = -\dfrac{a}{b} M_y$ and use it at Eq. 3.85, then

$$(\frac{a^2}{b} - b)M_y = c \qquad \text{gives} \qquad M_y = \frac{-bc}{a^2 + b^2} \tag{3.87}$$

Substitute the terms of a, b and c again

$$M_y = \frac{MBB_\perp}{\Delta_B^2 + B^2 - B_o^2 - i2\Delta_B B_o} \tag{3.88}$$

Multiply both numerator and denominator with conjugate of denominator $\Delta_B^2 + B^2 - B_o^2 + i2\Delta_B B_o$ then

$$M_y = \frac{MBB_\perp (\Delta_B^2 + B^2 - B_o^2) + i2MBB_o B_\perp \Delta_B}{\Delta_B^4 + B^4 + B_o^4 + 2\Delta_B^2 B^2 - 2B^2 B_o^2 - 2\Delta_B^2 B_o^2 + 4\Delta_B^2 B_o^2} \tag{3.89}$$

$$= \frac{MBB_\perp (\Delta_B^2 + B^2 - B_o^2) + i2MBB_o B_\perp \Delta_B}{\Delta_B^4 + B^4 + B_o^4 + 2\Delta_B^2 B^2 - 2B^2 B_o^2 + 2\Delta_B^2 B_o^2}$$

If we add and subtract the $2B^2 B_o^2$ term to the denominator

$$M_y = \frac{MBB_\perp (\Delta_B^2 + B^2 - B_o^2) + i2MBB_o B_\perp \Delta_B}{\Delta_B^4 + B^4 + B_o^4 + 2\Delta_B^2 B^2 + 2B^2 B_o^2 + 2\Delta_B^2 B_o^2 - 4B^2 B_o^2} \tag{3.90}$$

The denominator can be thought as $x^2 - y^2 = (x - y)(x + y)$, then

$$M_y = \frac{MBB_\perp(\Delta_B^2 + B^2 - B_o^2) + i2MBB_oB_\perp\Delta_B}{\left[\Delta_B^2 + B^2 + B_o^2\right]^2 - 4B^2B_o^2} \tag{3.91}$$

$$M_y = \frac{MBB_\perp(\Delta_B^2 + B^2 - B_o^2) + i2MBB_oB_\perp\Delta_B}{\left[\Delta_B^2 + B^2 + B_o^2 - 2BB_o\right]\cdot\left[\Delta_B^2 + B^2 + B_o^2 + 2BB_o\right]}$$

$$M_y = \frac{MBB_\perp(\Delta_B^2 + B^2 - B_o^2) + i2MBB_oB_\perp\Delta_B}{\left[\Delta_B^2 + (B - B_o)^2\right]\cdot\left[\Delta_B^2 + (B + B_o)^2\right]} \tag{3.92}$$

From the Eq. 3.73, take the imaginary part of M_y

$$\chi'' = \frac{M_y''}{B_\perp} = \frac{2MBB_o\Delta_B}{\left[\Delta_B^2 + (B - B_o)^2\right]\cdot\left[\Delta_B^2 + (B + B_o)^2\right]} \tag{3.93}$$

Take $B_o = -\dfrac{\omega}{\gamma} = \dfrac{-2\pi}{T_2\gamma} = -2\pi\Delta_B$ and $M = M_o = M(B) = \chi_o B$ (for **case 1**)

$$\chi''(B) = \frac{-4\pi\chi_o B^2\Delta_B^2}{\left[\Delta_B^2 + (B - B_o)^2\right]\cdot\left[\Delta_B^2 + (B + B_o)^2\right]} \tag{3.94}$$

Here χ'' is the function of B and to determine the χ_o constant, $\chi''(B)$ function is normalized to unity.

$$\int_{-\infty}^{\infty}\chi''(B)dB = 1 \tag{3.95}$$

$$\left[\begin{array}{l} -\dfrac{\pi\Delta_B^2\chi_o\log(\Delta_B^2 + B^2 - 2BB_o + B_o^2)}{2B_o} - \pi\Delta_B\chi_o\arctan(\dfrac{B - B_o}{\Delta_B}) + \\[4mm] \dfrac{\pi\Delta_B^2\chi_o\log(\Delta_B^2 + B^2 + 2BB_o + B_o^2)}{2B_o} - \pi\Delta_B\chi_o\arctan(\dfrac{B + B_o}{\Delta_B}) \end{array}\right]_{-\infty}^{\infty} = 1$$

Here log terms cancel each other and we know that $\lim\limits_{x\to\infty}(\arctan x) = \dfrac{\pi}{2}$ and

$$\lim\limits_{x\to-\infty}(\arctan x) = -\dfrac{\pi}{2}$$

$$\left\{ \left[-\pi\Delta_B\chi_o(\tfrac{\pi}{2}) - \pi\Delta_B\chi_o(\tfrac{\pi}{2}) \right] - \left[-\pi\Delta_B\chi_o(-\tfrac{\pi}{2}) - \pi\Delta_B\chi_o(-\tfrac{\pi}{2}) \right] \right\} = 1$$

gives $-2\pi^2\Delta_B\chi_o = 1$ and from here take $\chi_o = -\dfrac{1}{2\pi^2\Delta_B}$, then write it in the Eq. 3.94

$$\chi''(B) = \frac{-4\pi(-\dfrac{1}{2\pi^2\Delta_B})B^2\Delta_B^2}{\left[\Delta_B^2 + (B-B_o)^2\right]\cdot\left[\Delta_B^2 + (B+B_o)^2\right]} \tag{3.96}$$

As a result

$$\chi''(B) = \frac{2}{\pi}\frac{\Delta_B B^2}{\left[\Delta_B^2 + (B-B_o)^2\right]\cdot\left[\Delta_B^2 + (B+B_o)^2\right]} \tag{3.97}$$

This is solution of **Bloch-Bloembergen's** equation for **case 1** ($M = M_o = M(B) = \chi_o B$)

For the perfect soft ferromagnet which are characterized by stepwise dependence

$M_o(B) = M_o\,\text{sgn}(B)$ with constant M_o (**case 2**). $\text{sgn}(B) = \dfrac{B}{|B|} = \dfrac{|B|}{B}$ is used to simplify

the relation at Eq. 3.93 .

$$\chi'' = \frac{M_y''}{B_\perp} = \frac{2\chi_o|B|B_o\Delta_B}{\left[\Delta_B^2 + (B-B_o)^2\right]\cdot\left[\Delta_B^2 + (B+B_o)^2\right]} \tag{3.98}$$

Here χ'' is the function of B and to determine the χ_o constant, $\chi''(B)$ function is normalized to unity $\int\limits_{-\infty}^{\infty}\chi''(B)dB = 1$.

$$\left.\begin{array}{l} \dfrac{-\chi_o}{2}\left(\arctan(\dfrac{B-B_o}{\Delta_B}) - \arctan(\dfrac{B+B_o}{\Delta_B})\right)\Bigg|_{-\infty}^{0} - \\[4mm] \dfrac{\chi_o}{2}\left(\arctan(\dfrac{B-B_o}{\Delta_B}) - \arctan(\dfrac{B+B_o}{\Delta_B}) + 4\arctan(\dfrac{B_o}{\Delta_B})\right)\Bigg|_{0}^{\infty} \end{array}\right\} = 1 \qquad (3.99)$$

By using $\lim\limits_{x\to\infty}(\arctan x) = \dfrac{\pi}{2}$ and $\lim\limits_{x\to-\infty}(\arctan x) = -\dfrac{\pi}{2}$,

$$2\chi_o\arctan(\dfrac{B_o}{\Delta_B}) = 1 \qquad \text{or} \qquad \chi_o = \dfrac{1}{2\arctan(\dfrac{B_o}{\Delta_B})}. \qquad (3.100)$$

Substitute this result in Eq. 3.98

$$\chi'' = \dfrac{B_o\Delta_B|B|}{\arctan(B_o/\Delta_B)\left[\Delta_B^2 + (B-B_o)^2\right]\cdot\left[\Delta_B^2 + (B+B_o)^2\right]} \qquad (3.101)$$

This is the solution of **Bloch-Bloembergen's** equation for *case 2* ($M = M_o = \chi_o\,\text{sgn}(B)$).

3.5.2 Modified Bloch equation

The Bloch-Bloembergen equation in the preceding form is unsatisfactory in it, at least two aspects [45, 46]. First, it predicts that no absorption occurs in the absence of the magnetizing field while such zero-filed absorption can be observed experimentally. Second, it leads to the absurd conclusion that far resonance, negative absorption of circularly polarized microwaves should be observed [47, 48]. In order to avoid these inconsistencies, the Bloch-Bloembergen equation is sometimes modified in such a way

that longitudinal relaxation takes places along the direction of the effective filed and lateral relaxation occurs at right angles to it.

$$\vec{M}' = \gamma\vec{M} \times \vec{B}_{eff} - \frac{\vec{M} - M_o\vec{B}_{eff}/\vec{B}}{\vec{T}}$$

(3.102)

with $\vec{M} = (M_x \quad M_y \quad M_z)$, $\vec{T} = (T_2 \quad T_2 \quad T_1)$ and $\vec{\delta}_{iz} = (0 \quad 0 \quad 1)$ and T_1 and T_2 are referred to spin-lattice (in $\hat{z}$ direction) and spin-spin (in $\hat{x}$ and $\hat{y}$ direction) relaxation time respectively. By using the $\vec{M}'$ and $M \times B_{eff}$ from above part, the below equality is derived.

$$\frac{\vec{M} - M_o\vec{B}_{eff}/\vec{B}}{\vec{T}} = \left(\frac{M_x}{T_2} - \frac{M_oB_x}{T_2B}\right)\hat{i} + \left(\frac{M_y}{T_2} - \frac{M_oB_y}{T_2B}\right)\hat{j} + \left(\frac{M_z - M_oB_z}{T_1B}\right)\hat{k}$$

(3.103)

Use Eqs. 3.75, 3.76 and 3.103 in the Eq. 3.102, then

$$\frac{1}{\gamma}\frac{dM_x}{dt} = (M_yB_z - M_zB_y) - \frac{M_x}{\gamma T_2} + \frac{M_oB_x}{\gamma T_2B}$$

(3.104)

$$\frac{1}{\gamma}\frac{dM_y}{dt} = (M_zB_x - M_xB_z) - \frac{M_y}{\gamma T_2} + \frac{M_oB_y}{\gamma T_2B}$$

(3.105)

$$\frac{1}{\gamma}\frac{dM_z}{dt} = (M_xB_y - M_yB_x) - \frac{M_z - M_oB_z}{\gamma T_1B}$$

(3.106)

Substitude Eqs. 3.70 and 3.71 in Eqs. 3.104 and 3.105 then

$$i\frac{\omega}{\gamma}M_x = (M_yB_z - M_zB_y) - \frac{M_x}{\gamma T_2} + \frac{M_oB_x}{\gamma T_2B}$$

(3.107)

$$i\frac{\omega}{\gamma}M_y = (M_zB_x - M_xB_z) - \frac{M_y}{\gamma T_2} + \frac{M_oB_y}{\gamma T_2B}$$

(3.108)

Use the relations $\Delta_B = \dfrac{1}{\gamma T_2}$, $B_o = -\dfrac{\omega}{\gamma}$, $M_z = M$ and; the magnetic field traveling along

z-axis $B_z = B$ and in y-direction $B_y = B_\perp$ so $B_x = 0$,

$$(-iB_o + \Delta_B)M_x - BM_y = -MB_\perp$$
(3.109)

$$BM_x + (-iB_o + \Delta_B)M_y = \frac{M_o \Delta_B B_\perp}{B}$$
(3.110)

here take $a = -iB_o + \Delta_B$, $b = B$, $c = -MB_\perp$ and $d = \dfrac{M_o \Delta_B B_\perp}{B}$ then the Eqs. 3.109 and

3.110 take the forms of

$$aM_x - bM_y = c$$
(3.111)

$$bM_x + aM_y = d$$
(3.112)

From the above relation $M_x = \dfrac{c + bM_y}{a}$ and use it at Eq. 3.112.

$$\frac{bc}{a} + \frac{b^2 + a^2}{a} M_y = d \qquad \text{gives} \qquad M_y = \frac{ad - bc}{a^2 + b^2}$$
(3.113)

Substitute the terms of a, b, c and d again

$$M_y = \frac{(-iB_o + \Delta_B)\left(\dfrac{M_o \Delta_B B_\perp}{B}\right) + MBB_\perp}{\Delta_B^2 + B^2 - B_o^2 - i2\Delta_B B_o}$$
(3.114)

Multiply both numerator and denominator with conjugate of denominator $\Delta_B^2 + B^2 - B_o^2 + i2\Delta_B B_o$ then

$$M_y' = \frac{B_\perp}{B} \frac{(MB^2 + M_o\Delta_B^2)(\Delta_B^2 + B^2 - B_o^2) + 2M_o B_o \Delta_B^2}{\Delta_B^4 + B^4 + B_o^4 + 2\Delta_B^2 B^2 - 2B^2 B_o^2 + 2\Delta_B^2 B_o^2}$$

(3.115)

$$M_y'' = \frac{B_\perp}{B} \frac{(-M_o B_o \Delta_B)(\Delta_B^2 + B^2 - B_o^2) + 2MB^2 B_o \Delta_B + 2M_o B_o \Delta_B^3}{\Delta_B^4 + B^4 + B_o^4 + 2\Delta_B^2 B^2 - 2B^2 B_o^2 + 2\Delta_B^2 B_o^2}$$

If we add and subtract the $2B^2 B_o^2$ term to the denominator and rearrange the numerator

$$M_y'' = \frac{B_\perp}{B} \frac{B_o \Delta_B(-M_o B^2 + MB_o^2 + 2MB^2 + M_o\Delta_B^2)}{\Delta_B^4 + B^4 + B_o^4 + 2\Delta_B^2 B^2 + 2B^2 B_o^2 + 2\Delta_B^2 B_o^2 - 4B^2 B_o^2}$$

(3.116)

The denominator can be thought as $x^2 - y^2 = (x-y)(x+y)$, then

$$M_y'' = \frac{B_\perp}{B} \frac{B_o \Delta_B \left[M_o(\Delta_B^2 - B^2) + M(2B^2 + B_o^2) \right]}{\left[\Delta_B^2 + B^2 + B_o^2\right]^2 - 4B^2 B_o^2}$$

(3.117)

From the Eq. 3.73, the imaginary part of susceptibility is

$$\chi'' = \frac{M_y''}{B_\perp} = \frac{B_o \Delta_B}{B} \frac{\left[M_o(\Delta_B^2 - B^2) + M(2B^2 + B_o^2) \right]}{\left[\Delta_B^2 + B^2 + B_o^2\right]^2 - 4B^2 B_o^2}$$

(3.118)

Take $M = M_o = M(B) = \chi_o B$ (for the **case 1**)

$$\chi''(B) = \frac{B_o \Delta_B \chi_o (\Delta_B^2 + B^2 + B_o^2)}{\left[\Delta_B^2 + (B - B_o)^2\right] \cdot \left[\Delta_B^2 + (B + B_o)^2\right]}$$

(3.119)

Here χ'' is the function of B and to determine the χ_o constant, $\chi''(B)$ function is normalized to unity $\int_{-\infty}^{\infty} \chi''(B)dB = 1$.

$$\frac{1}{2} B_o \chi_o \arctan(\frac{B - B_o}{\Delta_B}) + \frac{1}{2} B_o \chi_o \arctan(\frac{B + B_o}{\Delta_B}) \Big|_{-\infty}^{\infty} = 1$$

Here the arctan terms goes to constant at limits as $\lim_{x \to \infty}(\arctan x) = \frac{\pi}{2}$ and

$\lim_{x \to -\infty}(\arctan x) = -\frac{\pi}{2}$, so

$$B_o \chi_o \left(\frac{\pi}{2}\right) - B_o \chi_o \left(-\frac{\pi}{2}\right) = 1$$

gives $\pi B_o \chi_o = 1$ and from here take $\chi_o = \frac{1}{\pi B_o}$, then write it in the Eq. 3.119,

$$\chi''(B) = \frac{B_o \Delta_B \left(\frac{1}{\pi B_o}\right)(\Delta_B^2 + B^2 + B_o^2)}{\left[\Delta_B^2 + (B - B_o)^2\right] \cdot \left[\Delta_B^2 + (B + B_o)^2\right]} \tag{3.120}$$

As a result

$$\chi''(B) = \frac{1}{\pi} \frac{\Delta_B (\Delta_B^2 + B^2 + B_o^2)}{\left[\Delta_B^2 + (B - B_o)^2\right] \cdot \left[\Delta_B^2 + (B + B_o)^2\right]} \tag{3.121}$$

This is solution of *modified Bloch's* equation for *case 1* ($M = M_o = M(B) = \chi_o B$)

For the perfect soft ferromagnet which are characterized by stepwise dependence

$M_o(B) = M_o \operatorname{sgn}(B)$ with constant M_o (*case 2*). $\operatorname{sgn}(B) = \frac{B}{|B|} = \frac{|B|}{B}$ is used to simplify

the relation at Eq. 3.118.

$$\chi'' = \frac{M_y''}{B_\perp} = \frac{M_o B_o \Delta_B (B^2 + B_o^2 + \Delta_B^2)}{|B| \left[\Delta_B^2 + (B - B_o)^2\right] \cdot \left[\Delta_B^2 + (B + B_o)^2\right]} \tag{3.122}$$

3.5.3 Gilbert equation

Gilbert suggested that equation of motion with a relaxation rate proportional to the total M'[49]:

$$\vec{M}' = \gamma \vec{M} \times \vec{B}_{eff} + \frac{G}{|\vec{M}|} \vec{M} \times \vec{M}' \qquad (3.123)$$

with G>0. Then the linewidth parameter can be defined as $\Delta_B = GB_o$ and with $\vec{M} = (M_x \quad M_y \quad M_z)$, $\vec{T} = (T_2 \quad T_2 \quad T_1)$ and T_1 and T_2 are referred to spin-lattice (in $\hat{z}$ direction) and spin-spin (in $\hat{x}$ and $\hat{y}$ direction) relaxation time respectively as before. From above parts $\vec{M}'$ and $M \times B_{eff}$ will be used in Eq. 3.123 from above parts and

$$M \times M' = \begin{vmatrix} \hat{i} & \hat{j} & \hat{k} \\ M_x & M_y & M_z \\ M_x' & M_y' & B_z' \end{vmatrix}$$

$$M \times M' = (M_y M_z' - M_z M_y')\hat{i} - (M_x M_z' - M_z M_x')\hat{j} + (M_x M_y' - M_y M_x')\hat{k}$$
$$(3.124)$$

will be used with Eqs. 3.75, 3.76 in Eq. 3.123, then

$$\frac{1}{\gamma}\frac{dM_x}{dt} = (M_y B_z - M_z B_y) - \frac{G}{\gamma|M|}(M_y M_z' - M_z M_y') \qquad (3.125)$$

$$\frac{1}{\gamma}\frac{dM_y}{dt} = (M_z B_x - M_x B_z) - \frac{G}{\gamma|M|}(M_z M_x' - M_x M_z') \qquad (3.126)$$

$$\frac{1}{\gamma}\frac{dM_z}{dt} = (M_x B_y - M_y B_x) - \frac{G}{\gamma|M|}(M_x M_y' - M_y M_x') \qquad (3.127)$$

Substitude $M_x' = i\omega M_x$, $M_y' = i\omega M_y$ and $M_x' = 0$) in Eqs. 3.125 and 3.126 and then

$$i\frac{\omega}{\gamma}M_x = (M_yB_z - M_zB_y) - \frac{G}{\gamma|M|}(-i\omega M_zM_y) \tag{3.128}$$

$$i\frac{\omega}{\gamma}M_y = (M_zB_x - M_xB_z) - \frac{G}{\gamma|M|}(i\omega M_zM_x) \tag{3.129}$$

Use the relations $\Delta_B = GB_o$, $B_o = -\frac{\omega}{\gamma}$, $M_z = M$ and; the magnetic field traveling along z-axis $B_z = B$ and in y-direction $B_y = B_\perp$ so $B_x = 0$,

$$(-iB_o)M_x - (iB_oG + B)M_y = -MB_\perp \tag{3.130}$$

$$(-iB_oG + B)M_x + (-iB_o)M_y = 0 \tag{3.131}$$

here take $a = -iB_o$, $b = iB_oG + B = i\Delta_B + B$, and $c = -MB_\perp$ then the Eqns 3.130 and 3.131 take the forms of

$$aM_x - bM_y = c \tag{3.132}$$

$$bM_x + aM_y = 0 \tag{3.133}$$

From the above relation $M_x = -\frac{b}{a}M_y$ and use it at Eqn 3.132.

$$\frac{-a^2 - b^2}{b}M_y = c \qquad \text{gives} \qquad M_y = \frac{-bc}{a^2 + b^2} \tag{3.134}$$

Substitute the terms of a, b, c and d again

$$M_y = \frac{-(i\Delta_B + B)(-MB_\perp)}{(-iB_o)^2 + (i\Delta_B + B)^2} \tag{3.135}$$

$$M_y = \frac{MBB_\perp + iM\Delta_B B_\perp}{B^2 - B_o^2 - \Delta_B^2 + i2B\Delta_B} \tag{3.136}$$

Multiply both numerator and denominator with conjugate of denominator $B^2 - B_o^2 - \Delta_B^2 - i2B\Delta_B$ then

$$M'_y = \frac{(B^2 - B_o^2 - \Delta_B^2)(MBB_\perp) + 2MB\Delta_B^2 B_\perp}{(B^2 - B_o^2 - \Delta_B^2)^2 + 4B^2\Delta_B^2} \tag{3.137}$$

$$M''_y = \frac{M\Delta_B B_\perp (B^2 - B_o^2 - \Delta_B^2) - 2MB^2 B_\perp \Delta_B}{(B^2 - B_o^2 - \Delta_B^2)^2 + 4B^2\Delta_B^2} \tag{3.138}$$

Use the latter one that gives the imaginary part of the susceptibility. If we add and subtract the $2B^2 B_o^2$ term to the denominator and rearrange the numerator of imaginary part:

$$M''_y = \frac{M\Delta_B B_\perp (B^2 - B_o^2 - \Delta_B^2 - 2B^2)}{\Delta_B^4 + B^4 + B_o^4 + 2\Delta_B^2 B^2 + 2B^2 B_o^2 + 2\Delta_B^2 B_o^2 - 4B^2 B_o^2} \tag{3.139}$$

$$M''_y = \frac{M\Delta_B B_\perp (-B^2 - B_o^2 - \Delta_B^2)}{(B^2 - B_o^2 - \Delta_B^2)^2 - 4B^2\Delta_B^2}$$

The denominator can be thought as $x^2 - y^2 = (x - y)(x + y)$, then

$$M''_y = \frac{-M\Delta_B B_\perp (B^2 + B_o^2 + \Delta_B^2)}{\left[\Delta_B^2 + B^2 + B_o^2 - 2B^2 B_o^2\right] \cdot \left[\Delta_B^2 + B^2 + B_o^2 + 2B^2 B_o^2\right]} \tag{3.141}$$

$$M''_y = \frac{-M\Delta_B B_\perp (B^2 + B_o^2 + \Delta_B^2)}{\left[\Delta_B^2 + (B - B_o)^2\right] \cdot \left[\Delta_B^2 + (B + B_o)^2\right]}$$

The imaginary part of susceptibility is

$$\chi'' = \frac{M_y''}{B_\perp} = \frac{-M\Delta_B(B^2 + B_o^2 + \Delta_B^2)}{\left[\Delta_B^2 + (B - B_o)^2\right] \cdot \left[\Delta_B^2 + (B + B_o)^2\right]} \tag{3.141}$$

Take $M = M_o = M(B) = \chi_o B$ (for the *case 1*)

$$\chi''(B) = \frac{-\chi_o B\Delta_B(B^2 + B_o^2 + \Delta_B^2)}{\left[\Delta_B^2 + (B - B_o)^2\right] \cdot \left[\Delta_B^2 + (B + B_o)^2\right]} \tag{3.142}$$

Here χ'' is the function of B and to determine the χ_o constant, $\chi''(B)$ function is not normalized to unity. Because $\int_{-\infty}^{\infty} \chi''(B) dB = 1$ are divergent.

$$\chi''(B) \propto \frac{\chi_o \Delta_B(B^2 + B_o^2 + \Delta_B^2)|B|}{\left[\Delta_B^2 + (B - B_o)^2\right] \cdot \left[\Delta_B^2 + (B + B_o)^2\right]} \tag{3.143}$$

This is solution of *Gilbert's* equation for *case 1* ($M = M_o = M(B) = \chi_o B$)

For the perfect soft ferromagnet which are characterized by stepwise dependence $M_o(B) = M_o \, \text{sgn}(B)$ with constant M_o (*case 2*). $\text{sgn}(B) = \frac{B}{|B|} = \frac{|B|}{B}$ is used to simplify the imaginary part of the susceptibility as

$$\chi'' = \frac{M_y''}{B_\perp} = \frac{-M_o\Delta_B(B^2 + B_o^2 + \Delta_B^2)}{\left[\Delta_B^2 + (B - B_o)^2\right] \cdot \left[\Delta_B^2 + (B + B_o)^2\right]}. \tag{3.144}$$

From $\int_{-\infty}^{\infty} \chi''(B) dB = 1$, $M_o = \frac{-1}{\pi}$. And so

$$\chi''(B) = \frac{1}{\pi} \frac{\Delta_B(B^2 + B_o^2 + \Delta_B^2)}{\left[\Delta_B^2 + (B - B_o)^2\right] \cdot \left[\Delta_B^2 + (B + B_o)^2\right]} \tag{3.145}$$

this show that **Gilbert's case 2** is same with the modified Bloch case1.

3.5.4 Landau-Lifshitz equation

Landau and Lifshitz suggested a damping term with relaxation rate proportional to the precessional component of M'[50]:

$$\vec{M}' = \gamma \vec{M} \times \vec{B}_{eff} + \frac{\lambda}{\left|\vec{M}\right|^2} \vec{M} \times (\vec{M} \times \vec{B}_{eff}) \tag{3.146}$$

where $\lambda > 0$. If one renormalizes the gyromagnetic ratio in Gilbert's equation as $\gamma' = \gamma(1 + G^2)$, above equation and Gilbert's are become equivalent. For small damping, the Gilbert and Landau-Lifshitz approaches become equivalent from physical viewpoint. In a same way, by using $\vec{M}'$ and $M \times B_{eff}$ with $C_x = (M_y B_z - M_z B_y)$, $C_y = (M_z B_x - M_x B_z)$ and $C_z = (M_x B_y - M_y B_x)$, one reachs $M \times B_{eff} = C_x \hat{i} + C_y \hat{j} + C_z \hat{k}$. Then

$$M \times (M \times B_{eff}) = \begin{vmatrix} \hat{i} & \hat{j} & \hat{k} \\ M_x & M_y & M_z \\ C_x & C_y & C_z \end{vmatrix} = (M_y C_z - M_z C_y)\hat{i} - (M_x C_z - M_z C_x)\hat{j} + (M_x C_y - M_y C_x)\hat{k}$$

$$\tag{3.147}$$

After using Eqs. 3.75 and 3.76, then Eq. 3.146 rewritten in its components as;

$$\frac{1}{\gamma}\frac{dM_x}{dt} = (M_y B_z - M_z B_y) - \frac{\lambda}{\gamma|M|^2}(M_y C_z - M_z C_y) \tag{3.148}$$

$$\frac{1}{\gamma}\frac{dM_y}{dt} = (M_z B_x - M_x B_z) - \frac{\lambda}{\gamma|M|^2}(M_z C_x - M_x C_z) \tag{3.149}$$

$$\frac{1}{\gamma}\frac{dM_z}{dt} = (M_x B_y - M_y B_x) - \frac{\lambda}{\gamma|M|^2} M \times (M_x B_y - M_y B_x) \qquad (3.150)$$

In Eq. 3.149, using $M_z' = 0$ condition:

$$0 = (M_x B_y - M_y B_x) - \frac{\lambda}{\gamma|M|^2} M \times (M_x B_y - M_y B_x)$$

it is obvious that $C_z = M_x B_y - M_y B_x = 0$.

$$\frac{1}{\gamma}\frac{dM_x}{dt} = (M_y B_z - M_z B_y) + \frac{\lambda}{\gamma|M|^2} M_z (M_z B_x - M_x B_z) \qquad (3.151)$$

$$\frac{1}{\gamma}\frac{dM_y}{dt} = (M_z B_x - M_x B_z) - \frac{\lambda}{\gamma|M|^2} M_z (M_y B_z - M_z B_y) \qquad (3.152)$$

Substitude $M_x' = i\omega M_x$ and $M_y' = i\omega M_y$ in the Eqs. 3.151 and 3.152 then

$$\left(i\frac{\omega}{\gamma} + \frac{\lambda}{\gamma|M|^2} M_z B_z \right) M_x - B_z M_y = -M_z B_y - \frac{\lambda}{\gamma|M|^2} M_z^2 B_x \qquad (3.153)$$

$$M_x B_z + \left(i\frac{\omega}{\gamma} + \frac{\lambda}{\gamma|M|^2} M_z B_z \right) M_y = B_x M_z + \frac{\lambda}{\gamma|M|^2} M_z^2 B_y \qquad (3.154)$$

Because the magnetic field is traveling along z-axis $B_z = B$, filed perpendicular in y-direction $B_y = B_\perp$ and so $B_x = 0$. Using the relations and $M_z = M$, $B_o = -\frac{\omega}{\gamma}$, and the linewidth parameter as $\Delta_B = \frac{\lambda}{\gamma\chi_o}$ (for case 1),

$$\left(-iB_o + \frac{\Delta_B \chi_o}{M} B \right) M_x - B M_y = -M B_\perp \qquad (3.155)$$

$$BM_x + \left(-iB_o + \frac{\Delta_B \chi_o}{M} B\right) M_y = \Delta_B \chi_o B_\perp \tag{3.156}$$

substitute the value of $M = M_o = M(B) = \chi_o B$ for *case 1, simplifies the relations as*

$$\left(-iB_o + \Delta_B\right) M_x - BM_y = -\chi_o BB_\perp \tag{3.157}$$

$$BM_x + \left(-iB_o + \Delta_B\right) M_y = \Delta_B \chi_o B_\perp \tag{3.158}$$

here take $a = -iB_o + \Delta_B$, $b = B$, $c = -\chi_o BB_\perp$ and $d = \Delta_B \chi_o B_\perp$ then the Eqs. 3.157 and 3.158 take the forms of

$$aM_x - bM_y = c \tag{3.159}$$

$$bM_x + aM_y = d \tag{3.160}$$

From the above relation $M_x = \dfrac{c + bM_y}{a}$ and use it at Eq. 3.160.

$$(a^2 + b^2) M_y = ad - bc \qquad \text{gives} \qquad M_y = \frac{ad - bc}{a^2 + b^2} \tag{3.161}$$

Substitute the terms of a, b, c and d again

$$M_y = \frac{\left(-iB_o + \Delta_B\right)\left(\Delta_B \chi_o B_\perp\right) + B(\chi_o BB_\perp)}{\left(-iB_o + \Delta_B\right)^2 + B^2} \tag{3.162}$$

$$M_y = \frac{\left(\Delta_B^2 \chi_o B_\perp + B^2 \chi_o B_\perp\right) - iB_o \Delta_B \chi_o B_\perp}{B^2 - B_o^2 + \Delta_B^2 - i2B_o \Delta_B}$$

$$M_y = \frac{\chi_o B_\perp \left(\Delta_B^2 + B^2\right) - iB_o \Delta_B \chi_o B_\perp}{B^2 - B_o^2 + \Delta_B^2 - i2B_o \Delta_B} \tag{3.163}$$

Multiply both numerator and denominator with conjugate of denominator $B^2 - B_o^2 + \Delta_B^2 + i2B_o\Delta_B$ then complex part of M_y is obtained as;

$$M''_y = \frac{2B_o\Delta_B\chi_oB_\perp\left(\Delta_B^2 + B^2\right) - B_o\Delta_B\chi_oB_\perp\left(B^2 - B_o^2 + \Delta_B^2\right)}{\left(B^2 - B_o^2 + \Delta_B^2\right)^2 + \left(2B_o\Delta_B\right)^2}$$ (3.164)

$$M''_y = \frac{B_o\Delta_B\chi_oB_\perp\left(\Delta_B^2 + B^2 + B_o^2\right)}{\left(B^2 - B_o^2\right)^2 + \Delta_B^4 + 2\Delta_B^2\left(B^2 - B_o^2\right) + 4B_o^2\Delta_B^2}$$

$$M''_y = \frac{B_o\Delta_B\chi_oB_\perp\left(\Delta_B^2 + B^2 + B_o^2\right)}{\left(B^2 - B_o^2\right)^2 + \Delta_B^4 + 2\Delta_B^2B^2 + 2B_o^2\Delta_B^2}$$ (3.165)

If we add and subtract the $2B^2B_o^2$ term to the denominator

$$M''_y = \frac{B_o\Delta_B\chi_oB_\perp\left(\Delta_B^2 + B^2 + B_o^2\right)}{\left(B^2 + B_o^2\right)^2 + \Delta_B^4 + 2\Delta_B^2\left(B^2 + B_o^2\right) - 4B^2B_o^2}$$

$$M''_y = \frac{B_o\Delta_B\chi_oB_\perp\left(\Delta_B^2 + B^2 + B_o^2\right)}{\left[\left(B^2 + B_o^2\right) + \Delta_B^2\right]^2 - 4B^2B_o^2}$$ (3.166)

The denominator can be thought as $x^2 - y^2 = (x-y)(x+y)$, then

$$M''_y = \frac{B_o\Delta_B\chi_oB_\perp\left(\Delta_B^2 + B^2 + B_o^2\right)}{\left[\left(B^2 + B_o^2\right) + \Delta_B^2 - 2BB_o\right]\left[\left(B^2 + B_o^2\right) + \Delta_B^2 + 2BB_o\right]}$$

$$M''_y = \frac{B_o\Delta_B\chi_oB_\perp\left(\Delta_B^2 + B^2 + B_o^2\right)}{\left[\left(B - B_o\right)^2 + \Delta_B^2\right]\left[\left(B + B_o\right)^2 + \Delta_B^2\right]}$$ (3.167)

From the Eq. 3.73, the imaginary part of M_y gives the imaginary part of susceptibility χ'';

$$\chi'' = \frac{M_y''}{B_\perp} = \frac{B_o \Delta_B \chi_o \left(\Delta_B^2 + B^2 + B_o^2\right)}{\left[(B - B_o)^2 + \Delta_B^2\right]\left[(B + B_o)^2 + \Delta_B^2\right]} \tag{3.168}$$

Here χ'' is the function of B and to determine the χ_o constant, $\chi''(B)$ function is normalized to unity $\int_{-\infty}^{\infty} \chi''(B)dB = 1$, and it gives $\chi_o = \frac{1}{\pi B_o}$

$$\chi'' = \frac{M_y''}{B_\perp} = \frac{1}{\pi} \frac{\Delta_B \left(\Delta_B^2 + B^2 + B_o^2\right)}{\left[(B - B_o)^2 + \Delta_B^2\right]\left[(B + B_o)^2 + \Delta_B^2\right]} \tag{3.169}$$

this is solution of **Landau-Lifshitz case 1** and it is same as the *modified Bloch case 1* (Eq. 3.121) and *Gilbert's case 2* (Eq. 3.146).

In **Landau-Lifshitz case 2** linewidth parameter $\Delta_B = \frac{\lambda B_o}{\gamma M_o}$, and others are

$B_z = B$, $B_y = B_\perp$, $B_x = 0$, $M_z = M$ an and $B_o = -\frac{\omega}{\gamma}$ substituted in Eqs. 3.153 and 3.154;

$$\left(-iB_o + \frac{\Delta_B}{B_o} B\right)M_x - BM_y = -MB_\perp \tag{3.170}$$

$$BM_x + \left(-iB_o + \frac{\Delta_B}{M_o} B\right)M_y = \frac{\Delta_B}{M_o} MB_\perp \tag{3.171}$$

here take $a = \left(-iB_o + \frac{\Delta_B}{M_o} B\right)$, $b = B$, $c = -MB_\perp$ and $d = \frac{\Delta_B}{B_o} MB_\perp$ then the Eqs. 3.170 and 3.171 take the forms of

$$aM_x - bM_y = c \tag{3.172}$$

$$bM_x + aM_y = d \tag{3.173}$$

From the above relation $M_x = \dfrac{c + bM_y}{a}$ and use it at Eq. 3.173

$$(a^2 + b^2)M_y = ad - bc \quad \text{gives} \quad M_y = \frac{ad - bc}{a^2 + b^2} \tag{3.174}$$

Substitute the terms of a, b, c and d again

$$M_y = \frac{\left(-iB_o + \dfrac{\Delta_B}{B_o}B\right)\left(\dfrac{\Delta_B}{B_o}MB_\perp\right) + MBB_\perp}{\left(-iB_o + \dfrac{\Delta_B}{B_o}B\right)^2 + B^2} \tag{3.175}$$

$$M_y = \frac{\left[MBB_\perp + \left(\dfrac{\Delta_B}{B_o}\right)^2 MBB_\perp\right] - i\Delta_B MB_\perp}{B^2 - B_o^2 + \left(\dfrac{\Delta_B}{B_o}\right)^2 B^2 - i2\Delta_B B} \tag{3.176}$$

Multiply both numerator and denominator with conjugate of denominator $B^2 - B_o^2 + \left(\dfrac{\Delta_B}{B_o}\right)^2 B^2 + i2\Delta_B B$ then complex part of M_y is obtained as;

$$M_y'' = \frac{-\Delta_B MB_\perp\left[B^2 - B_o^2 + \left(\dfrac{\Delta_B}{B_o}\right)^2 B^2\right] + 2\Delta_B B\left[MBB_\perp + \left(\dfrac{\Delta_B}{B_o}\right)^2 MBB_\perp\right]}{\left(B^2 - B_o^2\right)^2 + 2\left(B^2 - B_o^2\right)\left(\dfrac{\Delta_B}{B_o}B\right)^2 + \left(\dfrac{\Delta_B}{B_o}B\right)^4 + (2\Delta_B B)^2}$$

$$M_y'' = \frac{\Delta_B B^2 MB_\perp + \Delta_B B^2 MB_\perp\left(\dfrac{\Delta_B}{B_o}\right)^2 + \Delta_B MB_\perp B_o^2}{\left(B^2 - B_o^2\right)^2 + 2B^2\left(\dfrac{\Delta_B}{B_o}B\right)^2 + 2(\Delta_B B)^2 + \left(\dfrac{\Delta_B}{B_o}B\right)^4} \tag{3.177}$$

If we add and subtract the $2B^2 B_o^2$ term to the denominator

$$M''_y = \frac{\Delta_B M B_\perp \left[B^2 + B_o^2 + B^2 \left(\dfrac{\Delta_B}{B_o} \right)^2 \right]}{\left(B^2 + B_o^2 \right)^2 + 2 \left(B^2 + B_o^2 \right) \left(\dfrac{\Delta_B}{B_o} B \right) + \left(\dfrac{\Delta_B}{B_o} B \right)^4 - 4 B^2 B_o^2}$$

$$M''_y = \frac{\left(\dfrac{1}{B_o^2} \right) \Delta_B M B_\perp \left[B_o^2 B^2 + B_o^4 + \Delta_B^2 B^2 \right]}{\left[B^2 + B_o^2 + \left(\dfrac{\Delta_B}{B_o} B \right)^2 \right]^2 - 4 B^2 B_o^2} \tag{3.178}$$

The denominator can be thought as $x^2 - y^2 = (x - y)(x + y)$, then

$$M''_y = \frac{\left(\dfrac{1}{B_o^2} \right) \Delta_B M B_\perp \left[\left(B_o^2 + \Delta_B^2 \right) B^2 + B_o^4 \right]}{\left[B^2 + B_o^2 + \left(\dfrac{\Delta_B}{B_o} B \right)^2 - 2 B B_o \right] \left[B^2 + B_o^2 + \left(\dfrac{\Delta_B}{B_o} B \right)^2 + 2 B B_o \right]}$$

$$M''_y = \frac{\left(\dfrac{1}{B_o^2} \right) \Delta_B M B_\perp \left[\left(B_o^2 + \Delta_B^2 \right) B^2 + B_o^4 \right]}{\left[(B - B_o)^2 + \left(\dfrac{\Delta_B}{B_o} B \right)^2 \right] \left[(B + B_o)^2 + \left(\dfrac{\Delta_B}{B_o} B \right)^2 \right]}$$

$$M''_y = \frac{\left(\dfrac{1}{B_o^2} \right) \Delta_B M B_\perp \left[\left(B_o^2 + \Delta_B^2 \right) B^2 + B_o^4 \right]}{\left(\dfrac{1}{B_o^4} \right) \left[(B - B_o)^2 B_o^2 + \Delta_B^2 B^2 \right] \left[(B + B_o)^2 B_o^2 + \Delta_B^2 B^2 \right]}$$

$$M''_y = \frac{B_o^2 \Delta_B M B_\perp \left[\left(B_o^2 + \Delta_B^2 \right) B^2 + B_o^4 \right]}{\left[(B - B_o)^2 B_o^2 + \Delta_B^2 B^2 \right] \left[(B + B_o)^2 B_o^2 + \Delta_B^2 B^2 \right]}$$

(3.179)

The imaginary part of M_y gives the imaginary part of susceptibility χ'';

$$\chi'' = \frac{M''_y}{B_\perp} = \frac{B_o^2 \Delta_B M \left[\left(B_o^2 + \Delta_B^2 \right) B^2 + B_o^4 \right]}{\left[(B - B_o)^2 B_o^2 + \Delta_B^2 B^2 \right] \left[(B + B_o)^2 B_o^2 + \Delta_B^2 B^2 \right]}$$

(3.180)

Take $M = M_o = M(B) = \chi_o \, \text{sgn}(B)$ (for **case 2**)

$$\chi''(B) = \frac{B_o^2 \Delta_B M_o \left[\left(B_o^2 + \Delta_B^2 \right) B^2 + B_o^4 \right]}{\left[(B - B_o)^2 B_o^2 + \Delta_B^2 B^2 \right] \left[(B + B_o)^2 B_o^2 + \Delta_B^2 B^2 \right]}$$

(3.181)

Here χ'' is the function of B and to determine the M_o constant, $\chi''(B)$ function is normalized to unity $\int_{-\infty}^{\infty} \chi''(B) dB = 1$ and it gives

$$\frac{M}{2} \arctan\left(\frac{\left(B_o^2 + \Delta_B^2 \right) B + B_o^3}{B_o^2 \Delta_B} \right) + \frac{M}{2} \arctan\left(\frac{\left(B_o^2 + \Delta_B^2 \right) B - B_o^3}{B_o^2 \Delta_B} \right) \Bigg]_{-\infty}^{\infty} = 1$$

using the arctan at + or − infinity as $\lim_{x \to \infty} (\arctan x) = \frac{\pi}{2}$ and $\lim_{x \to -\infty} (\arctan x) = -\frac{\pi}{2}$, we obtain

$$\left[\frac{M_o}{2} (\frac{\pi}{2}) + \frac{M_o}{2} (\frac{\pi}{2}) \right] - \left[\frac{M_o}{2} (-\frac{\pi}{2}) + \frac{M_o}{2} (-\frac{\pi}{2}) \right] = 1$$

and so $M_o \pi = 1$ or $M_o = \frac{1}{\pi}$. Substitute it in Eq. 3.181.

$$\chi''(B) = \frac{1}{\pi} \frac{B_o^2 \Delta_B \left[\left(B_o^2 + \Delta_B^2 \right) B^2 + B_o^4 \right]}{\left[(B - B_o)^2 B_o^2 + \Delta_B^2 B^2 \right] \left[(B + B_o)^2 B_o^2 + \Delta_B^2 B^2 \right]}$$

(3.182)

As a result Eq. 3.182 is the form of In *Landau-Lifshitz case 2*.

3.5.5 Callen equation

The Callen dynamical equation with damping has been obtained using a quantum mechanical approach by quantizing the spin waves into magnons [51]:

$$\vec{M}' = \gamma \vec{M} \times \vec{B}_{eff} + \frac{\lambda}{|\vec{M}|^2} \vec{M} \times (\vec{M} \times \vec{B}_{eff}) - \alpha \vec{M} \tag{3.183}$$

Note that the first damping term in the equation coincides with the Landau-Lifshitz one, Eq. 3.146, while the second one has the same form as the Bloch-Bloembergen one, Eq. 3.74., in the case of the lateral relaxation, if one puts $\alpha = 1/T_2$.

In case 1, noting that $\Delta_B = \frac{\lambda}{|\gamma|\chi_o}$ and $\delta_B = \frac{\alpha}{|\gamma|}$. By using the relations from past section; $M \times B_{eff}$, $C_x = (M_y B_z - M_z B_y)$, $C_y = (M_z B_x - M_x B_z)$, $C_z = (M_x B_y - M_y B_x)$, $M \times B_{eff} = C_x \hat{i} + C_y \hat{j} + C_z \hat{k}$ and $\vec{M}'$, then Eq. 3.183 becomes:

$$\frac{1}{\gamma} \frac{dM_x}{dt} = (M_y B_z - M_z B_y) - \frac{\lambda}{\gamma |M|^2} (M_y C_z - M_z C_y) - \frac{\alpha}{\gamma} M_x \tag{3.184}$$

$$\frac{1}{\gamma} \frac{dM_y}{dt} = (M_z B_x - M_x B_z) - \frac{\lambda}{\gamma |M|^2} (M_z C_x - M_x C_z) - \frac{\alpha}{\gamma} M_y \tag{3.185}$$

$$\frac{1}{\gamma} \frac{dM_z}{dt} = (M_x B_y - M_y B_x) - \frac{\lambda}{\gamma |M|^2} M \times (M_x B_y - M_y B_x) - \frac{\alpha}{\gamma} M_z \tag{3.186}$$

As abovementioned condition $M_z' = 0$ gives $(M_x B_y - M_y B_x) = 0$ or $C_z = 0$. So

$$\frac{1}{\gamma} \frac{dM_x}{dt} = (M_y B_z - M_z B_y) + \frac{\lambda}{\gamma |M|^2} M_z (M_z B_x - M_x B_z) - \frac{\alpha}{\gamma} M_x \tag{3.187}$$

$$\frac{1}{\gamma}\frac{dM_y}{dt} = (M_z B_x - M_x B_z) - \frac{\lambda}{\gamma|M|^2}M_z(M_y B_z - M_z B_y) - \frac{\alpha}{\gamma}M_y \tag{3.188}$$

linewidth parameter $\Delta_B = \dfrac{\lambda}{|\gamma|\chi_o}$ and others are $\delta_B = \dfrac{\alpha}{|\gamma|}$ $B_z = B$, $B_y = B_\perp$, $B_x = 0$,

$M_z = M$ an and $B_o = -\dfrac{\omega}{\gamma}$ substituted in Eqs. 3.187 and 3.188;

$$(-iB_o + \delta_B + \Delta_B)M_x - BM_y = -\chi_o BB_\perp \tag{3.189}$$

$$BM_x + (-iB_o + \delta_B + \Delta_B)M_y = \chi_o \Delta_B B_\perp \tag{3.190}$$

here take $a = (-iB_o + \delta_B + \Delta_B)$, $b = B$, $c = -\chi_o BB_\perp$ and $d = \chi_o \Delta_B B_\perp$ then the Eqs 3.189 and 3.190 take the forms of

$$aM_x - bM_y = c \tag{3.191}$$

$$bM_x + aM_y = d \tag{3.192}$$

From the above relation $M_x = \dfrac{c + bM_y}{a}$ and use it at Eq. 3.192.

$$(a^2 + b^2)M_y = ad - bc \qquad \text{gives} \qquad M_y = \frac{ad - bc}{a^2 + b^2} \tag{3.193}$$

Substitute the terms of a, b, c and d again

$$M_y = \frac{\chi_o \Delta_B B_\perp(-iB_o + \delta_B + \Delta_B) + \chi_o B^2 B_\perp}{(-iB_o + \delta_B + \Delta_B)^2 + B^2} \tag{3.194}$$

$$M_y = \frac{(\delta_B + \Delta_B)\chi_o \Delta_B B_\perp + \chi_o B^2 B_\perp - i\chi_o B_o \Delta_B B_\perp}{B^2 - B_o^2 + (\delta_B + \Delta_B)^2 - iB_o(\delta_B + \Delta_B)} \tag{3.195}$$

Multiply both numerator and denominator with conjugate of denominator $B^2 - B_o^2 + (\delta_B + \Delta_B)^2 + iB_o(\delta_B + \Delta_B)$ then complex part of M_y is obtained as;

$$M_y'' = \frac{\chi_o \Delta_B B_\perp B_o \left[2(\delta_B + \Delta_B)^2 + B_o^2 - (\delta_B + \Delta_B)^2\right] + \chi_o B_\perp B_o B^2 \left[2\delta_B + \Delta_B\right]}{\left(B^2 - B_o^2\right)^2 + 2B^2(\delta_B + \Delta_B)^2 + (\delta_B + \Delta_B)^4 + 2B_o^2(\delta_B + \Delta_B)^2}$$

$$M_y'' = \frac{\chi_o \Delta_B B_\perp B_o \left[2\delta_B^2 + 4\delta_B \Delta_B + 2\Delta_B^2 + B_o^2 - \delta_B^2 - 2\delta_B \Delta_B - \Delta_B^2\right] + \chi_o B_\perp B_o B^2 \left[2\delta_B + \Delta_B\right]}{\left(B^2 - B_o^2\right)^2 + 2B^2(\delta_B + \Delta_B)^2 + (\delta_B + \Delta_B)^4 + 2B_o^2(\delta_B + \Delta_B)^2}$$

$$M_y'' = \frac{\chi_o \Delta_B B_\perp B_o \left[\delta_B^2 + 2\delta_B \Delta_B + \Delta_B^2 + B_o^2\right] + \chi_o B_\perp B_o B^2 \left[2\delta_B + \Delta_B\right]}{\left(B^2 - B_o^2\right)^2 + 2B^2(\delta_B + \Delta_B)^2 + (\delta_B + \Delta_B)^4 + 2B_o^2(\delta_B + \Delta_B)^2} \tag{3.196}$$

If we add and subtract the $2B^2 B_o^2$ term to the denominator

$$M_y'' = \frac{\chi_o B_\perp B_o \left\{\Delta_B \left[(\delta_B + \Delta_B)^2 + B_o^2\right] + B^2 \left[2\delta_B + \Delta_B\right]\right\}}{\left(B^2 + B_o^2\right)^2 + 2B^2(\delta_B + \Delta_B)^2 + (\delta_B + \Delta_B)^4 + 2B_o^2(\delta_B + \Delta_B)^2 - 4B^2 B_o^2}$$

$$M_y'' = \frac{\chi_o B_\perp B_o \left\{\Delta_B \left[(\delta_B + \Delta_B)^2 + B_o^2\right] + B^2 \left[2\delta_B + \Delta_B\right]\right\}}{\left(B^2 + B_o^2\right)^2 + 2\left(B^2 + B_o^2\right)(\delta_B + \Delta_B)^2 + (\delta_B + \Delta_B)^4 - 4B^2 B_o^2}$$

$$M_y'' = \frac{\chi_o B_\perp B_o \left\{\Delta_B \left[(\delta_B + \Delta_B)^2 + B_o^2\right] + B^2 \left[2\delta_B + \Delta_B\right]\right\}}{\left[\left(B^2 + B_o^2\right) + (\delta_B + \Delta_B)^2\right]^2 - 4B^2 B_o^2} \tag{3.197}$$

The denominator can be thought as $x^2 - y^2 = (x - y)(x + y)$, then

$$M_y'' = \frac{\chi_o B_\perp B_o \left\{\Delta_B \left[(\delta_B + \Delta_B)^2 + B_o^2\right] + B^2 \left[2\delta_B + \Delta_B\right]\right\}}{\left[\left(B^2 + B_o^2\right) + (\delta_B + \Delta_B)^2 - 2B^2 B_o^2\right]\left[\left(B^2 + B_o^2\right) + (\delta_B + \Delta_B)^2 + 2B^2 B_o^2\right]}$$

$$M_y'' = \frac{\chi_o B_\perp B_o \left\{\Delta_B \left[(\delta_B + \Delta_B)^2 + B_o^2\right] + B^2 \left[2\delta_B + \Delta_B\right]\right\}}{\left[(B - B_o)^2 + (\delta_B + \Delta_B)^2\right]\left[(B + B_o)^2 + (\delta_B + \Delta_B)^2\right]} \tag{3.198}$$

Again take the imaginary part of M_y to find the imaginary part of susceptibility χ'';

$$\chi'' = \frac{M_y''}{B_\perp} = \frac{\chi_o B_o \left\{ \Delta_B \left[(\delta_B + \Delta_B)^2 + B_o^2 \right] + B^2 \left[2\delta_B + \Delta_B \right] \right\}}{\left[(B - B_o)^2 + (\delta_B + \Delta_B)^2 \right] \left[(B + B_o)^2 + (\delta_B + \Delta_B)^2 \right]} \qquad (3.199)$$

Here χ'' is the function of B and to determine the χ_o constant, $\chi''(B)$ function is normalized to unity $\int_{-\infty}^{\infty} \chi''(B)dB = 1$, and it gives $\chi_o = \frac{1}{\pi B_o}$

$$\chi''(B) = \frac{\Delta_B \left[(\delta_B + \Delta_B)^2 + B_o^2 \right] + B^2 (2\delta_B + \Delta_B)}{\left[(B - B_o)^2 + (\delta_B + \Delta_B)^2 \right] \left[(B + B_o)^2 + (\delta_B + \Delta_B)^2 \right]}, \qquad (3.200)$$

this is solution of *Callen's* equation *case 1.*

In *case 2*, the linewidth parameter is taken as $\Delta_B = \frac{\lambda B_o}{|\gamma| M_o}$ and $\delta_B = \frac{\alpha}{|\gamma|}$ is same as before one. By using the relations in last section again and the conditions $B_z = B$, $B_y = B_\perp$, $B_x = 0$, $M_z = M$ and $B_o = -\frac{\omega}{\gamma}$ substituted in Eqs. 3.187 and 3.188, then Eq. 3.183 becomes:

$$\left(-iB_o + \delta_B + \frac{\Delta_B}{B_o} B \right) M_x - BM_y = -MB_\perp \qquad (3.201)$$

$$BM_x + \left(-iB_o + \delta_B + \frac{\Delta_B}{B_o} B \right) M_y = \frac{\Delta_B}{B_o} MB_\perp \qquad (3.202)$$

here take $a = \left(-iB_o + \delta_B + \frac{\Delta_B}{B_o} B \right)$, $b = B$, $c = -MB_\perp$ and $d = \frac{\Delta_B}{B_o} MB_\perp$ then the Eqs. 3.201 and 3.202 take the forms of

$$aM_x - bM_y = c \qquad \text{and} \qquad bM_x + aM_y = d \qquad (3.203\text{-}3.204)$$

From the above relation $M_x = \dfrac{c + bM_y}{a}$ and use it at Eq. 3.204

$$(a^2 + b^2)M_y = ad - bc \qquad \text{gives} \qquad M_y = \frac{ad - bc}{a^2 + b^2} \qquad (3.205)$$

Substitute the terms of a, b, c and d again

$$M_y = \frac{\dfrac{\Delta_B}{B_o} MB_\perp \left(-iB_o + \delta_B + \dfrac{\Delta_B}{B_o} B \right) + MBB_\perp}{\left(-iB_o + \delta_B + \dfrac{\Delta_B}{B_o} B \right)^2 + B^2} \qquad (3.206)$$

$$M_y = \frac{MBB_\perp + MBB_\perp \left(\dfrac{\Delta_B}{B_o} \right)^2 + MB_\perp \delta_B \left(\dfrac{\Delta_B}{B_o} \right) - i\Delta_B MB_\perp}{B^2 - B_o^2 + \left(\delta_B + \dfrac{\Delta_B}{B_o} B \right)^2 - i2B_o \left(\delta_B + \dfrac{\Delta_B}{B_o} B \right)}$$

$$M_y = \frac{\left(\dfrac{1}{B_o^2} \right) MB_\perp \left[BB_o^2 + \Delta_B (\delta_B B_o + \Delta_B B) - i\Delta_B B_o^2 \right]}{B^2 - B_o^2 + \left(\delta_B + \dfrac{\Delta_B}{B_o} B \right)^2 - i2B_o \left(\delta_B + \dfrac{\Delta_B}{B_o} B \right)} \qquad (3.207)$$

Multiply both numerator and denominator with conjugate of denominator $B^2 - B_o^2 + \left(\delta_B + \dfrac{\Delta_B}{B_o} B \right)^2 + i2B_o \left(\delta_B + \dfrac{\Delta_B}{B_o} B \right)$ then complex part of M_y is obtained as;

$$M_y'' = \frac{\left(\dfrac{1}{B_o^2} \right) MB_\perp \left\{ 2B_o \left(\delta_B + \dfrac{\Delta_B}{B_o} B \right) \left[BB_o^2 + \Delta_B (\delta_B B_o + \Delta_B B) \right] - \Delta_B B_o^2 \left[B^2 - B_o^2 + \left(\delta_B + \dfrac{\Delta_B}{B_o} B \right)^2 \right] \right\}}{(B^2 - B_o^2)^2 + 2(B^2 - B_o^2) \left(\delta_B + \dfrac{\Delta_B}{B_o} B \right)^2 + \left(\delta_B + \dfrac{\Delta_B}{B_o} B \right)^4 + 4B_o^2 \left(\delta_B + \dfrac{\Delta_B}{B_o} B \right)^2}$$

$$M''_y = \frac{\left(\frac{1}{B_o^2}\right)MB_\perp \left\{2(B_o\delta_B + \Delta_B B)\left[BB_o^2 + \Delta_B(\delta_B B_o + \Delta_B B)\right] - \Delta_B\left[B_o^2(B^2 - B_o^2) + (B_o\delta_B + \Delta_B B)^2\right]\right\}}{(B^2 - B_o^2)^2 + 2B^2\left(\delta_B + \frac{\Delta_B}{B_o}B\right)^2 + 2B_o^2\left(\delta_B + \frac{\Delta_B}{B_o}B\right)^2 + \left(\delta_B + \frac{\Delta_B}{B_o}B\right)^4}$$

If we add and subtract the $2B^2 B_o^2$ term to the denominator

$$M''_y = \frac{\left(\frac{1}{B_o^2}\right)MB_\perp \left\{(B_o\delta_B + \Delta_B B)^2(2\Delta_B - \Delta_B) + 2BB_o^3\delta_B + 2B^2 B_o^2\Delta_B - B^2 B_o^2\Delta_B + \Delta_B B_o^4\right\}}{(B^2 + B_o^2)^2 + 2(B^2 + B_o^2)\left(\delta_B + \frac{\Delta_B}{B_o}B\right)^2 + \left(\delta_B + \frac{\Delta_B}{B_o}B\right)^4 - 4B^2 B_o^2} \quad (3.208)$$

$$M''_y = \frac{\left(\frac{1}{B_o^2}\right)MB_\perp \left[\Delta_B(B_o\delta_B + \Delta_B B)^2 + B_o^2\left(2BB_o\delta_B + B^2\Delta_B + \Delta_B B_o^2\right)\right]}{\left[(B^2 + B_o^2) + \left(\delta_B + \frac{\Delta_B}{B_o}B\right)^2\right]^2 - 4B^2 B_o^2}$$

$$M''_y = \frac{\left(\frac{1}{B_o^2}\right)MB_\perp \left[\Delta_B\left(B_o^2\delta_B^2 + 2B_o\delta_B\Delta_B B + \Delta_B^2 B^2\right) + 2BB_o^3\delta_B + B_o^2\Delta_B\left(+ B^2 + B_o^2\right)\right]}{\left[(B^2 + B_o^2) + \left(\delta_B + \frac{\Delta_B}{B_o}B\right)^2\right]^2 - 4B^2 B_o^2}$$

$$M''_y = \frac{\left(\frac{1}{B_o^2}\right)MB_\perp \left[\Delta_B\left(B_o^2\delta_B^2 + \Delta_B^2 B^2\right) + 2B_o\delta_B\Delta_B^2 B + 2BB_o^3\delta_B + B_o^2\Delta_B\left(+ B^2 + B_o^2\right)\right]}{\left[(B^2 + B_o^2) + \left(\delta_B + \frac{\Delta_B}{B_o}B\right)^2\right]^2 - 4B^2 B_o^2} \quad (3.209)$$

The denominator can be thought as $x^2 - y^2 = (x - y)(x + y)$, then

$$M''_y = \frac{\left(\frac{1}{B_o^2}\right)MB_\perp \left[\Delta_B\left(B_o^2\delta_B^2 + \Delta_B^2 B^2\right) + 2B_o\delta_B B\left(\Delta_B^2 + B_o^2\right) + B_o^2\Delta_B\left(B^2 + B_o^2\right)\right]}{\left[(B^2 + B_o^2) + \left(\delta_B + \frac{\Delta_B}{B_o}B\right)^2 - 2BB_o\right]\left[(B^2 + B_o^2) + \left(\delta_B + \frac{\Delta_B}{B_o}B\right)^2 + 2BB_o\right]}$$

$$M_y'' = \frac{\left(\frac{1}{B_o^2}\right)MB_\perp\left[\Delta_B B_o^2 \delta_B^2 + \Delta_B^3 B^2 + 2B_o\delta_B B\left(\Delta_B^2 + B_o^2\right) + B^2 B_o^2 \Delta_B + B_o^4 \Delta_B\right]}{\left[(B-B_o)^2 + \left(\delta_B + \frac{\Delta_B}{B_o}B\right)^2\right]\left[(B+B_o)^2 + \left(\delta_B + \frac{\Delta_B}{B_o}B\right)^2\right]}$$

$$M_y'' = \frac{\left(\frac{1}{B_o^2}\right)MB_\perp\left[\Delta_B B_o^2\left(\delta_B^2 + B_o^2\right) + \Delta_B B^2\left(\Delta_B^2 + B_o^2\right) + 2B_o\delta_B B\left(\Delta_B^2 + B_o^2\right)\right]}{\left(\frac{1}{B_o^4}\right)\left[(B-B_o)^2 B_o^2 + (\delta_B B_o + \Delta_B B)^2\right]\left[(B+B_o)^2 B_o^2 + (\delta_B B_o + \Delta_B B)^2\right]}$$

$$M_y'' = \frac{B_o^2 MB_\perp\left[\Delta_B B_o^2\left(\delta_B^2 + B_o^2\right) + \left(\Delta_B B^2 + 2B_o\delta_B B\right)\left(\Delta_B^2 + B_o^2\right)\right]}{\left[(B-B_o)^2 B_o^2 + (\delta_B B_o + \Delta_B B)^2\right]\left[(B+B_o)^2 B_o^2 + (\delta_B B_o + \Delta_B B)^2\right]} \qquad (3.210)$$

Again take the imaginary part of M_y to find the imaginary part of susceptibility χ'';

$$\chi'' = \frac{M_y''}{B_\perp} = \frac{B_o^2 M\left[\Delta_B B_o^2\left(\delta_B^2 + B_o^2\right) + \left(\Delta_B B^2 + 2B_o\delta_B B\right)\left(\Delta_B^2 + B_o^2\right)\right]}{\left[(B-B_o)^2 B_o^2 + (\delta_B B_o + \Delta_B B)^2\right]\left[(B+B_o)^2 B_o^2 + (\delta_B B_o + \Delta_B B)^2\right]} \qquad (3.211)$$

Here $M = M_o\,\mathrm{sgn}(B)\,\chi''$ is the function of B and to determine the M_o constant, $\chi''(B)$ function is normalized to unity $\int_{-\infty}^{\infty}\chi''(B)dB = 1$, and it gives $M_o = N^{-1}$

$$\chi''(B) = \frac{1}{N}\frac{B_o^2\left[\Delta_B B_o^2\left(\delta_B^2 + B_o^2\right) + \left(\Delta_B B^2 + 2B_o\delta_B B\right)\left(\Delta_B^2 + B_o^2\right)\right]}{\left[(B-B_o)^2 B_o^2 + (\delta_B B_o + \Delta_B B)^2\right]\left[(B+B_o)^2 B_o^2 + (\delta_B B_o + \Delta_B B)^2\right]}, \qquad (3.212)$$

where $N = \pi - \arctan\left(\frac{B_o^2 + \Delta_B\delta_B}{B_o(\Delta_B - \delta_B)}\right) + \arctan\left(\frac{B_o^2 - \Delta_B\delta_B}{B_o(\Delta_B + \delta_B)}\right)$. This is solution of *Callen's* equation for *case 2.*

3.6 PROPERTIES OF MAGNETITE

3.6.1 Crystal structure of magnetite

Magnetite (Fe_3O_4) has an inverse spinel crystal structure with face centered cubic unit cell where oxygen ions are placed regularly in cubic close packed positions along the [111] axis [21]. Magnetite's oxygen ion array contains holes partially filled with ferric and ferrous ions [21, 52]. The unit cell is comprised of 56 atoms: 32 O^{2-} anions, 16 Fe^{3+} cations and 8 Fe^{2+} cations [16]. Magnetite's chemical formula is Fe_3O_4, however more appropriately it is defined as $FeO·Fe_2O_3$. The inverse spinel structure is arranged such that half of the Fe_{3+} ions are tetrahedrally coordinated and the remaining half of Fe^{3+} and all of the Fe^{2+} are octahedrally coordinated (Figure 3.5).
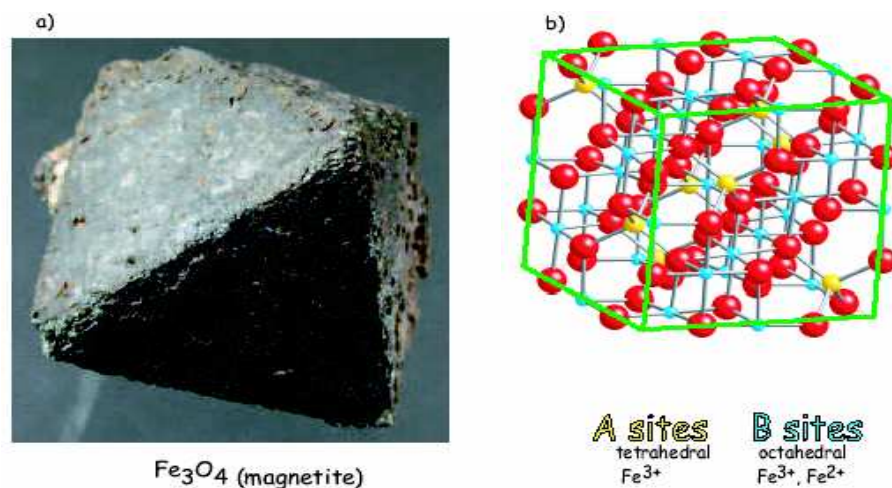

Figure 3.5 a) A magnetite octahedron. **b)** Internal crystal structure. Big red dots are the oxygen anions (O^{2-}). The blue dots are iron cations in octahedral coordination and the yellow dots are in tetrahedral coordination. Fe^{3+} sits on the A sites and Fe^{2+} and Fe^{3+} sit on the B sites[55].

3.6.2 Magnetic properties of magnetite

Magnetite's electronic configuration consists of unpaired 3d electrons, which impart net magnetic moments. The spins of the tetrahedrally (A) coordinated Fe^{3+} and

the spins of the octahedrally (B) coordinated Fe^{3+} and Fe^{2+} are antiparallel and unequal in magnitude (Figure 3.6.a) [18].
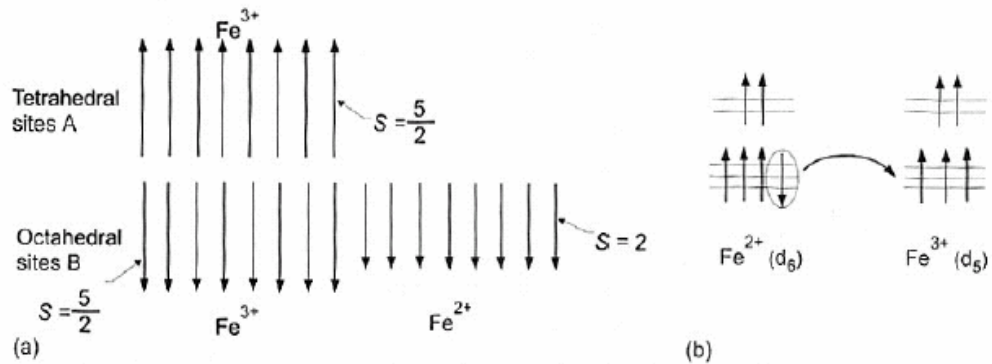
Figure 3.6. (a) Spin arrangements in magnetite, $FeO \cdot Fe_2O_3$, and **(b)** the double exchange interaction with inter-ion electron transfer [19].

Table 3.3 Summarized properties of magnetite

Name	Magnetite
Formula	Fe_3O_4
Magnetic response	Ferrimagnetic
Saturation Magnetization (M_S)(emu/cm^3)	480-500 at 298 K
Curie Temperature (K)	858
Crystal system	Cubic
Cell dimensions (nm)	a = 0.839
Density (g/cm3)	5.26
Color	black
Magnetic susceptibility (emu/g)	90 [56] – 98 [20]
Estimated maximum single-domain size for spherical particles [17, 28, 57] Ds (nm)	128

Below the Curie temperature (850K) these interpenetrating sublattices aligned antiparallel with unequal moments give rise to the observed ferrimagnetism [21]. The spin arrangements of the two interpenetrating sublattices of the octahedrally coordinated

Fe^{2+} and Fe^{3+} are coupled ferromagnetically via a double-exchange mechanism associated with inter-ion electron transfer (Figure 3.6.b) [19, 53]. The easy axis of magnetite is the cube edge. The crystalline magnetic anisotropy constant (K) for magnetite is 1.4 x 10^5 erg/cm^3 and the superparamagnetic maximum critical particle size estimated from KV ~25kT is ~25 nm, which is lower than the single domain critical size in Table 3.3 [54].

CHAPTER 4

EXPERIMENTAL

4.1 SYNTHESIS AND CHARACTERIZATION

4.1.1 Chemicals and materials

All chemicals were of reagent grade and used without further purification. Ferric chloride hexahydrate ($FeCl_3 \cdot 6H_2O > 99\%$), ferrous chloride tetrahydrate ($FeCl_2 \cdot 4H_2O > 99\%$), and starch (25-30KDa, $(C_6H_{10}O_5)_n > 99\%$) were obtained from Aldrich. Hydrogen peroxide ($H_2O_2 > 99\%$) and hydrochloric acid ($HCl > 37\%$) were obtained from KEBO. Milli-Q water was re-deionized (specific conductance < 0.1 s/cm) and deoxygenated by bubbling N_2 gas for 1 hr prior to use.

4.1.2 Preparation of magnetic colloid

The chemical reaction of Fe_3O_4 precipitation is given by,

$$Fe^{2+} + 2\ Fe^{3+} + 8\ OH^- \rightarrow Fe_3O_4 + 4\ H_2O.$$

according to the results of thermodynamic modeling of this system, a complete precipitation of Fe_3O_4 is expected in the pH range pH=7.5-14, while maintaining a molar ratio of Fe^{2+}: Fe^{3+} = 1:2 under a non-oxidizing environment. Under oxidizing conditions, Fe_3O_4 may be oxidized as given by the following reactions [58 - 60].

$$Fe_3O_4 + 0.25\ O_2 + 4.5\ H_2O \rightarrow 3Fe(OH)_3$$

$$Fe_3O_4 + 0.25O_2 + \rightarrow 1.5Fe_2O_3$$
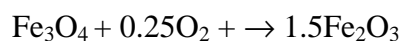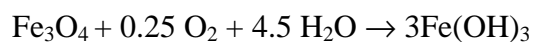
Aqueous dispersion of magnetic nanoparticles was prepared by the addition of an aqueous mixture of ferric and ferrous salts to a strong alkaline solution (NaOH or NH_4OH) at room temperature. In the present study, a solution of NaOH was used as alkali source instead of ammonia. Oxygen is eliminated from the solution by using N_2 gas flow through the reaction medium during synthesis operation in a closed system. SPION with average particles size of 6 nm were prepared without any additional stabilizer according to following procedure. Typically, 5 mL of iron solution with containing 0.1 M Fe^{2+} and 0.2 M Fe^{3+} is added drop-wise into 50 mL of alkali solution (NaOH) under vigorous mechanical stirring (2000 min^{-1}) for 30 min at room temperature. Color of the suspension was turned to black almost immediately. SPION with particle size of 12 nm was prepared by increasing the reaction temperature. All the procedures and experimental conditions were same as procedure for the synthesis of 6 nm SPION except alkaline solution was pre-heated to 80 ºC before the co-precipitation reaction.

The precipitated powders are collected and removed from the solution by external magnetic field. The supernatant solution was removed from the precipitate after decantation. Deoxygenated Milli-Q water was added to wash the powder and the solution was decanted after centrifugation at 3500 min^{-1}. After washing the powder four times, 1×10^{-2} M HCl solution was added to neutralize the anionic charge on the surface of particles. The positively charged colloidal particles were then separated by centrifugation and peptized by adding deoxygenated Milli-Q water [58-60].

4.1.3 Structural Characterization

The structural properties of Fe_3O_4 powders obtained were analyzed by X-ray powder diffraction (XRD) with a Philips PW 1830 diffractometer using the monochromatized X-ray beam from the nickel-filtered Cu K_α radiation. The average size of the crystals (D; nm) was estimated using Scherer's formula (Table 4.1) [58 - 60].

Table 4.1 Samples synthesized under different conditions and their average particle sizes (*D*); calculated from XRD data.

Sample	pH	NaOH (M)	Particle size (nm)
S1	14	0.9	1.1
S2	14	1.0	1.7
S3	14	1.5	3.0
S4	12.5	1.5	5.5
S5	11.54	1.5	6.0
S6	11.2	1.5	11.0

4.2 SPR MEASUREMENT

The polycrystalline powders of superparamagnetic iron oxide nanoparticles (SPION) placed in paraffin just above its melting temperature have been diluted and oriented in the presence of a strong magnetic field (15 kG). The samples were subsequently cooled down below the melting temperature of paraffin in this field to have magnetic orientation. A sample with dimensions 1.5x2x2.5 mm was cut from this ingot for SPR measurements. A conventional X-band (f $\cong$ 9.5 GHz) Bruker EMX model spectrometer employing an ac magnetic field (100 kHz) modulation technique was used to record the first derivative absorption signal (Figure 4.1).
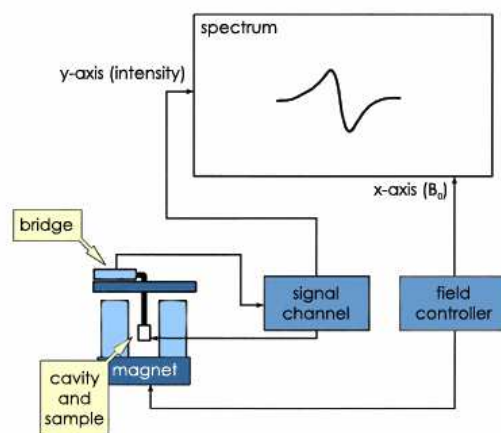
Figure 4.1 Block diagram of an ESR spectrometer

Operating conditions were 0.20 mW microwave power, 10 G modulation amplitude, center field 3500 G, sweep width 7000 G, time constant 20.48 s and sweep time 20.97 s with multiple accumulations to enhance the signal-to-noise ratio. An Oxford continuous helium gas flow cryostat has been used, allowing the X-band microwave cavity to remain at ambient temperature during ESR measurements at low temperatures. The temperature was stabilized by a conventional Lakeshore 340 temperature controller within an accuracy of 1 degree between 10 and 300 K. A goniometer was used to rotate the sample with respect to the external magnetic field in order to observe angular variations of the FMR spectra. For the frequency dependence measurements hand made K- and Q-band spectrometer used.

CHAPTER 5

THEORETICAL ANALYSIS

5.1 MAGNETIC SUSCEPTIBILITY

A correlation between the resonance magnetic field and the peak to peak line width is often observed in low temperature superparamagnetic resonance (SPR) studies of fine magnetic nanoparticles. In order to account for this correlation, we considered the resonance line shapes resulting from Landau-Lifshitz equation for the analysis of the data [61, 62].

$$\vec{M}' = \gamma \vec{M} \times \vec{B}_{eff} + \frac{\lambda}{\left|\vec{M}\right|^2} \vec{M} \times (\vec{M} \times \vec{B}_{eff}) \tag{3.146}$$

Especially in numerical computer simulation of SPR spectra and in theoretical modeling, at different low temperature regions, the resonance line broadening should be treated separately from the distribution of resonance magnetic field. The resonance field and line width of the SPR spectra were analyzed in this study. At low temperature the resonance of the individual magnetic particles occurs with a considerable line width.

The dynamic susceptibility is given by $\chi = \chi_1 - i\chi_2$ where χ_1 and χ_2 are the real and imaginary parts of the susceptibility, respectively. The microwave absorption is proportional to the imaginary part of the dynamic susceptibility. $\frac{dP}{dB} \alpha \frac{d\chi_2}{dB}$ And, therefore the following individual line shape is obtained for case 2 [61, 62].

$$\chi_2' = \frac{1}{\pi} \cdot \frac{B_0^2 \Delta_B \left[\left(B_0^2 + \Delta_B^2 \right) B^2 + B_0^4 \right]}{\left[B_0^2 (B - B_0)^2 + \Delta_B^2 B^2 \right] \cdot \left[B_0^2 (B + B_0)^2 + \Delta_B^2 B^2 \right]} \qquad (5.1)$$

Here we defined $B_0 = -\omega/\gamma$ as the resonance magnetic field and the line width $\Delta_B = \lambda B_0 / |\gamma||M_0|$.

5.2 RESONANCE FIELD

The analytical expression for the apparent resonance-field shift has been obtained. Computer simulations using the derivative magnetic susceptibility provide good fits of the resonance spectra at different temperatures for the same magnetic and morphological parameters of the particles.

In contrast to Lorentzian (or Gaussian), the line shape of Eq. 3.182 is characterized by an apparent resonance field (that at the maximum of resonance absorption) depending on the line width given by [61, 62].

$$B_r = \frac{B_0^2}{B_0^2 + \Delta_B^2} \left[2B_0 \left(B_0^2 + \Delta_B^2 \right)^{\frac{1}{2}} - B_0^2 - \Delta_B^2 \right]^{\frac{1}{2}} \qquad (5.2)$$

5.3 SPR LINE WIDTH

In a recent investigation on the SPR of nanoparticles at different temperatures [61-63], it has been shown that the individual line width for the SPR of nanoparticles at different temperatures can be well fitted by

$$\Delta_B = \Delta_T L(x) \qquad (5.3)$$

In this equation Δ_T is a saturation line width at a temperature T, $L(x) = \coth x - 1/x$ is the Langevin function with $x = M_s V B_{eff}/k_B T$, V being the particle volume.

Table 5.1 Fit parameters by using Hr equation derived from Landau-Lifshitz line shape function.

	S 1	S 2	S 3	S 4	S 5	S 6
Size (nm)	1.1	2.0	3.0	5.5	6.0	11.0
Vs (nm3)	800	3500	3800	8600	12500	10500
K (kJm-3)	25	13	10	8	7.5	5.5
Ms (kAm-1)	495	500	505	520	525	540
V(nm3)	1.331	8	27	166.38	216	1331
Ho (T)	0.338	0.338	0.338	0.338	0.338	0.338
ΔHo (T)	3.200	0.580	0.350	0.250	0.180	0.215

Besides, the thermal fluctuation-induced modulation of the magnetocrystalline anisotropy energy has been taken into account to describe the rapid increase of the individual line width by decreasing the temperature. This mechanism leads to a temperature dependence of Δ_T. The resulting volume and temperature dependence of the individual line width is then [61-63],

$$\Delta_B = \Delta_o L(x) G(y) \tag{5.4}$$

where Δ_o is the saturation line width at 0 K and G(y) is the superparamagnetic averaging factor given as $G(y) = \dfrac{1}{L(y)} - \dfrac{10}{y} + \dfrac{35}{y^2 L(y)} - \dfrac{105}{y^3}$ With $y = K_1 V_s / kT$ where K_1 is the first order magnetocrystalline anisotropy constant and V_s is the reference volume (presumably the greatest volume in the statistical ensemble). The magnetic parameters of magnetite (Fe_3O_4) nanoparticles have been used in the simulations. The best-fit values of the adjustable simulation parameters have been determined as shown in Table 5.1.

Note that one and the same set of these parameters provides the best fits to the spectra recorded in the whole temperature range of this study.

CHAPTER 6

RESULTS AND DISCUSSION

6.1 SAMPLE 1: Fe_3O_4 (D = 1.1 nm)

In this section, the SPR spectra of smallest Fe_3O_4 with diameter of 1.1 nm were recorded as a function of temperature. The derivative of microwave power absorbed by the sample with respect to the static magnetic field *dP/dH* is plotted as a function of static field for some selected temperatures as shown in Figure 6.1.
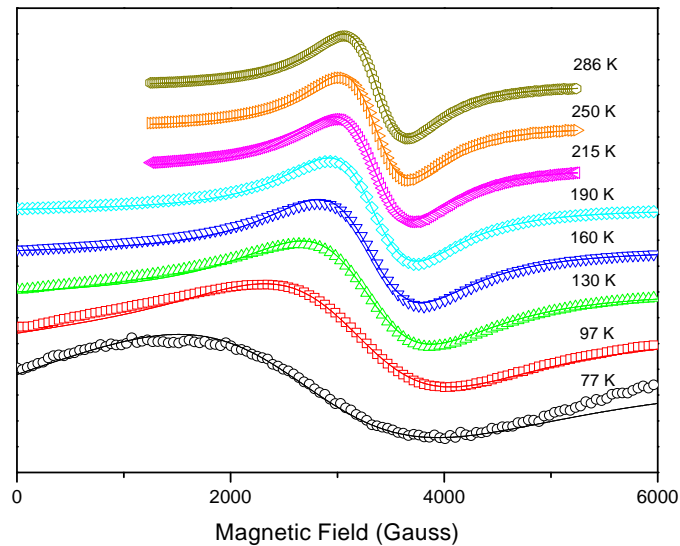
Figure 6.1 SPR spectra of Fe_3O_4 with a diameter of 1.1 nm at some selected temperatures; markers and solid lines show the experimental and theoretical fit values, respectively.

It contains that markers and solid lines show the experimental and theoretical fit values, respectively. The theoretical fit was done according to the Eqn 5.1.

It is observed that the SPR signals are completely temperature dependant. The absorption power and the resonance field decreases with the decrease in temperature while the line width increases. The values of the line width and the resonance field are 590 G and 3355 G at room temperature, respectively. The absorption power is too weak below 77 K compared with absorptions at higher temperatures. All the changes are plotted as a function of temperature and explained in detail in the following sections

6.1.1 Line width

Figure 6.2 shows the variation of the line width values of the SPR spectra and the theoretical fits according to the Eqn 5.4. The best fit values of the adjustable simulation parameters have been determined as follows: $Ms = 495$ kAm^{-1}, $\Delta Ho = 3.200$ T and $Vs = 800$ nm (Table 5.1). As seen from the figure, the line width increases smoothly as the temperature decreases down to 92 K.
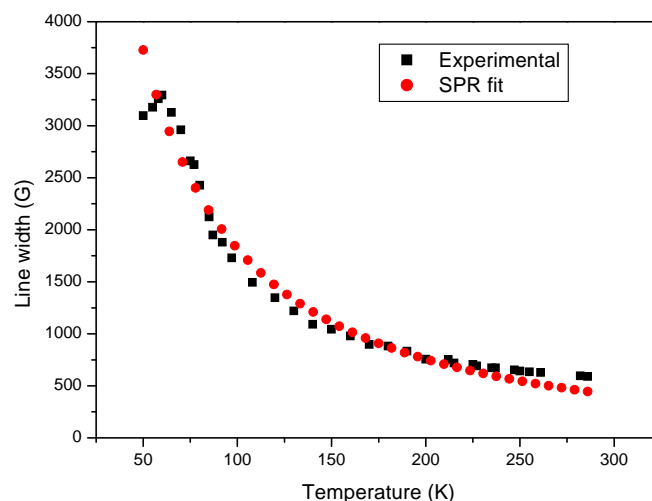
Figure 6.2 Line width vs. temperature for Fe_3O_4 with diameter of D = 1.1 nm; rectangular markers and circle markers show experimental and theoretical fit values, respectively.

Then the increase rate rises up below this temperature when the temperature decreased further to 60 K. The maximum in line width is reached at this temperature. Between 50 and 60 K line width decreases again. Below 50 K the signal is too weak and shifted to the low fields and no measurements can be done. It is known that in randomly oriented dispersed ferromagnet the absorption line width turns out to be a non-monotonic function of temperature. At low temperatures the line width is large due to the scatter in direction of anisotropic field of particles (inhomogeneous broadening). As the temperature increases the tendency to make magnetic moment isotropic causes the line width to decrease.

6.1.2. Resonance Field

Figure 6.3 shows the variation of the resonance field values (measured from the magnetic field at the centre of the SPR resonance curve) with the temperature and their theoretical simulations according to the Eqn. 5.2. The figure implies that the resonance field decreases smoothly when the temperature decreases down to 92 K. Below this temperature the resonance field decreases sharply, and no measurement can be done below 62 K, since the signal intensity goes to zero. At low temperature, 50 K, the resonance field of the SPR spectra is 1915 gauss while it has a value of 3355 G at room temperature.

For the resonance field there arises two distinct regions (I) for T > 92 K and (ii) T < 92 K. The behavior for T > 92 K can be explained as follows. It is known that the dependence of uniaxial anisotropy energy on temperature is similar to that of magnetostatic (demagnetization) energy [64]. Thus the resonance field will increase with the temperature.

The decrease of resonance field for T < 92 K is intriguing. This behavior can be explained on the line similar to that suggested by Kodama et al. [65]. Below 92 K the surface spin freezes and they freeze in the direction of dc magnetic field. This yields an exchange coupling between the surface and core spins. This gives rise to a 'unidirectional' anisotropy with easy axis in the direction of the field [64, 66]. As a result there is sudden decrease in the resonance field below 92 K.
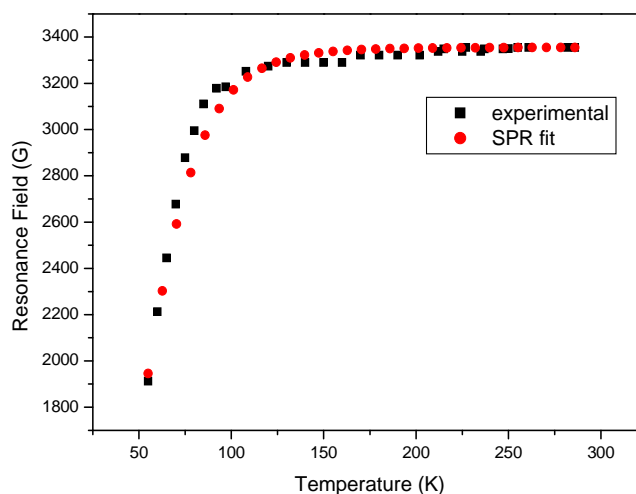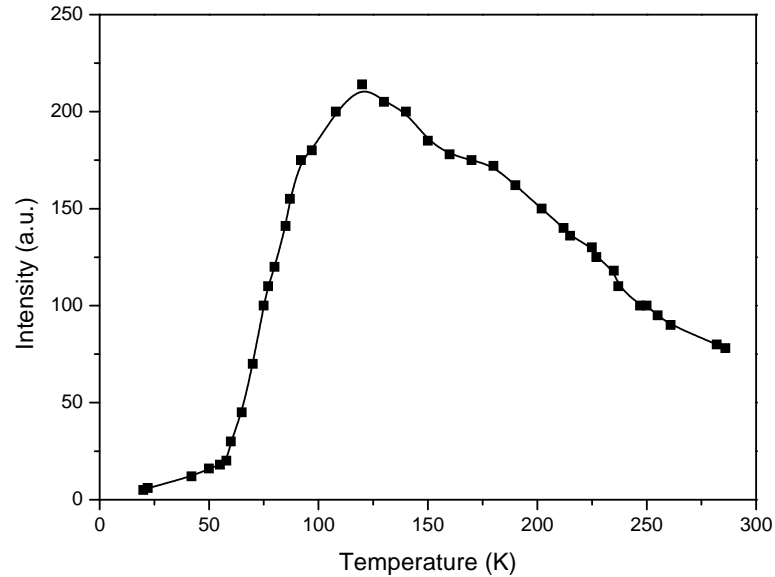
Figure 6.3 Resonance field vs. temperature for Fe_3O_4 with diameter of D = 1.1 nm; rectangular markers and circle markers show experimental and theoretical fit values, respectively.

6.1.3. Intensity

Figure 6.4 represents the temperature variation of SPR signal intensity (corresponding to dc susceptibility derived from magnetization) obtained from second integral of the SPR signals. According to the figure, the signal intensity is decreased slowly with increasing temperature above 120 K. Below this temperature; it decreases slowly between 92 and 120 K. From this figure, one can see that the magnetization curve of this sample shows a maximum at around 120 K. The intensity of the SPR signals starts to decrease sharply between 58 and 92 K. Below 58 K, it decreases slowly again. It seems almost constant between 85 and 120 K. The changes in the line width, resonance field and the signal intensity graphs are considerably important at around 92 K. The changes are not same with the general trend in all graphs. Below 92 K; it decreases sharply by decreasing the temperature. Since the intensity curve is equivalent to dc susceptibility, this kind of behavior of the signal intensity can be attributed to the spin glass nature of the sample, originating from antiferromagnetic interactions between the magnetic spins of the sample. When the temperature reaches the lowest value, the ESR intensity goes to zero value. This shows that the sample shows antiferromagnetic behavior at low temperatures. That is the antiferromagnetic interaction can over dominate and cause a spin disorder at low temperatures. Thus, since the spin alignments

become wholly in disordered and in random directions, the macroscopic magnetization approximately vanishes at lowest temperature [67]


Figure 6.4 Intensity vs. temperature for Fe_3O_4 with diameter of D = 1.1 nm

As a result, the general broadening of the line width and the decrease in the resonance filed by decreasing temperature can be explained by spin disorder (spin frustration). It is possibly coming from mainly antiferromagnetic interactions between the neighboring spins. At low temperatures the disorder of dipolar fields is increasing because the magnetization is not increasing with the same ratio. Its crucial to note that gyromagnetic (Larmour) precession frequency is observed in an effective field. The shift in the resonance filed and the broadening in the line width clearly indicate the exchange anisotropy field (induced), they mainly cause the frustration of spins.

6.2 SAMPLE 2: Fe_3O_4 (D = 2 nm)

Figure 6.5 just like the sample above reveals that SPR spectra of Fe_3O_4 with diameter of 2 nm are strongly temperature dependent. It is also theoretically fitted by

Eqn. 5.1 and drawn as in same figure. However the first derivative of the absorption signals at lower temperature turns out to be weaker. On the other hand, we observe that they contains DPPH at approximately 3400 G. Below the 50 K the intensity of the spectra are so low that it makes difficult to identify line width and resonance field of them. At lower temperatures, the fitting the SPR spectra became difficult. Because the wings of the experimental spectra are broader than that of the theoretical fits.
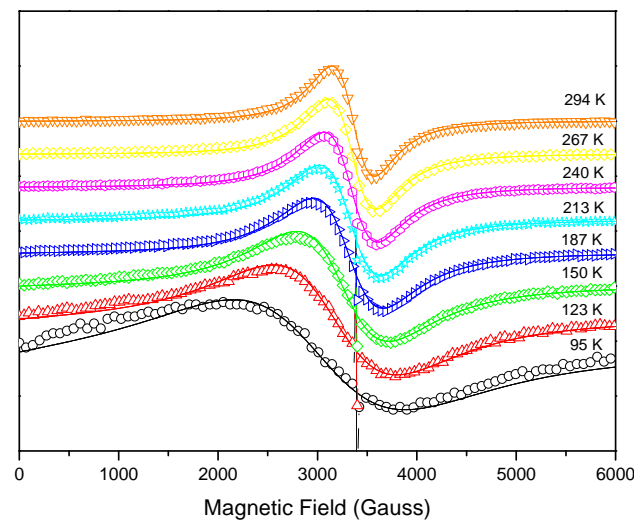
Figure 6.5 SPR spectra of Fe_3O_4 with diameter of 2 nm at some selected temperatures; markers and solid lines show the experimental and theoretical fit values, respectively.

6.2.1 Line width

Generally, the line width of the spectra increases as the temperature decreases as in the Figure 6.6. Line width is increasing smoothly with decreasing temperatures down to 125 K. It also contains the best fit value parameters: $Ms = 500$ kAm^{-1}, $\Delta Ho = 0.580$ T and $Vs = 3500$ nm which are listed in Table 5.1. The theoretical fit was done according to the Eqn. 5.4. In the range of 50 – 125 K, the change rate of line width respect to temperature rises. Below 50 K it slightly increases then it cannot be measured because of low absorption signals.
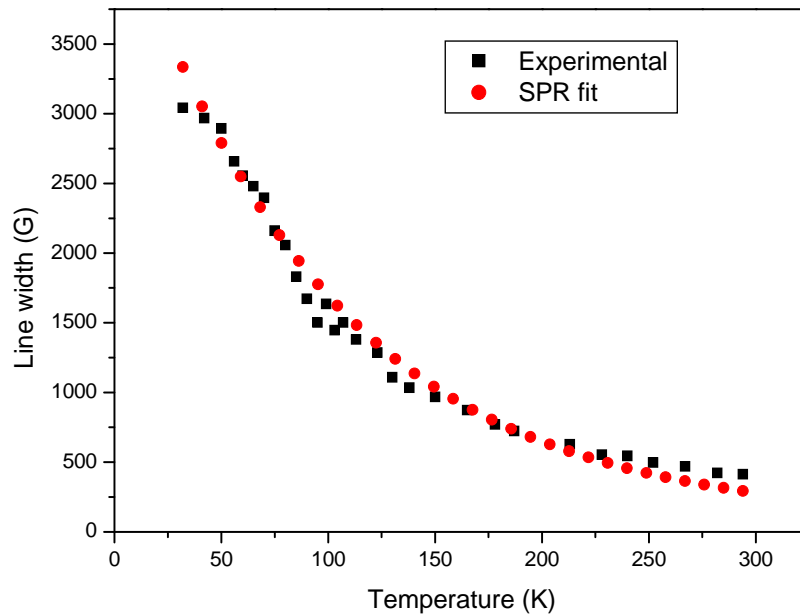
Figure 6.6 Line width vs. temperature for Fe_3O_4 with diameter of $D = 2$ nm ; rectangular markers and circle markers show experimental and theoretical fit values, respectively.

6.2.2. Resonance Field

The temperature dependency of the resonance field can be seen in Figure 6.7. Both experimental and the theoretical simulations of related temperatures are done according to the Eqn. 5.2. Both line width and the resonance field curves fitted with same parameters as mentioned in Table 5.1. The temperature is not effective as such between 125 and 300 K. The sharp decrease comes true below 125 K. The surface spin freezes in the direction of dc filed below 125 K and it causes the exchange coupling between the surface and the core spin. As a result, the sharp decrease occurred in the resonance filed below 125 K.
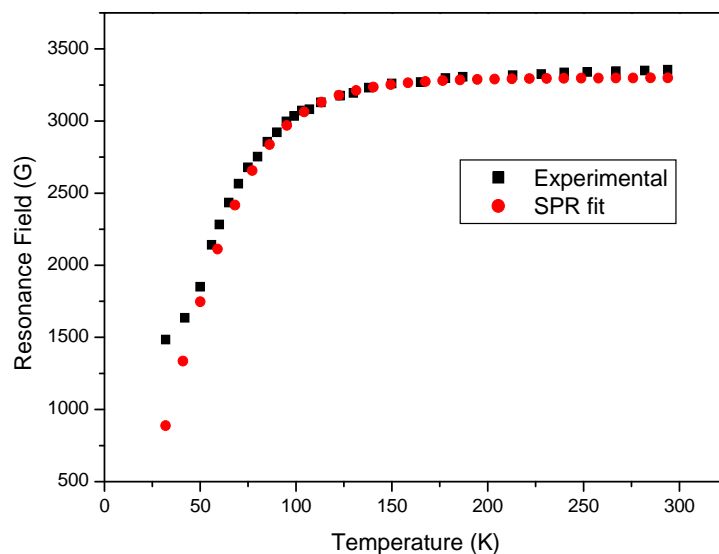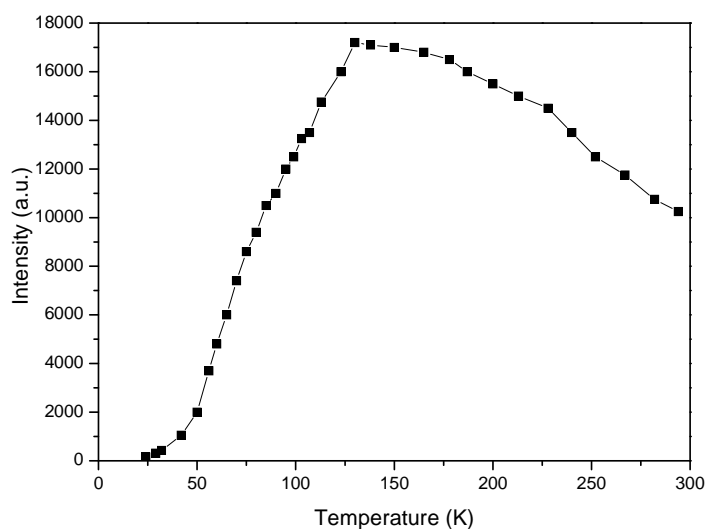
Figure 6.7 Resonance field vs. temperature for Fe_3O_4 with diameter of D = 2 nm; rectangular markers and circle markers show experimental and theoretical fit values, respectively.

6.2.3. Intensity

Two distinct regions can be considered in the absorption intensity versus temperature curve (Figure 6.8). In the first region between 130 and 300 K, the absorption intensity kept on increasing smoothly and reached its maximum value at 130 K. And the second region, below 130 K reveals that the absorption intensity sharply decreases down to 25 K however below this value it cannot be detected further due to weak signals.

As a result, magnetic characteristics of Fe_3O_4 with diameter of 2 nm below 125 K are similar to those of Sample 1 in the temperature below 92 K. Broadening of the line width and the decrease in the resonance filed in low temperature is caused by spin frustration. Therefore, we can come to conclusion that these two samples at low temperatures show the spin disorder system. This sample shows antiferromagnetic behavior at low temperatures as the fist one. This spin disorder at low temperatures is the effect of that the antiferromagnetic interaction can over dominate [67].

Figure 6.8 Intensity vs. temperature for Fe_3O_4 with diameter of D = 2 nm

6.3 SAMPLE 3: Fe_3O_4 (D = 3 nm)

This section includes the derivative of microwave power absorbed by the sample with respect to the static magnetic field, the temperature dependent curves of line width, resonance field and the intensity of the absorption signals of the Fe_3O_4 with diameter of 3 nm. The experimental and the theoretical SPR spectra are shown in Figure 6.9. It contains that markers and solid lines show the experimental and theoretical fit values, respectively. The theoretical fit was done according to the Eqn. 5.1.

As in this figure, the signal is clearly temperature dependant. The absorption power and the resonance field decreases with the decrease in temperature while the line width increases. The values of the line width and the resonance field are 385 G and 3300 G respectively at room temperature. The absorption power is too weak below 15 K compared with absorptions at higher temperatures. All the changes are plotted as a function of temperature and explained in detail in the following sections.
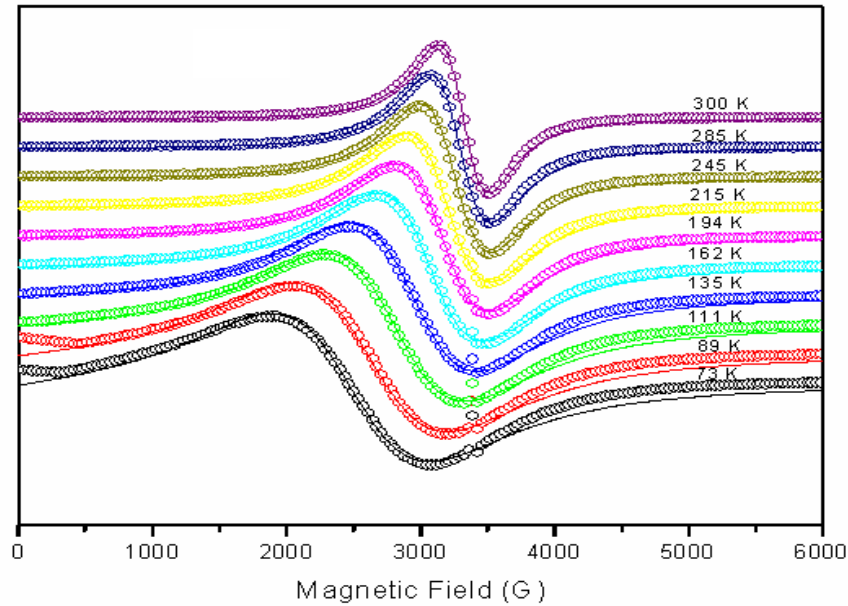
Figure 6.9 SPR spectra of Fe_3O_4 with diameter of 3 nm at some selected temperatures; markers and solid lines show the experimental and theoretical fit values, respectively.

6.3.1 Line width

Figure 6.10 shows the variation of the line width values of the SPR spectra and the theoretical fits according to the Eqn 5.4. The best fit values of the adjustable simulation parameters have been determined as follows: Ms = 505 kAm^{-1}, ΔHo = 0.350 T and Vs = 3800 nm (Table 5.1). As seen from the figure, the line width increases smoothly as the temperature decreases. While the peak to peak line width has the value of 3856 G at room temperatures, it reduces to 1515 G at 26 K. The line width is larger at low temperatures than it is at high temperatures. Because the scatter in direction of anisotropic field of particles (tendency to make magnetic moment isotropic), line width to decreases at higher temperatures. The experimental values are quite different than the theoretical fits below 60 K. These differences may be caused by the change in the magnetic behavior of the small particles at lower temperatures.
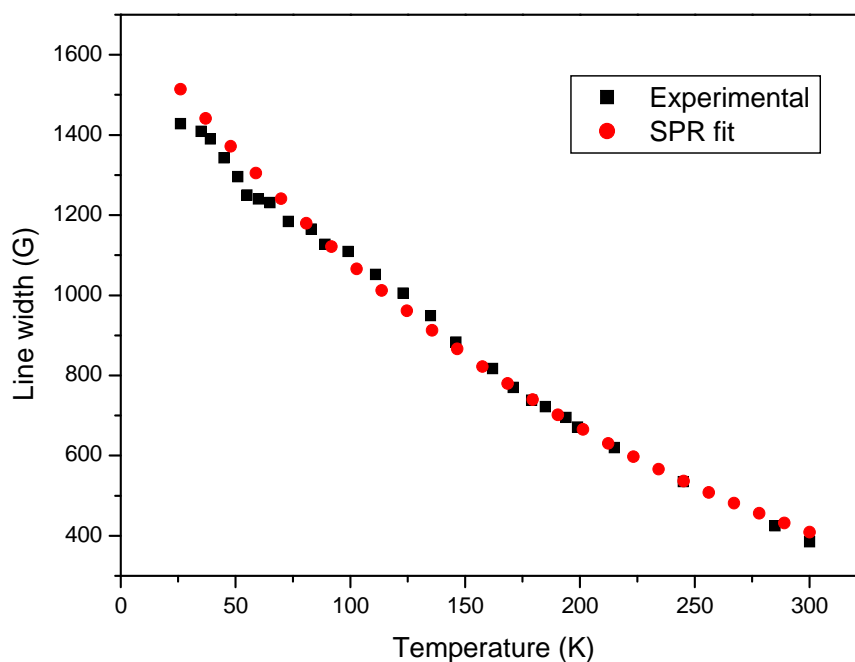
Figure 6.10 Line width vs. temperature for Fe_3O_4 with diameter of D = 3 nm; rectangular markers and circle markers show experimental and theoretical fit values, respectively.

6.3.2. Resonance Field

Both experimental values and the theoretical simulations at related temperatures can be seen in Figure 6.11. The theoretical simulations are done with Eqn. 5.2 again. In the figure below, the rectangular markers and circle markers show the experimental and theoretical fit values, respectively. The theoretical fit values are in accordance with the experimental resonance values. It is clear that the resonance field is temperature dependant like ones before. The effect of the temperature is increasing with decreasing temperature. The theoretical fits of the resonance field values are obtained with the same parameters that of the line width values (Table 5.1). The resonance field versus temperature curve is concave type curve. Around the room temperature the resonance field reaches 3300 G and it decreases 1600 G at 25 K. Below this temperature the resonance field of the SPR spectra can not be determined because the absorption intensity will goes to zero below this temperature.
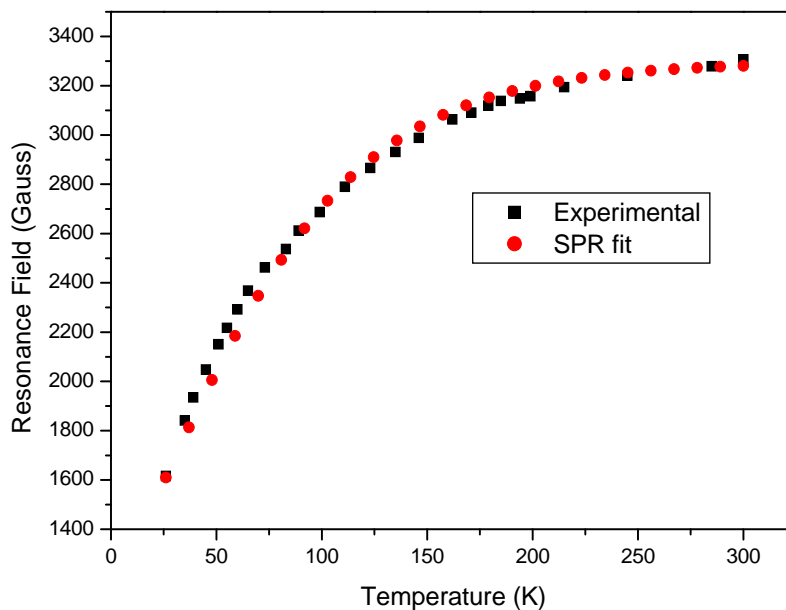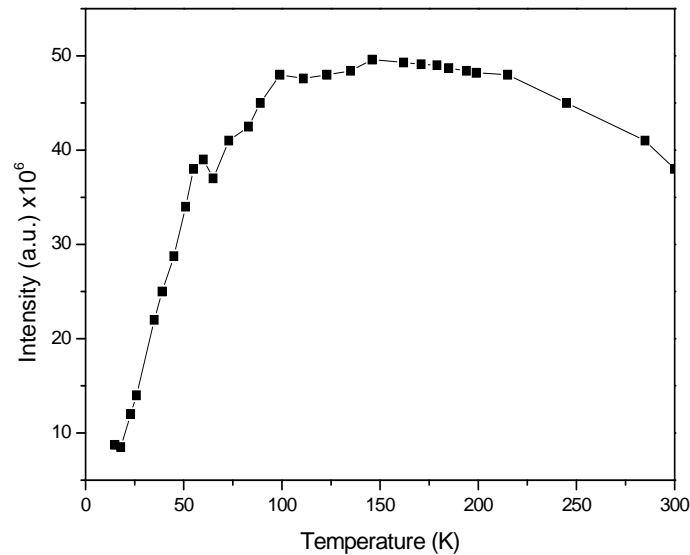
Figure 6.11 Resonance field vs. temperature for Fe_3O_4 with diameter of
$D = 3$ nm; rectangular markers and circle markers show experimental
and theoretical fit values, respectively.

6.3.3. Intensity

Figure 6.12 represents the temperature variation of SPR signal intensity obtained from second integral of the SPR signals. According to the figure, the signal intensity is decreased slowly with increasing temperature above 146 K. Below this temperature; it decreases slowly between 65 and 146 K. From this figure, one can see that the magnetization curve of this sample shows a maximum at around 146 K. The intensity of the SPR signals starts to decrease sharply below 65 K. Since the intensity curve is equivalent to dc susceptibility, this kind of behavior of the signal intensity can be attributed to the spin glass nature of the sample, originating from antiferromagnetic interactions between the magnetic spins of the sample. When the temperature reaches the lowest value, the SPR intensity goes to zero value. This has a physical meaning that the sample shows antiferromagnetic behavior at low temperatures. That is the antiferromagnetic interaction can over dominate and cause a spin disorder at low temperatures. Thus, since the spin alignments become wholly in disordered and in

random directions, the macroscopic magnetization approximately vanishes at lowest temperature [67].

**Figure 6.12** Intensity vs. temperature for Fe_3O_4 with diameter of D = 3 nm

As a conclusion, the broadening in the line width and the decrease in the resonance filed at lower temperatures refer to spin frustration. The possible sources of it are antiferromagnetic interactions between the neighboring spins. Because the magnetization is not increasing with the same ratio at low temperatures, the disorder of dipolar fields increases. The shift in the resonance filed and the broadening in the line width clearly indicate the exchange anisotropy field, they mainly cause the frustration of spins. In other words, the antiferromagnetic behavior is dominated at lower temperatures.

6.4 SAMPLE 4: Fe_3O_4 (D = 5.5 nm)

Figure 6.13 reveals that a SPR spectrum of Fe3O4 with diameter of 5.5 nm is clearly temperature dependent. It is also theoretically fitted and drawn by Eqn. 5.1 as in same figure. The theoretical fit curves at lower temperatures differ from the

experimental ones by their wings. The theoretical curves have quite narrower than the experimental at such temperatures.

However the first derivative of the absorption signals at lower temperature turns out to be weaker. Below the 26 K the intensity of the spectra are so low that it makes difficult to identify line width and resonance field of them. The line width, resonance field and the absorption intensity change with temperature are going to be explained in following sections.
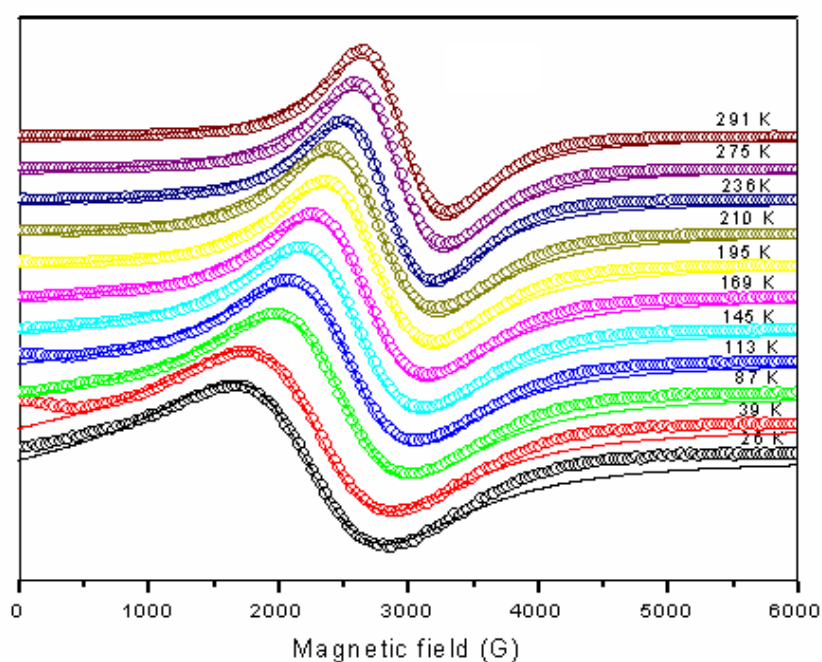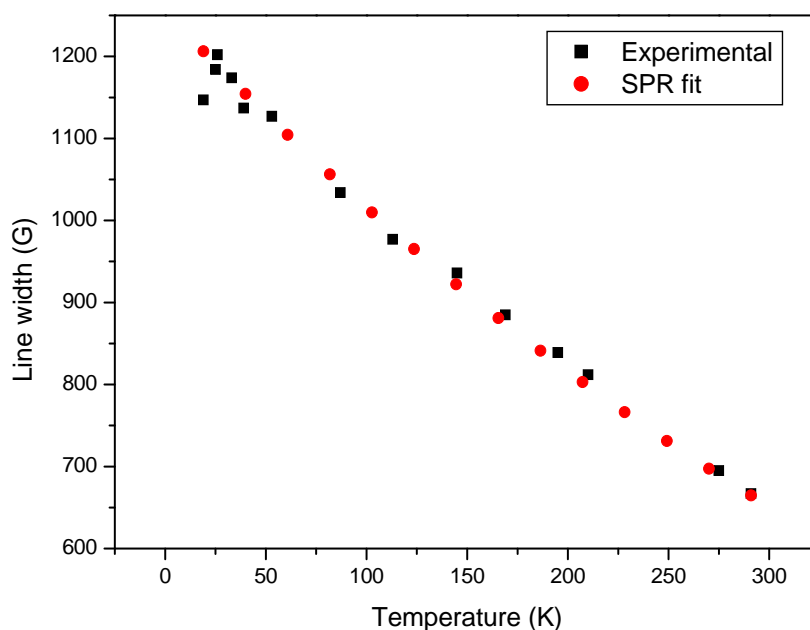

Figure 6.13 SPR spectra of Fe_3O_4 with diameter of 5.5 nm at some

selected temperatures; markers and solid lines show the experimental

and theoretical fit values, respectively.

6.4.1 Line width

In the Figure 6.14, the line width generally increases as the temperature decreases. Line width's increase is nearly linear with decreasing temperatures down to 25 K. It is about 650 G at room temperature and reaches 1200 G at 25 K, then it decreases 1150 G below this temperature. This figure also contains the best fit values

with parameters: Ms = 5200 kAm^{-1}, ΔHo = 0.250 T and Vs = 8600 nm which are listed in Table 5.1. The theoretical fit was done according to the Eqn. 5.4. Below 25 K it sharply decreases with decreasing temperature it cannot be measured because of low absorption signals. It has

Figure 6.14 Line width vs. temperature for Fe$_3$O$_4$ with diameter of D = 5.5 nm; rectangular markers and circle markers show experimental and theoretical fit values, respectively.

6.4.2. Resonance Field

The temperature dependency of the resonance field can be seen in Figure 6.15. Both experimental and the theoretical simulations of related temperatures are done according to the EThe resonance field curves fitted with same parameters as mentioned above section (Table 5.1). The resonance field is inversely changing with temperature. While the resonance field of the ESR spectra is 2970 G at around room temperatures, it reduces to 2100 G at 25 K. It is decreasing sharply with decreasing temperature below 25 K.
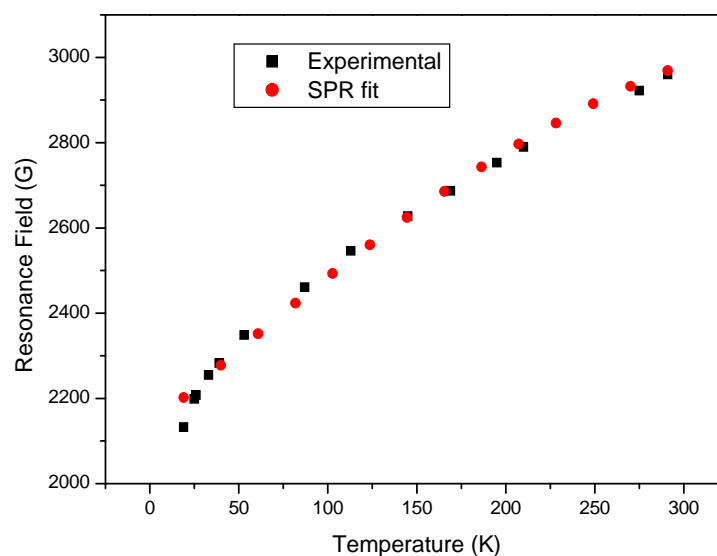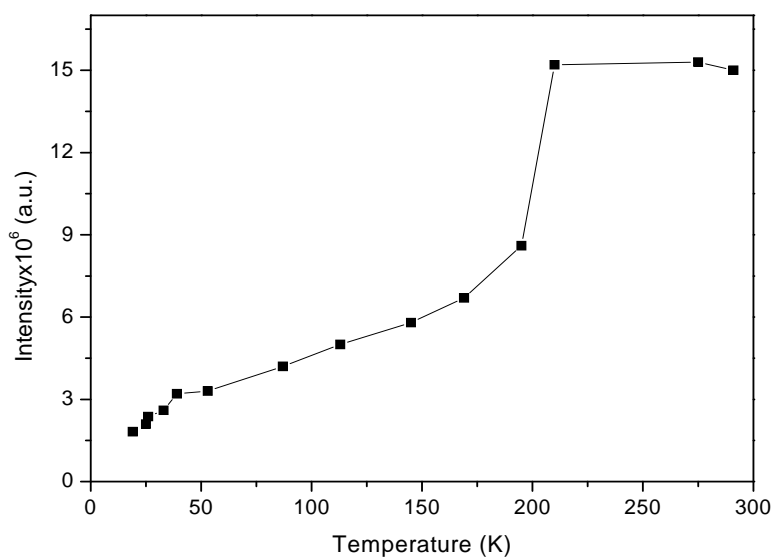
Figure 6.15 Resonance field vs. temperature for Fe_3O_4 with diameter of D = 5.5 nm; rectangular markers and circle markers show experimental and theoretical fit values, respectively.

6.4.3. Intensity

The absorption intensity versus magnetic filed curve is plotted in Figure 6.16. In the region between 210 and 300 K, the absorption intensity kept on increasing smoothly and reached its maximum value at 210 K by decreasing temperature. And then it decreases sharply down to 170 K. In the range of 40 - 170 K, decrease is going on slightly with decreasing temperature. The decreasing rate rises between 20 and 40 K and below this value it cannot be detected further due to weak signaThe changes in the line width, resonance field and the signal intensity graphs are considerably important below 40 K. Since the intensity curve is equivalent to dc susceptibility, this sharp decrease in intensity signal implies the spin glass nature of the iron oxides. Also we can add that antiferromagnetic interactions between the magnetic spins cause it. At lower temperatures the signal intensity goes to zero value as antiferromagnets.

Figure 6.16 Intensity vs. temperature for Fe_3O_4 with diameter of D = 5.5 nm

6.5 SAMPLE 5: Fe_3O_4 (D = 6 nm)

The SPR spectra of Fe_3O_4 sample with diameter of 6 nm and its derivatives were analyzed in this section. The derivative of microwave power absorbed by the sample with respect to the static magnetic field is plotted as a function of static field for some selected temperatures as shown in Figure 6.17. The markers and solid lines show the experimental and theoretical fit values, respectively. The theoretical fit was done according to the Eqn. 5.1.

It is observed that the SPR signals are completely temperature dependant. The resonance field decreases with the decrease in temperature while the line width increases. These changes are same in all analyzed samples, but the absorption intensity is increasing with decreasing temperature as a different observation from ones before.

So the absorption power does not go to the zero value. The values of the line width and the resonance field are 573 G and 3084 G at room temperature, respectively. All the changes are plotted as a function of temperature and explained in detail in the following sections.
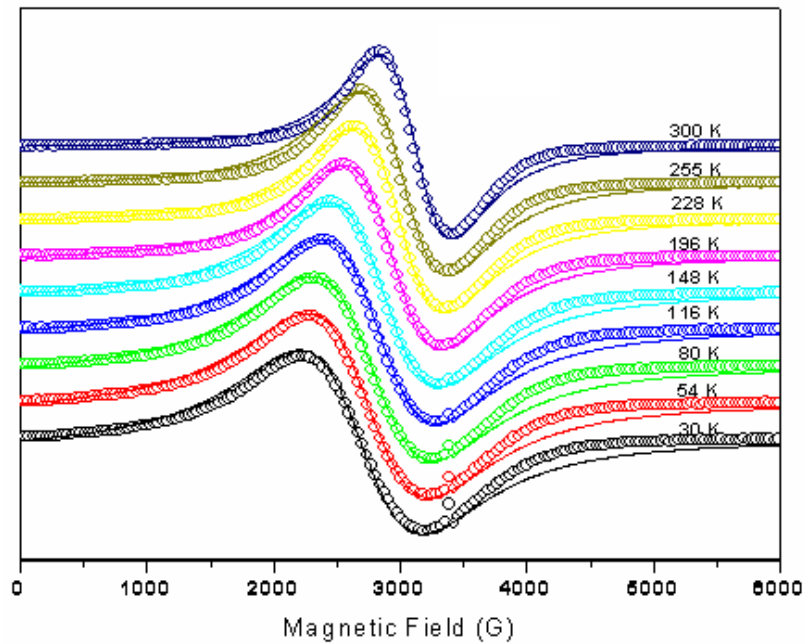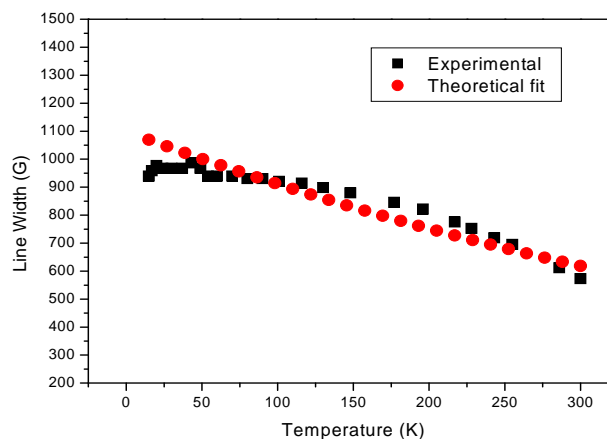

Figure 6.17 SPR spectra of Fe_3O_4 with diameter of 6 nm at some selected temperatures; markers and solid lines show the experimental and theoretical fit values, recpectively.

6.5.1 Line width

Figure 6.18 shows the variation of the line width values of the SPR spectra and the theoretical fits according to the Eqn 5.4. The best fit values of the adjustable simulation parameters have been determined as follows: $Ms = 525$ kAm^{-1}, $\Delta Ho = 0.180$ T and $Vs = 12500$ nm (Table 5.1). As seen from the figure, the line width increases smoothly with the decrease in temperature down to 54 K, and it has concave shape. Then there is a stepwise increase and decrease which are following each other between 14 and 54 K. The experimental setup can not provide the decrease in temperature below 10 K. The Eqn 5.4 supplies nearly linear curve as in the figure below. However the

experimental curve has a small concavity. The experimental values are fitted by the best proper parameters as mentioned above.
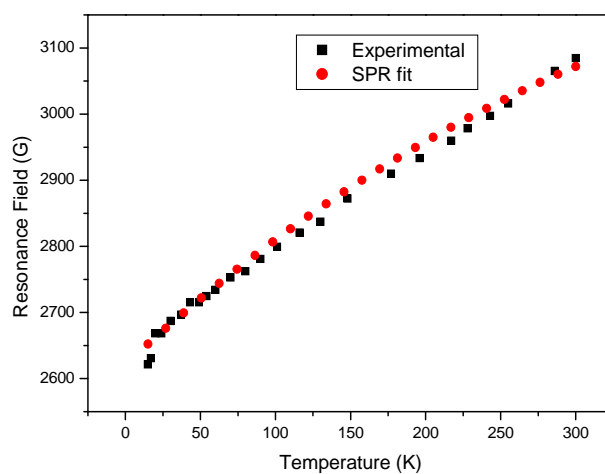

Figure 6.18 Line width vs. temperature for Fe_3O_4 with diameter of D = 6 nm; rectangular markers and circle markers show experimental and theoretical fit values, respectively.

6.5.2. Resonance Field

Figure 6.19 shows the variation of the resonance field values with the temperature and their theoretical simulations according to the Eqn. 5.2. The figure implies that the resonance field decreases smoothly when the temperature decreases down to 20 K. Below this temperature the resonance field decreases sharply, and no measurement can be done below 15 K, since the decrease below this temperature is impossible. At lowest temperature, 20 K, the resonance field of the FMR spectra is 2622 G while it has a value of 3085 G at room temperature.

The decrease of resonance field by decreasing temperature can be explained on the line similar to that suggested by Kodama et al. [65]. The surface spin freezes and they freeze in the direction of dc magnetic field. This yields an exchange coupling between the surface and core spins. This gives rise to a 'unidirectional' anisotropy with easy axis in the direction of the field [64,66]. As a result there is linear decrease in the resonance field.

Figure 6.19 Resonance field vs. temperature for Fe_3O_4 with diameter of D = 6 nm

6.5.3. Intensity

The Figure 6.20 shows the absorption intensity of the SPR spectra with respect to temperature in a range of 15 - 300 K. Unlike the samples analyzed before, the absorption intensity of this sample surprisingly increases with decreasing temperature.
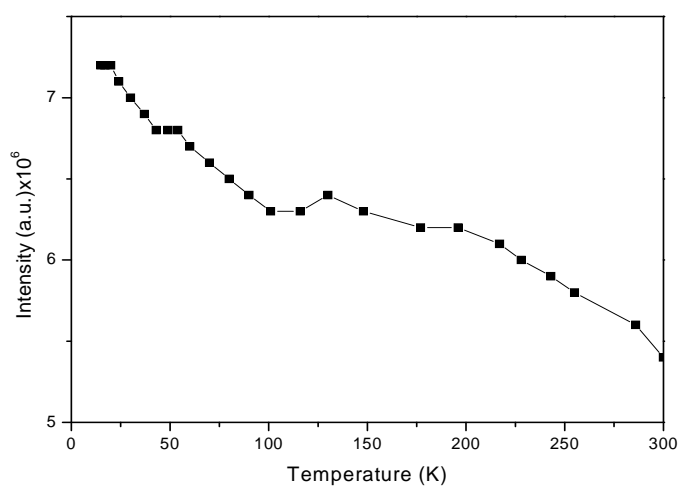
Figure 6.20 Intensity vs. temperature for Fe_3O_4 with diameter of D = 6 nm

6.6 SAMPLE 6: Fe$_3$O$_4$ (D = 11 nm)

Figure 6.21 reveals that SPR spectra of Fe$_3$O$_4$ with diameter of 11 nm are strongly temperature dependent. It is also theoretically fitted by Eqn. 5.1 and drawn as in same figure. However the first derivative of the absorption signals at lower temperature turns out to be weaker. Below the 9 K the intensity of the spectra are so low that it makes difficult to identify line width and resonance field of them. At lower temperatures, the fitting the SPR spectra became difficult. Because the wings of the experimental spectra at higher fields are narrower than that of the theoretical fits.
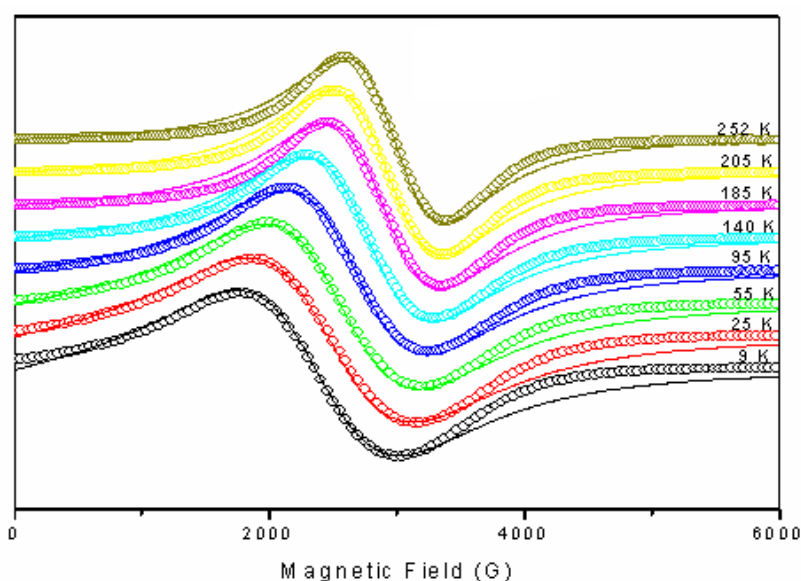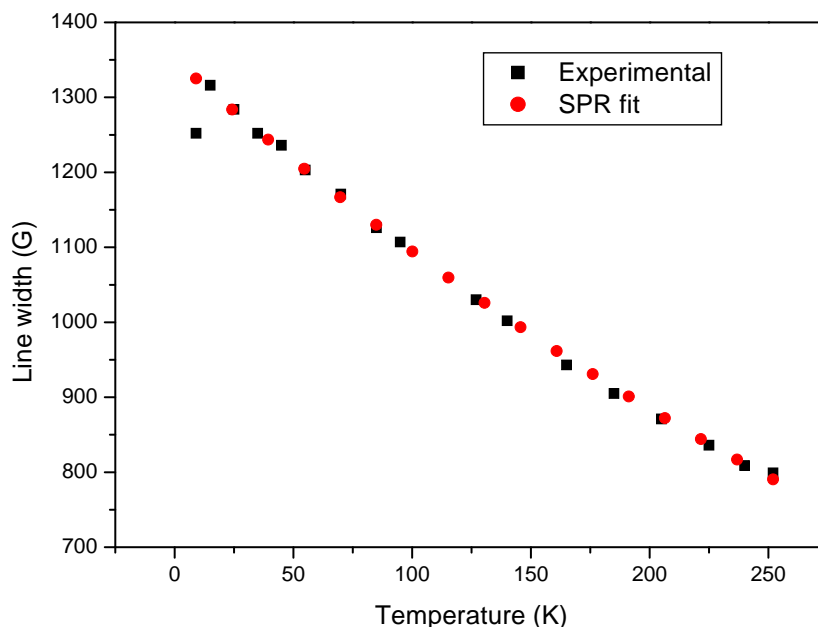

Figure 6.21 SPR spectra of Fe$_3$O$_4$ with diameter of 11 nm at some

selected temperatures; markers and solid lines show the experimental

and theoretical fit values, recpectively.

6.6.1 Line width

Generally, the line width of the spectra increases as the temperature decreases as in the Figure 6.22. Line width is increasing linearly with decreasing temperatures down to 15 K. It also contains the best fit value parameters: Ms = 540 kAm^{-1}, ΔHo = 0.215 T and Vs = 10500 nm which are listed in Table 5.1. The theoretical fit was done according to the Eqn 5.4. The line width of the SPR spectra sharply decreases below 15 K. While

it has 799 G at around room temperature, it reaches 1316 G at 15 K. It reduces to 1252 G at the lower temperature of 9 K.
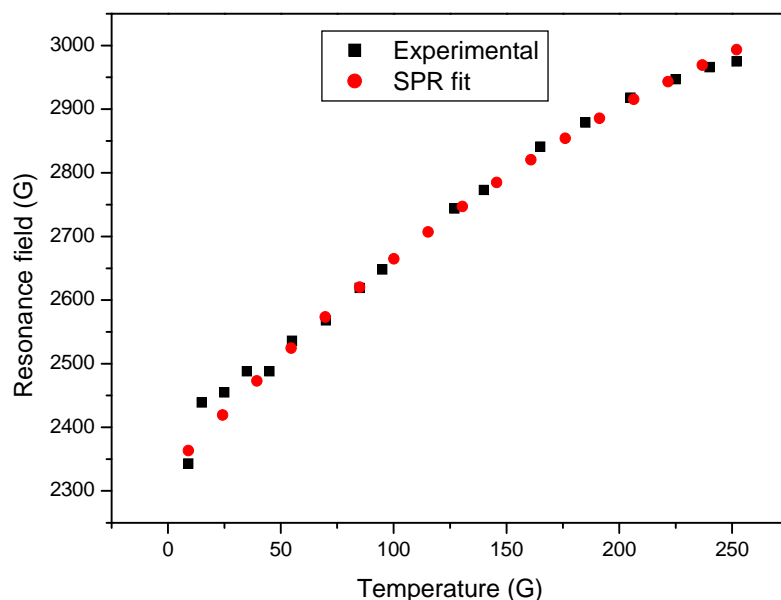

Figure 6.22 Line width vs. temperature for Fe_3O_4 with diameter of D = 11 nm; rectangular markers and circle markers show experimental and theoretical fit values, respectively.

6.6.2. Resonance Field

The temperature dependency of the resonance field of the largest sample can be seen in Figure 6.23. Both experimental and the theoretical simulations of related temperatures are done according to the Eqn. 5.2. Both line width and the resonance field curves fitted with same parameters as mentioned in Table 5.1. The resonance field decreases sharply between 45 and 252 K by decreasing temperature. It has the values of 2975 G and 2488 G at 252 and 45 K, respectively. In other words it reduces almost 500 G. In the range of 15 – 45 K the rate of decrease slows down. However it again decreases sharply below 15 K and it reduces to 2343 G at 9 K. Therefore we can say that the temperature has varying effect on resonance field. At low temperatures, the surface spin freezing in the direction of dc filed then it causes the exchange coupling

between the surface and the core spin. As a result, the sharp decrease occurred at low temperatures.
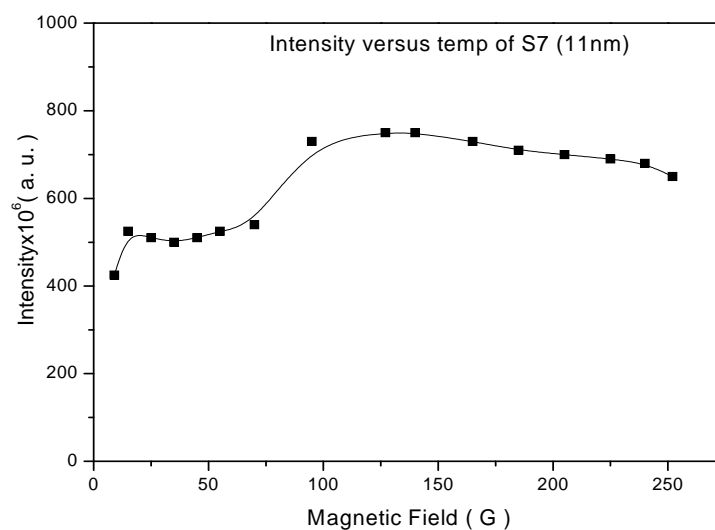

Figure 6.23 Line width vs. temperature for Fe_3O_4 with diameter of D = 11 nm; rectangular markers and circle markers show experimental and theoretical fit values, respectively.

6.6.3. Intensity

Two distinct regions can be considered in the absorption intensity versus temperature curve (Figure 6.24). In the high temperature region between 95 and 300 K, the absorption intensity kept on increasing quietly and reached the maximum value at around 95 K. The absorption intensity decreases sharply down to 70 K. And the other region in the range of 15 – 70 K reveals no change that the absorption intensity is nearly constant. Below 15 K the absorption intensity sharply decreases again. However below this temperature it cannot be detected further due to weak signals.

As a result, magnetic characteristics of Fe_3O_4 with diameter of 11 nm at low temperature are similar to the smaller particles. Broadening of the line width and the decrease in the resonance filed in low temperature is caused by spin frustration.

Therefore, we can come to conclusion that this sample at low temperatures shows the spin disorder system that means antiferromagnetic behavior dominant at low temperatures. In other words, this spin disorder at low temperatures is the effect of that the antiferromagnetic interactions can over dominate in the system [67].


Figure 6.24 Intensity vs. temperature for Fe_3O_4 with diameter of D = 11 nm

CHAPTER 7

CONCLUSIONS

The room temperature X-band SPR spectra taken from 1.1-11 nm samples and their simulations according to Eqn. 5.1 are shown in Figure 7.1. At room temperature an intense resonance line is observed with slightly asymmetric line shape for all samples. The spectra seem to significantly be size dependent. As it is seen from the figure, at room temperature, the peak to peak line width and the resonance field is changing with the particle size. While the line width is varying between 385 G and 817 G, the resonance field changes from 3426 G to 2999 G, as the particle size changes (see Figure 7.2). While the resonance field is shifted to lower fields (decreasing) the linewidth is increasing by the increase in the particle size.
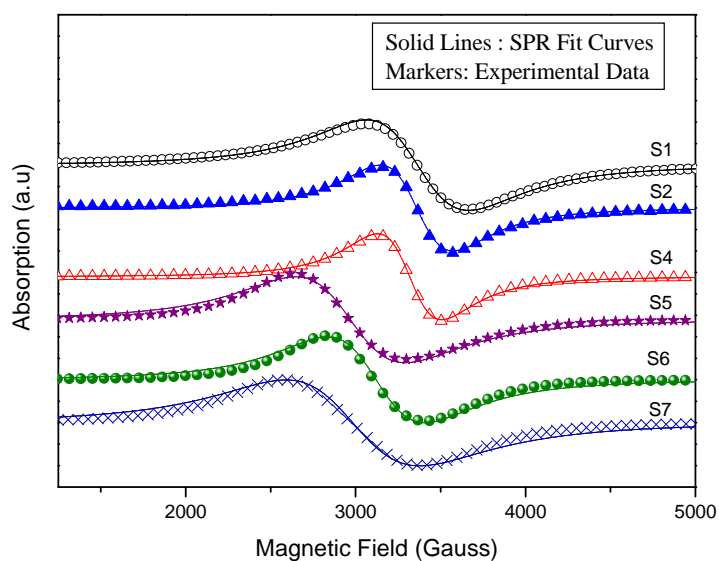
Figure 7.1 X-band SPR spectra of F_3O_4 with 1.1-11 nm and their simulations.

Figure 7.2 shows the particle size dependence of the room temperature resonance field and SPR line width. As seen from the figure, the changes in the resonance line center and SPR line width with the particle size also point out interesting aspects.
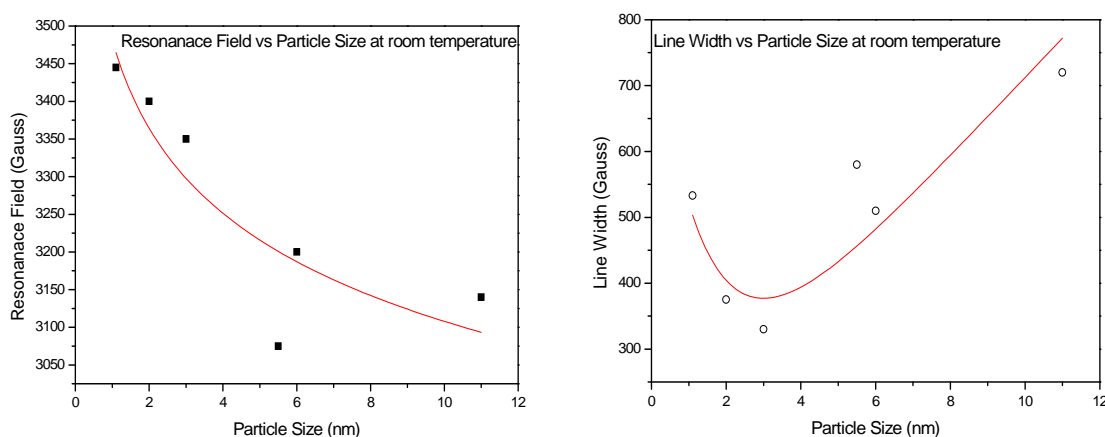
Figure 7.2 Particle size dependence of the X-band SPR (a) resonance field and (b) line width at room temperature.

When the particle size is increasing the resonance field of the SPR signal is decreasing while the SPR line width is increasing at room temperature. As shown in the Figure 7.2, the resonance field is inversely proportional with the particle diameter, means Hr≈1/d because of the large surface to volume ratio. This behavior can be explained by the core-shell morphology of the nanoparticles consisting of ferrimagnetically aligned core spins and the spin-glass like surface. The magnetic behavior of nanoparticles has a marked dependence with the decrease in particle size and the surface effects start to dominate. In nanoparticles having large ratio of surface to volume, the spin disorder (surface-spin-driven arrangements) may modify the magnetic properties. This spin disorder may be caused by lower coordination of the surface

atoms, broken exchange bonds that produce a spin-glass like state of spatially disordered (canted) spins in the surface cations with high anisotropy surface layer [32,68]. As the particle size increases the ratio of surface-to-volume decreases. Since the magnetization at the surface is smaller than the core, by increasing the size of nanoparticles decrease the ratio, means, increase the magnetization. Therefore, the particles come to resonance easily causing the decrease in the resonance field by increasing the particle size.

Figure 7.3 shows the temperature variation of the line width of the SPR spectra at X-band for all samples. As seen from the figure, overall behavior of the line width values of all samples is similar at high temperatures. They increase slowly by decreasing the temperature down to 130 K and they have linear temperature dependence. As the temperature decreased further the line width values for the samples 2.9 nm to 11 nm behaves like before and the values continue to change linearly with the temperature. For the samples 1.1 nm and 2 nm, below 140 K, the line width values increase faster than before by decreasing the temperature. The line width values for the sample 1.1 nm reaches its maximum value at around 60 K. Below 60 K, it starts to decrease. These line broadenings can be attributed to spin disorder (frustrations) at low temperatures. The surface spin fluctuations slow down as the temperature is decreased, leading at low temperatures to a frozen disorder of the surface spins. The degree of spin frustrations is expected to increase with decreasing the particle size. From the viewpoint of SPR, at some temperatures, the surface is transiently 'condensed' into a spin glass state for times larger than a Larmor period. The distribution of canting angles of frustrated spins at the surface then results in a wide spread of internal fields and thus in the line broadening [69,70]. This frustration may be partially attributed to

antiferromagnetic interactions between the magnetic clusters. That is, the line broadening might arise from the dipolar interactions between the superparamagnetic nanoparticles.
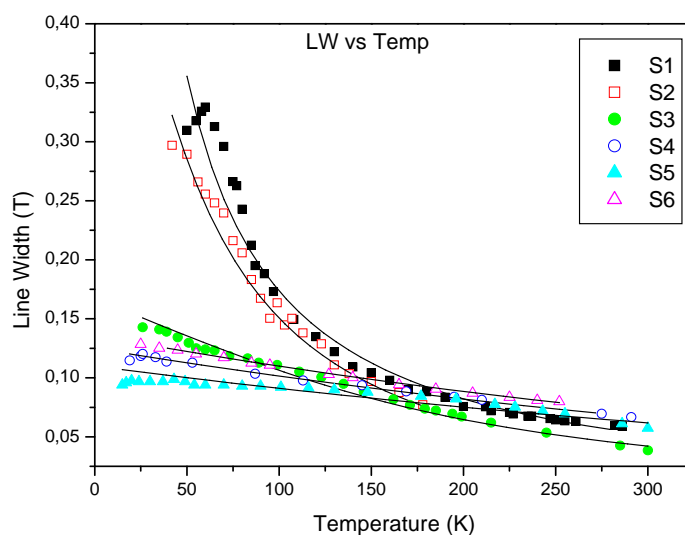
Figure 7.3 Temperature dependence of the line width of the X-band SPR spectra for all samples.

Temperature dependence of the resonance field values (measured from the magnetic field at the center of the SPR resonance line) of all samples are shown in Figure 7.4. The resonance field values of the samples 5.5 nm to 11 nm behave approximately the same. The values increases slowly by decreasing the temperature and there is an almost linear temperature dependence of the resonance field values for these samples.

But, it is different for the samples of 1.1 nm to 3 nm. For 1.1 nm and 2 nm samples, the resonance field values are approximately constant at high temperature regime. There is a turning point at 120 K. Below this temperature, the resonance field values of these samples decrease sharply. Then we can say that, 120K is the blocking

temperature of these samples (the blocking temperature is the transition temperature between the ferromagnetic and superparamagnetic state). For the 3 nm sample, the resonance field values are decreasing slowly by decreasing temperature down to 160 K. Below160 K, the decrease in the resonance field values increases. The amount of the shift in the resonance field varies between 479 G and 2029 G at lowest temperatures. The resonance shift increases by decreasing the particle size. This behavior is also consistent with the line width behavior. It should be remembered that, in any SPR measurement, gyromagnetic (Larmour) precession frequency is observed in an effective field. Therefore, the shift in the resonance field values is a clear indication to the induced field (exchange anisotropy field, perhaps in individual particles), which is the main cause of the disorder or frustration of any magnetic system [70]. The increase in the anisotropy fields (microscopic fields) at low temperatures reveals itself as the line broadening and a decrease in the signal intensity at low temperatures.
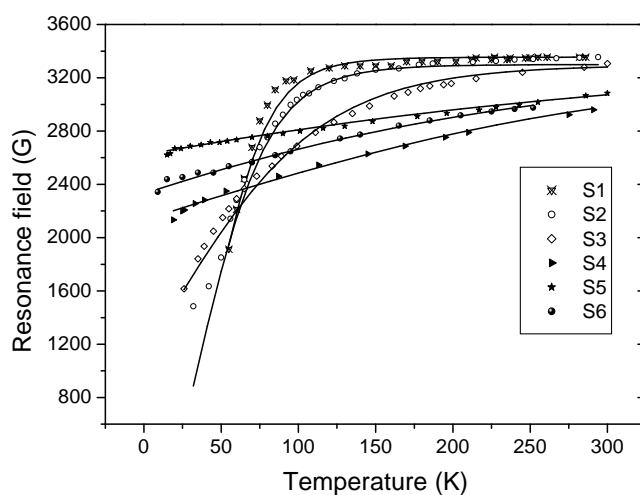
Figure 7.4 Temperature dependence of the resonance field at X-band. Solid lines are SPR fits for all samples.

The same behavior can be observed in Figure 7.5. The figure shows the temperature variations of the anisotropy fields found as the difference at room temperature and the value at any temperature for all samples. As it is seen, the anisotropy field values are increasing by decreasing the temperature and particle size.
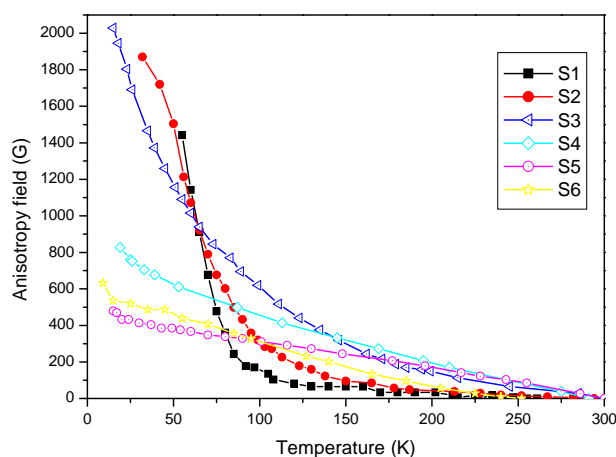
Figure 7.5 Temperature dependence of the anisotropy fields (H(r) - H (0)) at X-band for all samples.

The anisotropy field values obtained by H(r) - H(0); where H(r) is the resonance field at any temperature and H(0) is the resonance field at room temperature. As seen from the figure, the anisotropy field is inversely proportional with the temperature. For the samples S4-to-S6, there is a linear dependence on the temperature. For S3, it is inversely proportional with the temperature. But, for samples S1 and S2, it is increasing slowly down to 100 K. Below this temperature there is a sharp increase by decreasing the temperature.

These results show that, when the sizes of the particles decrease, the overall behaviors of the samples are changed. The reason for this, at low temperatures, the anisotropic energy KV is larger than the thermal energy k_BT to render the nanoparticles to be blocked readily. Also, the reduction of the magnetic domain size at low

temperatures increases with the microwave power absorption [61]. At high temperatures, k_BT is greater than the energy barrier, only thermal energy is required to reorient the domains/particles and diminishing hysteresis is observed as expected in the superparamagnetic behavior. We remark the existence of two behaviors, one at high and the other at low temperature. In the high temperature regime we observed a superparamagnetic behavior. That means the effective anisotropy is small and thermal fluctuations governs the physics of the system. At low temperature the SPR behavior shows signs of a high anisotropy. Extrapolation to low-T of the high-T behavior evidences the effects of a large anisotropy developing at low-T. This anisotropy cannot be originated by the shape of the particle, so it can be expected to be originated on the particle surface and this agrees with the magnetization measurements and Monte-Carlo simulations performed on the nanoparticle system [41]. So, the results can be interpreted by a simple model, in which each single-domain nanoparticle is considered as a core-shell system, with uniaxial anisotropy on the core and surface anisotropy on the shell. The surface contribution is more evident in the absence of interparticle interactions [62, 68, 71].
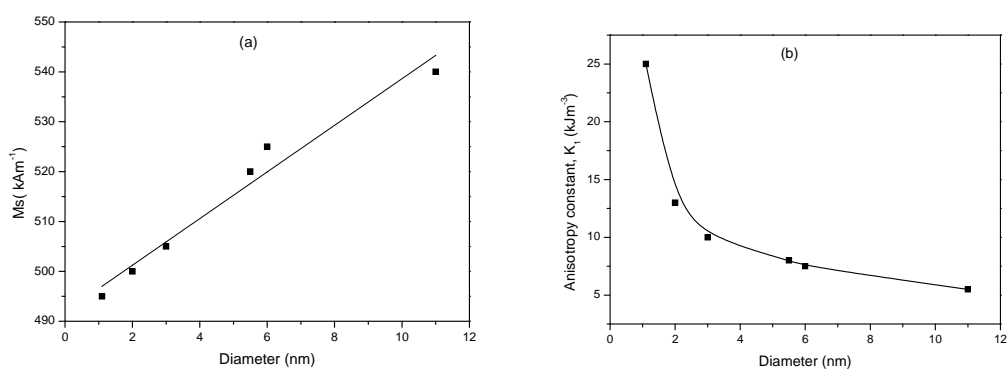
Figure 7.6 Variation of saturation magnetization, Ms (a) and anisotropy constant, K (b) with the particle size

Figure 7.6 shows the size dependence of saturation magnetization and the anisotropy constant. As seen from the figure, saturation magnetization, Ms is directly proportional to the nanoparticle size. The saturation magnetization is increasing with the size as expected. Magnetocrystalline anisotropy constant, K is inversely proportional to the particle size. One sees that the smaller is the particle size, the larger K that does not at all fit the concept of a purely volumic origin of the anisotropy. This anisotropy stems from discontinuity of magnetic interactions between individual spins which reside at the particle surface. This fact is well known for many of thin film systems [69, 70].

Superparamagnetic resonance experiments render information on the internal magnetic order of the nanoparticles. At high temperature, the SPR line shape is governed by the core anisotropy and the thermal fluctuations. By decreasing temperature, as the shell spins increase their magnetic susceptibility, they produce an effective field on the core, leading to a decrease of resonance field from its high temperature value. As the shell spins begin to order the effective anisotropy increases following its surface value more closely.
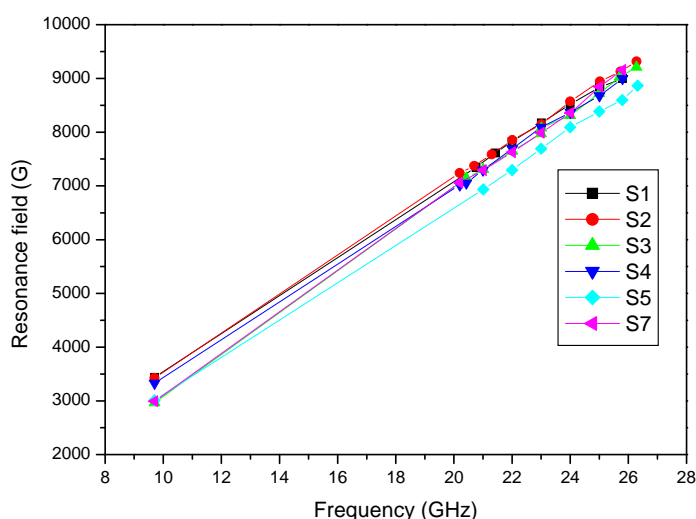
Figure 7.7 Frequency dependence of the resonance fields for all samples.

The resonance field values for all of the samples also change with the microwave frequency. The frequency dependence of the resonance field values are shown in Figure 7.7. As seen from the above figure, there is a linear frequency dependence of the resonance fields. As the frequency of the microwave is increased, the resonance field values of all samples increase linearly. When the experimental values are fitted to the theoretical resonance equation $h\nu = g\beta(B_r + B_i)$ [72, 73], the effective g-value is calculated from the slope of the curve as 1.9846 for Fe_3O_4.

As a conclusion, Magnetic properties of Fe_3O_4 nanoparticles have been studied in terms of temperature, microwave frequency and the particle size. Strong temperature and particle size dependence of SPR properties of the samples was observed. While the resonance field is decreasing by decreasing temperature, the peak to peak line width is increasing. As the particle size decreases, while the saturation magnetization is decreasing, the magnetocrystalline anisotropy constant is increasing. Linear microwave frequency dependence of the resonance field has also been observed. As the frequency increased the resonance field also increases. At low temperatures, the anisotropy energy KV is larger than the thermal energy $k_B T$ to render the nanoparticles to be blocked readily. At even lower temperatures, the anisotropy energy of magnetic nanoparticles enhanced too much. The enhancement of the line width and the anisotropy is increased by the reduction of the particle size at low temperatures. Since the relation between the blocking temperature and the particle volume as [74] $T_B = \dfrac{KV}{k_B \ln ft}$, when the volume of the nanoparticles decreased, the blocking temperature is also decreased as seen from the line width, resonance field and the anisotropy field graphs. Where t is the experimental measuring time, K is the anisotropy energy density constant and V is the volume of the

particle. The particles with very small size distribution showed the blocking temperatures below the room temperature.

REFERENCES

[1]   B.D. Cullity, *Introduction to Magnetic Materials*, Addison-Wesley
        Publishing Company, Philippines, 1972.

[2]   R.D.K. Misra, A. Kale, R.S. Srivatsava, O. Senkov, Mater. Sci. Technol.,
        2003 19, 826.

[3]   H. Nathani, R.D.K. Misra, Mater. Sci. Eng. B, 2004 113, 228.

[4]   J. Popplewell, L. Sakhnini, J. Magn. Magn. Mater., 1995, 149, 72.

[5]   K. Raj, B. Moskowitz, R. Casciari, J. Magn. Magn. Mater., 1995 149, 174.

[6]   E.J.W. Verwey, Nature, 1939, 144, 327.

[7]   B. Aktas, Thin Sold Films, 1997, 307, 250.

[8]   R.W. Chantrell, G.N. Coverdale, M. El Hilo, K. O'Grady, J. Magn. Magn.
        Mater., 1996, 157/158, 250.

[9]   V.I. Nikolaev, T.A. Bushina, Kim Eng Chan, J. Magn. Magn. Mater.,
        2006, 213, 213.

[10]   Juh-Tzeng Lue, J. Phys. and Chem. Solids, 2001, 62, 1599.

[11]   M.F. Hansen, S. Morup, J. Magn. Magn. Mater., 1998, 184, 262.

[12]   D. Jiles, *Introduction to Magnetism and Magnetic Materials*, Chapman &
        Hall, New York, 1991.

[13]   R.A. Serway, R.J. Beicher, R. McGrew, J. Soul, C. Teague, *Physics for
        Scientists and Engineers*, 5th Ed., Sunders College Pub., 2003.

[14]   R. Nave, http://hyperphysics.phy-astr.gsu.edu/hbase/solids/magpr.html,
        2001.

[15]   C. Chen, *Magnetism and Metallurgy of Soft Magnetic Materials*, Dover
        Publications,Inc., New York, 1986.

[16]   http://www.aacg.bham.ac.uk/magnetic_materials/origin_of_magnetism.ht
        ml,

[17]   C. M. Sorensen, in *Nanoscale Materials in Chemistry* (Ed.: K. J.
        Klabunde), John Wiley and Sons, Inc., New York, 2001, pp. 169.

[18]   C. Kittel, *Introduction to Solid State Physics*, Wiley, New York, 1976.

[19]   S. R. Elliott, *The Physics and Chemistry of Solids*, John Wiley & Sons, New York, 1998.

[20]   R. S. Tebble, D. J. Craik, *Magnetic Materials*, Wiley-Interscience, London, 1969.

[21]   R. M. Cornell, U. Schertmann, *The Iron Oxides: Structure, Properties, Reactions,Occurrence and Uses*, VCH Publishers, Weinheim, 1996.

[22]   R. E. Rosensweig, *Ferrohydrodynamics*, Cambridge University Press, Cambridge, 1985.

[23]   E. C. Stoner and E. P. Wohlfarth, Philos. Trans. London Ser., 1948, A 240, 599.

[24]   L. Neel, Ann. Geophys., 1949, 5, 99

[25]   W. F. Brown, Jr., Phys. Rev., 1963, 130, 1677.

[26]   J. Frenkel and J. Dorfman, Nature, 1930, 126, 274.

[27]   E. Blum, A. Cebers, M. M. Maiorov, *Magnetic Fluids*, Walter de Gruyter, Berlin, 1997

[28]   D. L. Leslie-Pelecky, R. D. Rieke, *Chemistry of Materials* 1996, *8*, 1770.

[29]   M. Ozaki, in *Fine Particles: Synthesis, Characterization, and Mechanisms of Growth, Vol. 92* (Ed.: T. Sugimoto), Marcel Dekker, Inc., New York, 2000.

[30]   E. P. Wohlfarth, *Journal of Magnetism and Magnetic Materials* 1983, *39*, 39.

[31]   R. H. Kodama, A. E. Berkowitz, *Physical Review B* 1999, *59*, 6321.

[32]   R. H. Kodama, *Journal of Magnetism and Magnetic Materials* 1999, *200*, 359.

[33]   R. Kotitz, P. C. Fannin, L. Trahms, *Journal of Magnetism and Magnetic Materials* 1995, *149*, 42.

[34]   I. S. Jacobs, C. P. Bean, in *Magnetism, Vol. III* (Eds.: G. T. Rado, H. Suhl), Academic Press, New York, 1963, pp. 271.

[35]   A. H. Morrish, The Physical Principles of Magnetism. New York, Wiley, 1975.

[36]   A. Aharoni, Introduction to the Theory of Ferromagnetism. Monographs on Physics, Oxford University Press, 1996.

[37]   Dieter Süss, Thesis, Technical Physics, Vienna University of
        Tecnology,1999

[38]   http://repositories.cdlib.org/sio/library/8

[39]   Stephen Blundell, Magnetism in Condensed Matter, New York, Oxford,
        2001

[40]   W. F. Brown, Micromagnetics. New York: Interscience, 1963.

[41]   R.Berger, J.C. Bissey, J. Kliva, J. Phys. Condens. Matter, 2000, 12, 9347.

[42]   Poole C. and Farach H. A., Theory of magnetic Resonanace, Willey, New
        York, 1972.

[43]   F. Bloch, Phys. Rev. 20, 460.

[44]   B. Bloembergen, Phys. Rev., 1950, 78, 572.

[45]   R.S. Codrington, J.D. Olds, H.C. Torrey, Phys. Rev., 1954, 95, 607.

[46]   M.A. Garstens, J.I. Kaplan, Phys. Rev., 1955, 99, 459.

[47]   J. Kliva, R.Berger, J. Magn. Magn. Mater., 1999, 205, 328.

[48]   B. Lax, K.J. Button, *Microwave Ferrites and Ferrimagnetic,*1962,
        McGraw-Hill.

[49]   T.L Gilbert, Phys. Rev., 1955, 100, 1243.

[50]   L. Landau, E. Lifshitz, Phys. Z. Sowjetunion, 1935, 8,153.

[51]   H.B. Callen, J. Phys. Chem. Solids, 1958, 4,256.

[52]   V. A. M. Brabers, *Handbook of Magnetic Materials, Vol. 8* (Ed.: K. H. J.
        Buschow), Elsevier Science, 1995, pp. 189.

[53]   P. A. Cox, *Transition Metal Oxides*, Oxford University Press, Oxford,
        1992.

[54]   T. Sato, T. Iijima, M. Sekin, N. Inagaki, *Journal of Magnetism and
        Magnetic Materials* 1987, *65*, 252.

[55]   W. Willams and D. Dunlop, J. Geophys. Res., 1995, 100,3859.

[56]   X. Qui, *Chinese Journal of Chemistry* 2000, *18*, 834.

[57]   C. Kittel, *Physical Reviews* 1946, *70*, 965.

[58]   D. K. Kim, Y. Zhang, J. Kehr, T. Klason, B. Bjelke, and M. Muhammed, J.
        Magn. Magn. Mater., 2001, 225, 256.

[59]   D. K. Kim, Ph.D. Thesis, MATCHEM, MET, KTH, 2002.

[60]   D. K. Kim, Y. Zhang, W. Voit, K. V. Rao, and M. Muhammed, J. Magn.
        Magn. Mater., 2001, 255, 30.

[61]   R. Berger, J. Bissey, J. Kliava, H. Daubric, C. Estournes, J. Magn. Magn. Mater., 2001, 234, 535.

[62]   Y. Köseoğlu, H. Kavas and B. Aktaş, Phys. Stat. Solid. (a), 2006, 203, 7, 1595.

[63]   E. De Biasi, C.A. Ramos, R.D. Zysler, J. Magn. Magn. Mater., 2003, 262, 235.

[64]   Misbah-ul-Islam, K.A. Hasmi, M.U. Rana and T. Abbas, Solid State Comm., 121, 2002, 51.

[65]   R. H. Kodama, A. E. Berkowitz, E.J. McNiff, Jr.S. Foner, *J. Appl. Phys.,* 1999, 81, 52.

[66]   Landolt-Börnstein, New Series III/4b, Springer, New York, 1970.

[67]   Y. Köseoğlu and B. Aktaş, Physica Status Solidi (c) 1, No.12, 2004, 3511.

[68]   Y. Köseoğlu, F. Yıldız, B. Aktaş, G.S. Alvarez, M. Toprak, M. Muhammed, Physica Status Solidi (b) 242, 8, 2005, 1712.

[69]   M. Özdemir, B. Aktas, Y. Öner, T. Sato, T. Ando, J. Magn. Magn. Mater. 164, 1996, 53.

[70]   F. Gazeau, J.C. Bacri, F. Gendron, R. Perzynski, Yu.L. Raikher, V.I. Stepanov, E. Dubois, J. Magn. Magn. Mater. 186, 1998, 175.

[71]   R.D. Zysler, H. Romero, C.A. Ramos, E. De Biasi, D. Fiorani, J. Magn. Magn. Mater. 266, 2003, 233.

[72]   Y. Köseoğlu, R. Yilgin, J.V. Yakhmi, J. Qin, X. Chen, B. Aktaş, J. Magn. Magn. Mater. 141, 2003, 258.

[73]   Y. Köseoğlu, F. Yıldız, J.V. Yakhmi, J. Qin, X. Chen, B. Aktaş, J. Magn. Magn. Mater., 416, 2003, 258.

[74]   J. Chatterjee, Y. Haik, C. J. Chen, J. Magn. Magn. Mater., 113, 2003, 257.